3-2003

Reduction of Thermal Residual Strains in Adhesively Bonded Composite Repairs

Heather R. Crooks

REDUCTION OF THERMAL RESIDUAL STRAINS IN ADHESIVELY BONDED COMPOSITE REPAIRS

THESIS

Heather R. Crooks, First Lieutenant, USAF

AFIT/GAE/ENY/03-11J

DEPARTMENT OF THE AIR FORCE
AIR UNIVERSITY

AIR FORCE INSTITUTE OF TECHNOLOGY

Wright-Patterson Air Force Base, Ohio

AFIT/GAE/ENY/03-11J

REDUCTION OF THERMAL RESIDUAL STRAINS IN ADHESIVELY BONDED COMPOSITE REPAIRS

THESIS

Presented to the Faculty

Department of Aeronautical and Astronautical Engineering

Graduate School of Engineering and Management

Air Force Institute of Technology

Air University

Air Education and Training Command

In Partial Fulfillment of the Requirements for the

Degree of Master of Science in Aeronautical Engineering

Heather R. Crooks, BS

First Lieutenant, USAF

June 2003

AFIT/GAE/ENY/03-11J

REDUCTION OF THERMAL RESIDUAL STRAINS IN ADHESIVELY BONDED COMPOSITE REPAIRS

Heather R. Crooks, BS
First Lieutenant, USAF

Approved:

Dr. Anthony N. Palazotto (Chairman)	June 16, 2003 date
Maj Richard G. Cobb (Member)	16 June 03 date
Dr. Theodore Nicholas (Member)	16 June 03 date

Acknowledgements

First and foremost, I would like to thank my thesis committee: Dr. Anthony Palazotto, Maj Richard Cobb, and Dr. Ted Nicholas. I am thankful for their guidance and support throughout this endeavor. I would also like to thank the other faculty members in the ENY department for their dedication to the students at AFIT.

I would like to thank the following people from AFRL/MLS for their expertise and assistance throughout my research efforts. Without these people, I would still be deciding on a topic. My team members Dr. Brett Bolan, Molly Brown, Kelly Feirstine, Capt Chris LaPietra, Jim Mazza, Dan McCray, Brian Milligan, Justin Rausch, Jeff Smith, and Lt David Tolk. My MLSC test and evaluation friends Jack Coate, Dayle Pearson, Steve Thompson, and Don Woleslagle. My NDI guys Lt Sandy Davis, Dan Laufersweiler, Ed Porter, and Noel Tracy. Also, I would like to thank Jay Fiebig of WR-ALC and Kees Guijt of the USAFA for their assistance.

Last, but certainly not least, I would like to thank my family and friends. Their unwavering support, and superb listening abilities, helped me out tremendously as I pursued this degree. Thanks to my parents and siblings. I would also like to thank my AFIT "peeps". I was lucky enough to break into the full-time student circle and become friends with a great group of people. You guys rock, even though you graduated before I did: Michael "Nugget" Giebner, Scott Bergren, Christine Ellering, Dave "Crash, Bitter Dave" Garay, Christopher Hamilton, James "Haney" Hanley, Greg "Gregarious Hibbiddy Dibbiddy" Hoffman, Russ

Magaziner, Matt “Paps, Princess” Papaphotis, AJ Rolling, Jennifer “Hey, Lady” Schwartz, and Ray “Buzz” Toth.

Table of Contents

Page

List of Figures

Page

Page

Page

Page

List of Tables

List of Symbols

$2a$ = total crack length

$2L_R$ = total patch length

$12/\beta$ = load transfer length on each side of the crack

α = degree of conversion, crosslinking

α_T = coefficient of thermal expansion

$^{\circ}C$ = degrees Celsius

ε = strain

E_p = elasticity modulus of the patch material

E_s = elasticity modulus of the aluminum

$^{\circ}F$ = degrees Fahrenheit

G_A = sheer modulus of adhesive between patch and aluminum

ΔH_{TOT} = total exothermic heat release

ΔH_{ISO} = total isothermal exothermic heat release

ΔH_{RES} = total residual exothermic heat release

J/g = Joules per gram

ΔK = stress intensity factor

P_{max} = max load

P_w = total patch width

S = stiffness ratio

ΔT = change in temperature

t_A = adhesive bondline thickness

T_C = crystallization temperature

T_g = glass transition temperature

t_p = thickness of the patch

T_m = melting temperature

t_{ply} = cured ply thickness of one ply of patch material

t_s = thickness of the aluminum

W/g = Watts per gram

Abstract

Many military and commercial aircraft are being called upon to fly well beyond their original intended service lives. This has forced the United States Air Force (USAF) to increasingly rely on structural repairs to address fatigue induced damage and to extend aircraft useful life. The focus of this research is the use of a high-strength composite patch technique to repair a fatigue crack on an aluminum aircraft structure. This study investigates the thermal residual strains that occur as a direct result of the coefficient of thermal expansion (CTE) mismatch between the repair patch and the underlying cracked metallic structure to which the patch is bonded. This research examines the response of a precracked, 24 inches x 6 inches x 0.125 inch, 7075-T6 aluminum panel repaired with a 15-ply graphite/epoxy patch. Two adhesives: EA 9696 and FM 73M were used with varying cure cycles. The hypothesis is that by reducing cure temperatures, the CTE mismatch will be less dramatic, thus yielding a more robust repair with a comparable fatigue crack growth rate. The research concluded that reducing the cure cycle temperature could decrease the thermal residual strains by as much as 26.5% between the graphite/epoxy composite patch and the aluminum structure when FM 73M adhesive is used to bond them together and 7.4% when EA 9696 is used. The research also concluded that a lower cure cycle temperature did not detrimentally affect the panels' fatigue crack growth rates.

REDUCTION OF THERMAL RESIDUAL STRAINS IN ADHESIVELY BONDED COMPOSITE REPAIRS

CHAPTER 1: INTRODUCTION

Aircraft repair methods have existed since *before* the first powered flight of the Wright Brothers in 1903.

> "By the afternoon of December 12, 1903, the machine was again ready. Orville Wright recorded in his diary that day:
>
> 'Got machine outside in afternoon with intention of making a trial…In starting one time the frames supporting the tail were caught on the end of the track and broken.'"
>
> The Wrights spent the morning of December 14th "making repairs to the damaged tail of the Flyer." Later that day, Wilbur made the first real trial of the Flyer with only partial success. The gravity-assisted (and thus unofficial) flight covered only 32 meters, and on landing, the front landing skids and part of the front rudder were broken. "Repairs to the damaged machine occupied the next couple of days," leading up to the historic first powered flight on December 17th [1].

Structural failures are as much a problem today as they were in 1903. A well-known airline accident, as the result of a structural failure, is Aloha Airlines' Flight 243 on April 28, 1988. At flight level (FL) 240 (24,000 feet), Flight 243 enroute from Hilo, Hawaii to Honolulu, Hawaii, experienced structural failure and rapid decompression. Approximately eighteen feet of structure aft of the cabin entrance door and above the floorline separated from the aircraft. Remarkably, the aircraft safely diverted to Maui, Hawaii. All passengers survived the mishap; however, one flight attendant was lost during the decompression. A picture of the damaged aircraft is shown in Figure 1.

Figure 1: Flight 243 After In-flight Structural Failure

The National Transportation and Safety Board (NTSB) investigation found that disbonding and fatigue damage led to the structural failure. As a result of this accident, two programs were put into place: the National Aging Aircraft Research Program, operated under the Federal Aviation Administration (FAA) and the Airframe Structural Integrity Program (ASIP), operated under the National Aeronautics and Space Administration (NASA) [2].

Structural problems do not solely plague commercial aircraft; the United States military also deals with aging aircraft issues including fatigue and corrosion cracking. In 1993, a widespread fatigue cracking problem on the C-141 aircraft was identified in the inner wing, lower surface weep holes. Warner-Robins Air Logistics Center's (WR-ALC) Technical and Engineering Sciences Division, aided by the Air Force Research Laboratory Materials and Manufacturing Directorate's Systems Support Division, designed, tested, and installed bonded composite repairs to mitigate fatigue cracking in the aforementioned area. The

repair effort began in September 1993 and was completed in December 1994 with a total of 243 aircraft repaired and returned to service [3].

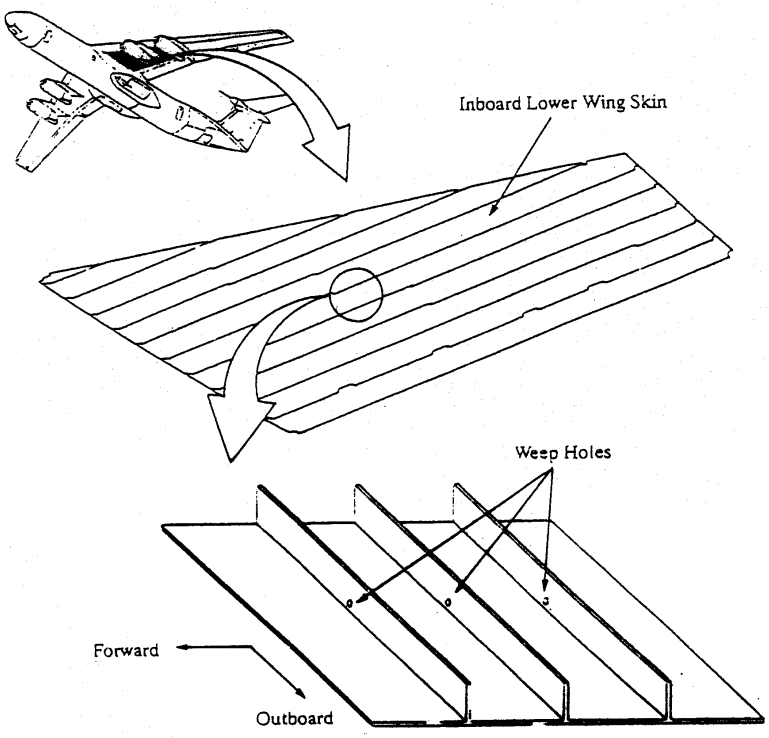

Figure 2: C-141 Weep Hole Location [3]

Fatigue cracking also plagued the F-16 aircraft near the fuel vent hole. Some F-16 aircraft developed cracks between 2,500 and 3,500 flight hours, forward and aft of the fuel vent hole in the lower left wing skin, 0.2 inch thick [4]. A pictorial representation of this is shown in Figure 3.

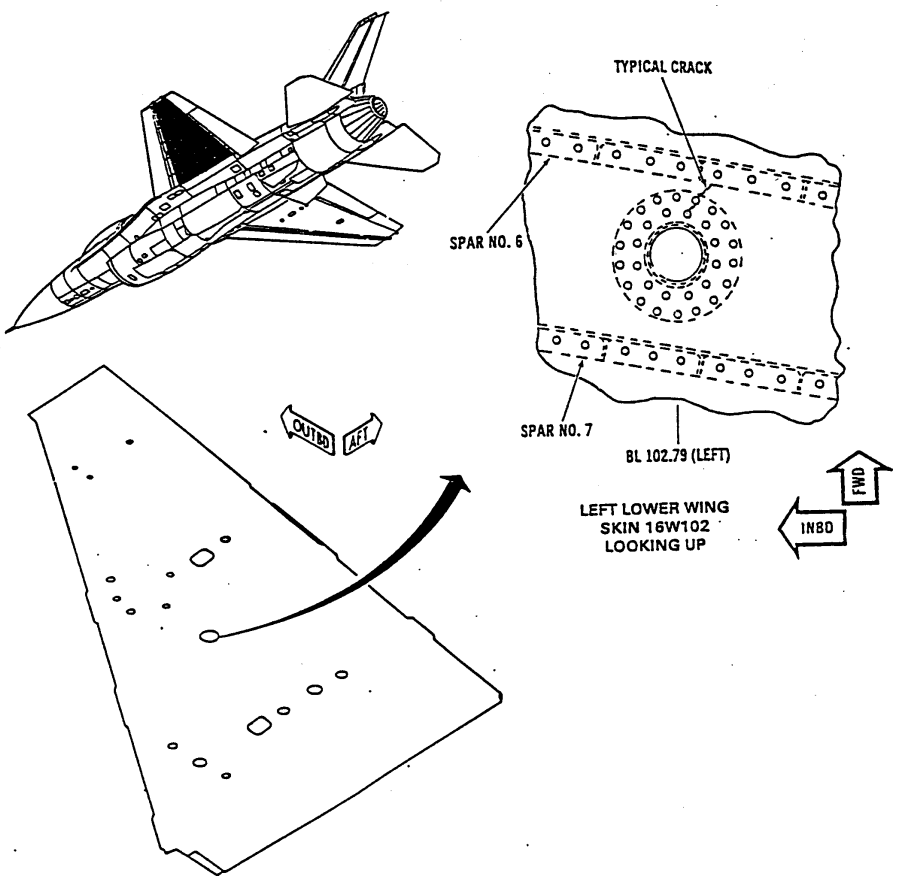

Figure 3: Typical Crack Location on the F-16 Near the Fuel Vent Hole [4].

In both cases, the crack growth was arrested by the use of a composite patch bonded over the damaged area, which will be discussed in section 1.2.1.

1.1 Aging Aircraft

Service Life Extension Programs are becoming more prevalent as aircraft are being utilized beyond their original design and service lives [5]. This situation is no more widespread than for the United States Air Force (USAF), whose own repair and maintenance goals require

increased combat capability through extended structural service lives, while reducing manpower requirements and decreasing costs through simplified repairs and reduced downtime [6].

The USAF aircraft inventory is rapidly aging as seen in Table 1.

Table 1: Aging USAF Aircraft Inventory [7]

Aircraft	Date Deployed	Age
A-10	1976	27
B-52	1955	48
C-141A	1964	39
C-5A	1969	34
E-3	1977	26
F-15	1972	31
F-16	1979	24
F-117	1982	21
KC-135	1956	47
T-37	1956	47
T-38	1959	44

The oldest aircraft in service, the B-52, is forty-eight years old, and the Air Force plans on extending its life another fifty years. The current fighter/bomber trainers are averaging forty-six years in service, while the Air Force tanker and cargo fleets are both near forty plus years of service.

1.2 Addressing Aging Aircraft Issues

There are two primary means of repairing metal fatigue and corrosion cracking on aging aircraft: bonded repairs and mechanically fastened repairs. Both types of repairs have their strengths and weaknesses, as described below.

1.2.1 Bonded Repairs

A technique known as "crack patching" was pioneered in the early 1970's at the Aeronautical Research Laboratory (ARL) in Australia. This method bonds a composite patch over the cracked structure to repair fatigue and stress corrosion cracking in metallic aircraft structures [6]. This practice has the advantage of attaining high structural efficiency and durability. An example of a composite repair is the use of graphite/epoxy composite doublers installed on the vertical stabilizers of F-15's to stiffen the boron/epoxy composite structure and reduce flutter during flight. One of these repairs is shown below in Figure 4.

Figure 4: F-15 Vertical Repair

Disadvantages of composite patches include the use of expensive materials with limited shelf-lives (at room temperature) and specialized storage requirements, ensuring sufficient surface preparation of the bonding surfaces, and the introduction of thermal strains due to curing the adhesive at an elevated temperature. Because of the coefficient of thermal expansion (CTE) mismatch between the metal structure and the repair material, tensile strains are introduced into the aircraft metallic component, thus opening the crack. This occurs during the cool-down phase of the cure cycle that bonds the patch to the structure. These strains are on the order of 1,000 με, which yields a tensile stress of 1,000 psi on 7075-T6 aluminum. Because of this, the strains affect the lifetime of the repaired structure. This will be further discussed in section 1.3.

1.2.2 Mechanically Fastened Repairs

Another method of repair is mechanical fastening, which utilizes metallic reinforcements with bolts or rivets. This type of repair is best known and most widely used in the USAF maintenance community; it is meant to restore strength and can be accomplished easily and inexpensively. This approach is ideal for Aircraft Battle Damage Repair (ABDR) purposes when the aircraft needs the absolute shortest turn-around time, for example, during wartime conditions. The materials for this type of repair offer advantages since they are easy to find, inexpensive, have no shelf-life limitations, and are easy to store. On the other hand, disadvantages of mechanically fastened repairs include: more damage to the aircraft in the form of drilled holes for bolts and rivets, thus adding stress concentrations, as well as the possibility of damage to underlying structures, components [8], and fuel areas; improperly machined holes; loss of corrosion protection systems; and potential load redistribution [9].

1.3 Thermal Strains

This section describes how thermal strains are introduced into a bonded repair. Refer to Figure 5 below for a better understanding.

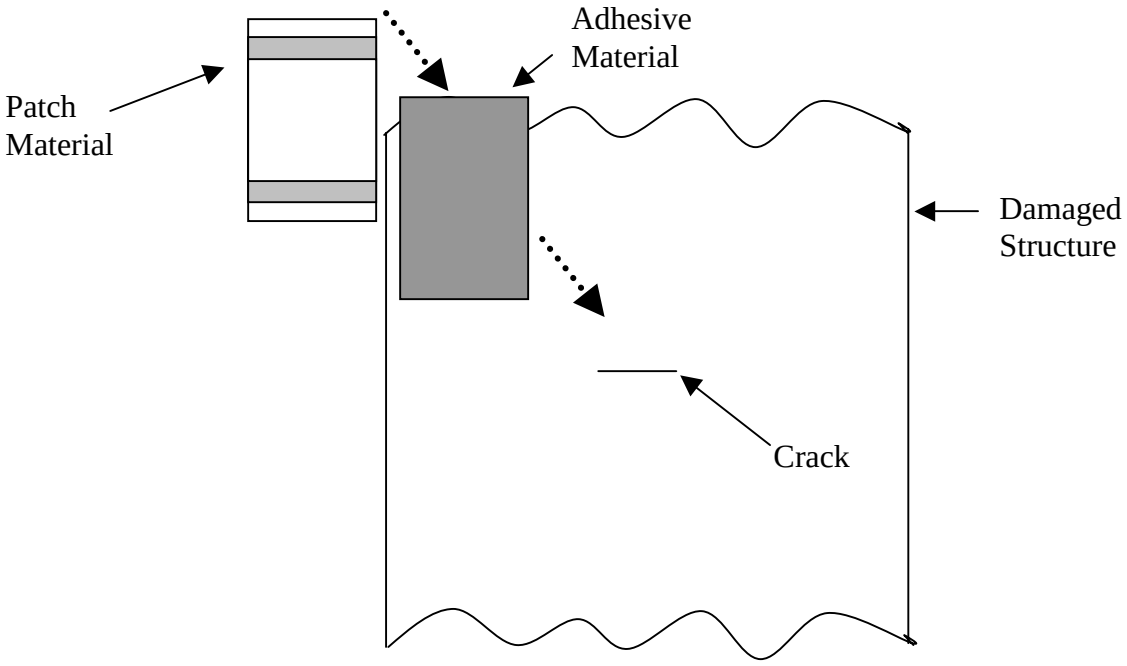

Figure 5: Bonded Repair Schematic

Each repair consists of a cracked structure, an adhesive material, and a patch material. This research used 7075-T6 aluminum and a graphite/epoxy patch. As mentioned previously, the thermal strains are introduced during the cure cycle, and in particular, the cool-down phase. During the heat-up phase, both materials are allowed to expand or contract freely because the adhesive has not yet cured and locked in its structure. When the adhesive is sufficiently cured, the three-dimensional molecular crosslinked structure limits its ability to

viscoelastically respond to stress [10]. When the repair has been cooled to ambient temperature, the CTE mismatch becomes clearly visible. This is the result of the aluminum structure having a positive CTE and the graphite patch having a negative CTE; therefore, the patch will expand when cooled, while the structure will contract. This causes the structure to be in tension, which is detrimental because this will open the crack on the structure [11]. In a study conducted by Cho and Sun [12], thermal residual strains were significantly reduced when a two-step bonding cycle was used. Also, the reduction of thermal residual stresses improved the fatigue performance in the given repair.

1.4 Thesis Objective

The objective of this research is to evaluate a methodology to reduce thermal residual strains in bonded repairs. The hypothesis is that a reduction in cure cycle temperature will yield a reduction in thermal residual strains [12]. This thesis will experimentally test this hypothesis. This section briefly outlines the testing materials and procedures followed in this research.

The thermal residual strains are present because of the CTE mismatch between the aluminum and the graphite patch material. The aluminum used in this research, 7075-T6, has a CTE of $23*10^{-6}$/°C [13]. Since the CTE is positive, the aluminum will expand when heated and contract when cooled. The patch material, graphite/epoxy, has a CTE of $-0.38*10^{-6}$/°C [14]. This negative CTE will cause the material to contract when heated and expand when cooled. At the conclusion of the patch bonding process when the materials have been cooled to room temperature, the aluminum is contracting, while the patch is

expanding. This causes tensile strains on the aluminum, also known as thermal residual strains.

The test specimens used in this research were of the Middle-Tension geometry and were machined from a 7075-T6 aluminum sheet nominally 0.125 inch in thickness to 24 inch by 6 inch panels. The specimens had a one-inch notch machined into the center of the panel. The panels were subsequently precracked to achieve a total crack length of approximately two inches. Each panel was patched on both sides (to mitigate out-of-plane bending) with a graphite/epoxy unidirectional patch. There were a total of eight strain gauges per specimen: two far-field strain gauges, two gauges under each patch, and one gauge on top of each patch. These gauges were used to determine the thermal strains throughout the patch bonding process. The thermal strains of interest are the residual strains that occur during the cool-down phase of the cure cycle.

Two types of adhesives were used in this research: Hysol EA 9696 from Henkel Loctite and FM 73M from Cytec Engineering Materials, Inc. The manufacturers' suggested cure cycles were used as a control in each case. To research the hypothesis that a lower cure temperature would reduce thermal residual strains, modified cure cycles were determined based upon Differential Scanning Calorimetry performed on each adhesive. Two modified cure cycles were researched for EA 9696, and one modified cure cycle was researched for FM 73M. There were a total of three panels per cure cycle for each adhesive. The 0° direction for the panel, patches, and strain gauges is shown in Figure 6.

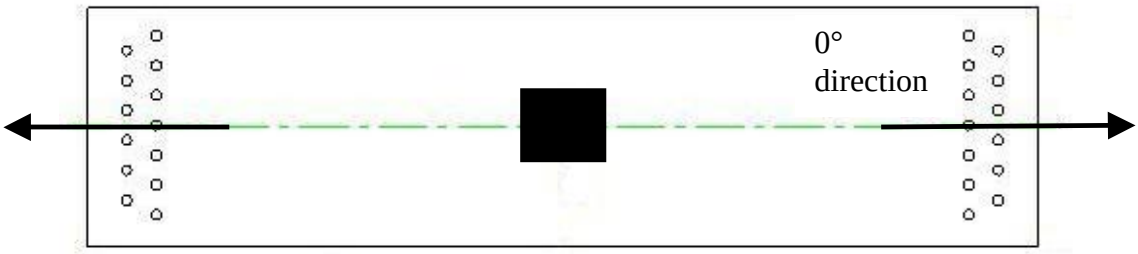

Figure 6: 0° Direction for Panel, Patches, and Strain Gauges

After the strain readings were taken, one panel from each test group was fatigue crack growth rate tested at room temperature to determine if the modified cure cycles yielded a repair with an improved (reduced) fatigue crack growth rate to that of the manufacturers' suggested cure cycle.

1.5 Chapter Summary

This chapter introduced aging aircraft and the need to repair these aircraft. Both mechanically fastened repairs and bonded repairs were discussed, as was the introduction of thermal residual strains when bonded repairs for used. The thesis objective was also outlined in this chapter.

CHAPTER 2: MATERIALS and ADHESIVE CYCLE DESIGN

For this research, the following types of materials and processes were selected: two adhesives, a patch material, a metallic structure material, and a surface preparation for the specimen. A graphite/epoxy patch material (FiberCote T700/E765 prepreg material) was chosen, as was 7075-T6 aluminum. 7075-T6 aluminum has the highest strength of aluminums with acceptable toughness and is used for strength critical structures such as fuselage floor beams, stabilizers, spar caps in control surfaces, and upper wing skins [15].

2.1 Surface Preparation

A grit-blast/sol-gel process with a waterborne corrosion inhibiting adhesive primer (CIAP), Cytec BR® 6747-1, was the surface preparation of choice for this research. Laboratory testing under optimal conditions on aluminum structures has shown sol-gel processes meet or exceed current surface preparation Technical Order (T.O.) callouts, are much easier to use, and are more environmentally friendly [16].

Some aircraft repair manuals and T.O.'s require techniques that use hazardous acids and complex processing steps. These techniques include tank-line phosphoric acid anodize (PAA), manual PAA, HF/Alodine, or acid paste etches to repair aluminum alloy structures. To alleviate some of these hazards, WR-ALC utilizes a grit-blast/silane surface preparation

for aircraft repairs. The sol-gel process is similar to the silane process; however, it has a more reactive chemistry that leads to several advantages including reduced surface preparation time.

Sol-gel surface preparation is used to molecularly bond the metallic structure to the adhesive primer as seen in Figure 7. The following is an excerpt explaining the sol-gel process and how it works.

> The sol-gel surface preparation process works by producing a gradient interphase coating. One side is molecularly bonded to the oxide structure on the metal and the other side is molecularly crosslinked with the adhesive primer, Figure 7. The type of bonding at the metal interface determines the long-term durability of the system. For high performance, durable bonding, the metal alloy surface has to be scrupulously clean and have an active metal oxide surface chemistry. Contamination on the surface can reduce the number of surface reactive sites, and subsequently reduce the surface density of bonds with the sol-gel coating. This will reduce the ultimate durability of the system.

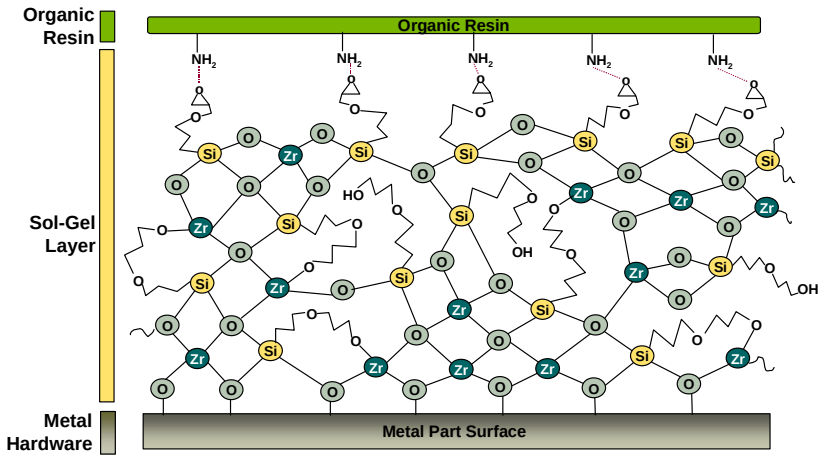

Figure 7: Notional Schematic of Sol-gel Adhesion Promoting Coating on a Metal Part [17]

2.2 Patch Design Process

The patches used in this research were designed using the *Composite Repair of Aircraft Structures (CRAS) Design Manual* [18]. This manual reports the general guidelines for bonded patches that are provided in RAAF-ENG-STD-C5033 [19] as follows.

- The patch should not have an elastic modulus less than the material being patched.
- Bonded patches should match the surface profile to which they are bonded such that the adhesive film conforms within a tolerance of ± 0.002 inches on the nominal adhesive thickness during application of normal bonding pressure.
- Composite patches are to maximize strength by use of fiber dominated lay-ups. Lay-up configurations in which the laminate strength is limited by the strength of the resin system are not desirable.

2.2.1 Stiffness

The stiffness ratio, *S*, is defined in Equation 1 as the ratio of the stiffness of the repair material to the stiffness of the original structure prior to damage.

$$S = \frac{E_p t_p}{E_s t_s} \quad (1),$$

where E_p is the Young's modulus of the patch, E_s is the Young's modulus of the aluminum structure, t_p is the thickness of the patch, and t_s is the thickness of the aluminum structure.

Since the repair should return the structure to its original strength, S should always be greater than 1. The CRAS manual suggests $1.0 \leq S \leq 1.6$; for this research, an S of 1.2 will be used. From the stiffness ratio, the patch thickness is determined as outlined in section 2.2.2.

2.2.2 Patch Thickness and Number of Plies

The next step is to determine the required thickness of the patch and, subsequently, the number of plies needed.

Rearranging Equation (1)

$$t_p = S\left(\frac{E_s t_s}{E_p}\right) \qquad (2),$$

where

S = 1.2 (chosen value)

E_s = 10E6 psi (for aluminum 7075-T6) [13]

t_s = 0.125 inch (chosen thickness of cracked aluminum panel for this study)

E_p = 18.71E6 psi (of composite patch) [20].

Solving for t_p,

$$t_p = 1.2\left[\frac{(10E6)(0.125)}{18.71E6}\right] = 0.08inch \quad (3).$$

This means that the entire patch must be at least 0.08 inch thick. The cured ply thickness, t_{ply}, for one ply of the T700/E765 composite patch material is 0.0056 inch. Dividing this into the patch thickness, the result is 14.2 plies.

$$\frac{0.08inch}{0.0056inch} = 14.2 \quad (4).$$

Rounding this up to 15, a patch thickness of

$$t_p = 15\ [plies] * 0.0056\ \frac{[inch]}{[ply]} = 0.084 \text{ inch} \quad (5)$$

is obtained. Now, the stiffness ratio must be recalculated. The above values are inserted into Equation (1),

$$S = \frac{(18.71E6)(0.084)}{(10E6)(0.125)} = 1.26 \quad (6).$$

The final values for the patch design are as follows:

$S = 1.26$

$t_p = 0.084$ inch

15 plies (7)

2.2.2.1 Patch Width (For Use With Both Adhesives)

The CRAS manual states that the minimum patch width must be at least twice the crack length, where crack length is defined as *2a*, and overlap the crack length by at least one inch. Following these guidelines has been found to reduce the stress near the crack tip. Therefore, to minimize or stop crack growth, a patch width of

$$P_W > (2a + 1) \quad (8) \text{ and}$$

$$P_W \leq PatchLength \quad (9)$$

must be obtained, where *2a = crack length* (a=one inch in this study), is required. In this case, $P_w > 3$ *inches;* therefore, the patch width was set to four inches.

2.2.2.2 Patch Length

The patch length was found by studying the adhesive shear stress developed in the bond. To determine the overall patch length, two other calculations were made: the values of the load transfer length and the taper length. WR-ALC/TIEDD [21] suggests the load transfer length should be double the length suggested by Baker [6] ($12/\beta$ rather than $6/\beta$, where $12/\beta$ = load transfer length on each side of the crack). Total overall patch length is defined as $2L_R$, where L_R = half length of patch:

$$2L_R = 2\left(\frac{12}{\beta}\right) + 2(taper - length) \quad (10).$$

The value of β is determined as follows:

$$\beta^2 = \frac{G_A}{t_A}\left(\frac{1}{E_s t_s} + \frac{1}{E_p t_p}\right) \quad (11),$$

where G_A = shear modulus of the adhesive between the patch and the aluminum and t_A = adhesive bondline thickness.

2.2.2.2.1 Patch Length for Use With EA 9696 Adhesive

For EA 9696, the following calculations apply:

$$\beta^2 = \frac{10^5}{0.006}\left(\frac{1}{10E6 * 0.125} + \frac{1}{18.71E6 * 0.084}\right) = 1.44E2 \quad (12)$$

$$\beta = 12\ in^{-1} \quad (13).$$

Because the patch is arranged in a wedding cake fashion, there must be a taper length between respective plies. The taper length is determined by the number of plies (minus one) and the thickness of the plies, as well as a drop off ratio, which is set to 10:1 as suggested by WR-ALC. Therefore,

$$taper\ length = 14*0.0056*10 = 0.784\ inch \quad (14).$$

This leads to an overall patch length calculation:

$$2L_R = 2\left(\frac{12}{12}\right) + 2(0.784) = 3.57 inches \quad (15).$$

The value was rounded up to 4.0 inches, such that the width was not larger than the length, to yield the following patch length dimensions:

$$\begin{array}{|c|}\hline \beta = 12\ in^{-1} \\ taper\ length = 0.784\ inch \\ total\ patch\ length = 4\ inches \\ \hline \end{array} \quad (16)$$

The following table depicts the entire patch design to be used with EA 9696 film adhesive (all widths = 4.0 inches):

Table 2: EA 9696 Patch Ply Dimensions

Ply #	Length [in]
1	4.0
2	3.89
3	3.78
4	3.66
5	3.55
6	3.44
7	3.33
8	3.22
9	3.10
10	2.99
11	2.88
12	2.77
13	2.66
14	2.54
15	2.43

Complete patch orientation for EA 9696 is shown in Figure 8.

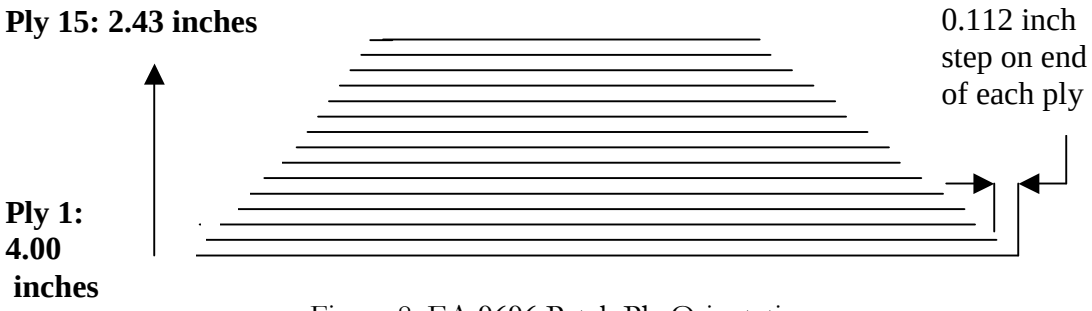

Figure 8: EA 9696 Patch Ply Orientation

2.2.2.2.2 Patch Length for use with FM 73M Adhesive

The β, taper length, and patch length for FM 73M are determined as follows:

$$\beta^2 = \frac{1.2E5}{0.005}\left(\frac{1}{10E6*0.125}+\frac{1}{18.71E6*0.084}\right)=34.5 \quad (17)$$

$$\beta = 5.87\ in^{-1} \quad (18)$$

$$taper\ length = 14*0.0056*10 = 0.784\ inch \quad (19)$$

$$2L_R = 2\left(\frac{12}{5.87}\right)+2(0.784)=5.66 inches \quad (20).$$

$$\boxed{\begin{array}{c}\beta = 5.87\ in^{-1}\\ taper\ length = 0.784\ inches\\ total\ patch\ length = 5.66\ inches\end{array}} \quad (21)$$

The following table depicts the entire patch design to be used with FM 73M film adhesive (all widths = 4.0 inches):

Table 3: FM 73M Patch Ply Dimensions

Ply #	Length [in]
1	5.66
2	5.55
3	5.44
4	5.32
5	5.21
6	5.10
7	4.99
8	4.88
9	4.76
10	4.65
11	4.54
12	4.43
13	4.32
14	4.20
15	4.09

Complete patch orientation for FM 73M is shown in Figure 9.

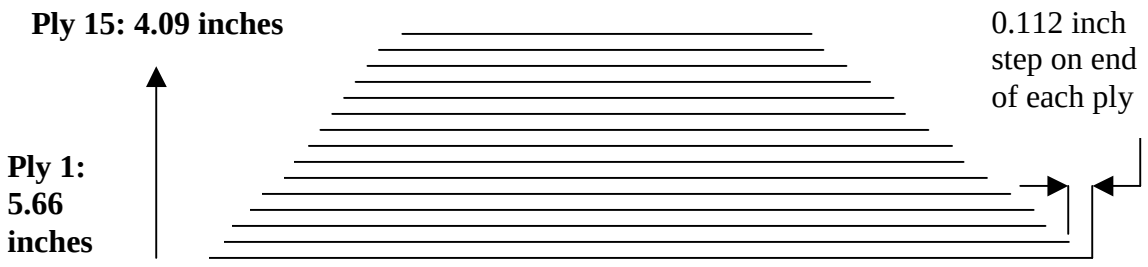

Figure 9: FM 73M Patch Ply Orientation

2.3 Adhesive Cycle Design

The two adhesives used in this study, EA 9696 and FM 73M, are modified epoxy film adhesives. EA 9696 is an adhesive designed for applications requiring both high toughness and service temperatures to 250°F/121°C [22]. EA 9696 exhibits a high retention of strength under vacuum, which is the preferred in-field-repair pressure application method.

FM 73M, manufactured by Cytec, is a toughened, general-purpose aerospace epoxy designed to provide excellent structural performance from -67°F to 180°F (-55°C to 82°C). FM 73M is formulated to provide outstanding durability in bonding metals and is also suitable for bonding many structural composite systems [23].

2.3.1 Manufacturers' Suggested Cure Cycles

The first cure cycles investigated were the manufacturers' suggested cure cycles. For both EA 9696 and FM 73M, the suggested cycle was to ramp the temperature at 5˚ per minute to 250˚F and then hold at 250˚F for one hour under full vacuum. In this research, full vacuum is defined as 29 inches Hg.

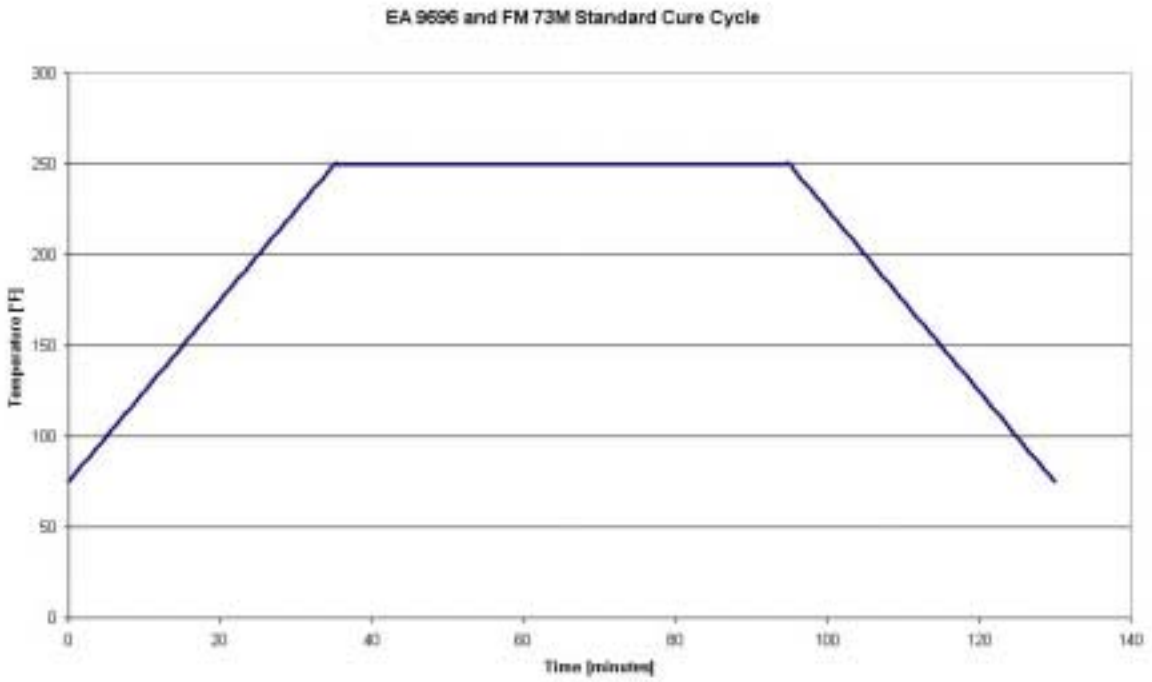

Figure 10: EA 9696 and FM 73M 250°F Cure

2.3.2 Differential Scanning Calorimetry (DSC)

DSC was the method used to determine the modified cure cycles. DSC is used to study the thermal transitions of materials, in this case, the adhesives. The thermal transition of importance in this research is the glass transition temperature, T_g, as well as the exothermic heat release of the adhesive system, which are discussed later in this section. The glass transition temperature is important because it is a useful quantity characterizing the progression of cure in thermosets [13]. By definition, T_g is the temperature of the intersection of the expansion curves of the glassy and rubbery states, and it appears as an endothermic shift over the glass transition interval in the DSC scan [10]. Note that T_g is a material property for a certain cure temperature. As the cure temperature changes, the T_g changes, as well. This change in T_g is due to material properties and the amount of cross-linking in the system. The closer the T_g of the modified cure cycle is to the T_g of the

standard cure cycle, the more cross-linking (α) is present. Cross-linking is discussed further in section 2.3.2.2.

The DSC description in Figure 11 demonstrates the need for two pans; one pan holds the adhesive sample, while the other is the reference pan. Both pans sit atop a heater that is controlled by a computer. The computer heats the two pans at a specific rate, making sure that one pan heats at the same rate as the other. DSC measures the difference of the heat flow between the two pans.

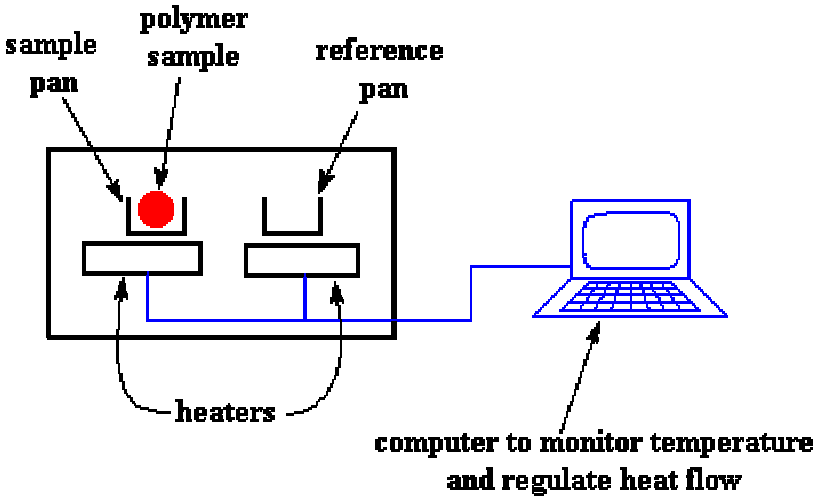

Figure 11: DSC Description [24]

The glass transition temperature T_g, the crystallization temperature T_c, and the melting point T_m can be determined by making a plot of heat flow versus temperature. One depiction of this type of graph is shown below. The only temperature transition this research is interested in is the glass transition temperature, T_g.

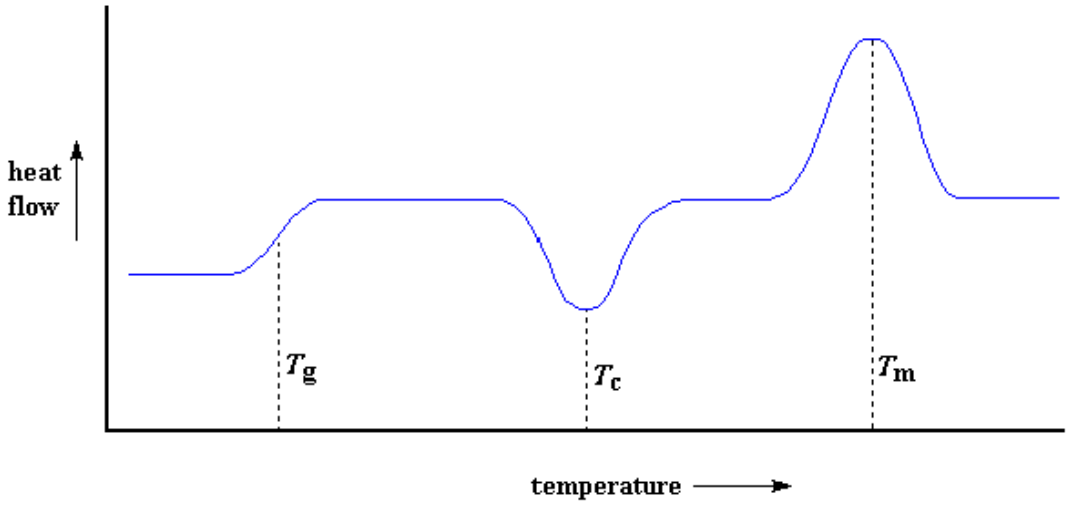

Figure 12: Figure Depicting T_g, T_c, and T_m [24]

2.3.2.1 Baseline Testing

Baseline testing is conducted to determine the total exothermic heat release of the adhesive system. An exothermic heat release is the amount of heat produced by the chemical reactions that occur in the adhesive during a given cure cycle. This value is important, as it is key in determining the extent of cure in an adhesive system. An adhesive system is considered to be fully cured when it no longer exhibits an exothermic heat release [10]. This is investigated further in section 2.3.2.2.

Baseline testing begins by placing approximately 10mg of adhesive into the sample pan and heating to 300°C at 10°C per minute. Throughout this test, temperature, time, and heat flow data are recorded. From these baseline data, the total exothermic heat release (H_{Total}) of the system is determined [10].

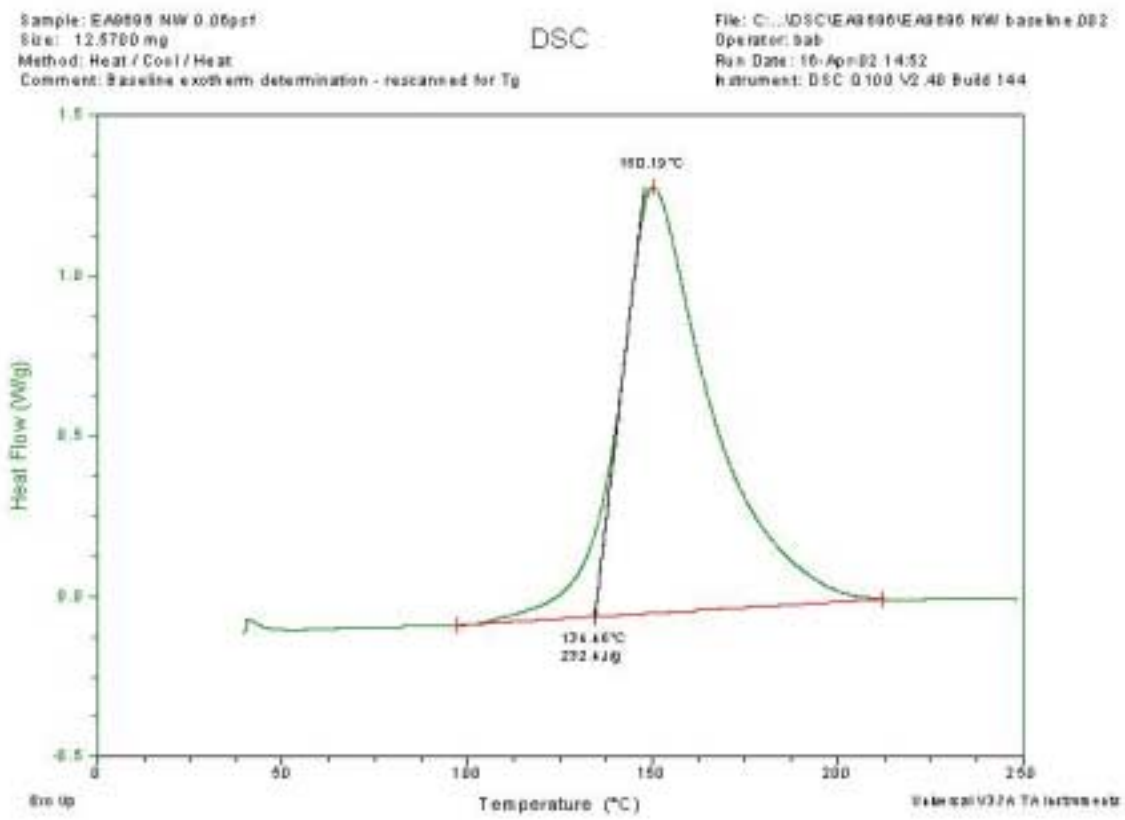

Figure 13: EA 9696 Baseline Exothermic Heat Release Determination

Figure 13 shows the heat flow of the adhesive system (measured in Watts per gram, W/g, of material) versus temperature in degree Celsius. The total exothermic heat release (measured in Joules per gram, J/g, of material) is determined by integrating the area under the curve and above the red line. As shown in Figure 13, the total exothermic heat release for EA 9696 is 232.4 J/g. Figure 14 shows the total exothermic heat release for FM 73M as 196.2 J/g. The variation in total exothermic heat release between the two adhesives is expected, as this is a function of material properties.

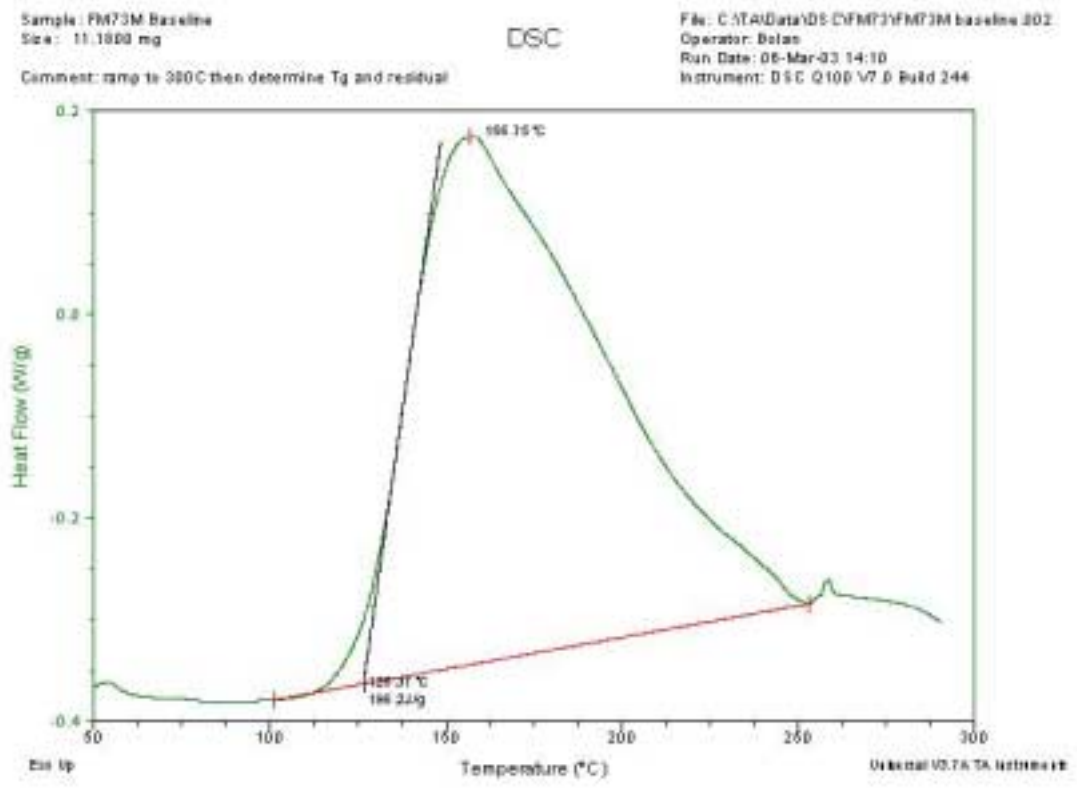

Figure 14: FM 73M Baseline Exothermic Heat Release Determination

2.3.2.2 Modified Cure Cycle Time Determination

Modified cure cycle temperatures were chosen (based on previous research conducted by AFRL/MLSA) at 220°F and 200°F for EA 9696 and 200°F for FM 73M. Once modified cure cycle temperatures were chosen, the time for those modified cure cycles was determined. To do this, 10mg of the adhesive were once again placed into the sample pan. The sample was then tested at the lower temperature for a longer period of time than one hour (the manufacturers' suggested curing time for 250°F). For example, for the EA 9696 200°F cure, the DSC test was conducted for 12 hours.

The information gained from this portion of the DSC test was the amount of isothermal exothermic heat release ($\Delta H_{isothermal}$). The isothermal exothermic heat release is defined as the amount of exothermic heat release for the given adhesive system when held isothermally at a selected temperature [10]. The test also reveals the time it takes for the adhesive system to be completely cured. An adhesive system is considered to be completely cured when there is no more exothermic heat release at the given temperature [10]. The data shown in Figure 15 indicate the adhesive system is completely cured for 200°F at 300 minutes and that the isothermal exothermic heat release is 160.8 J/g.

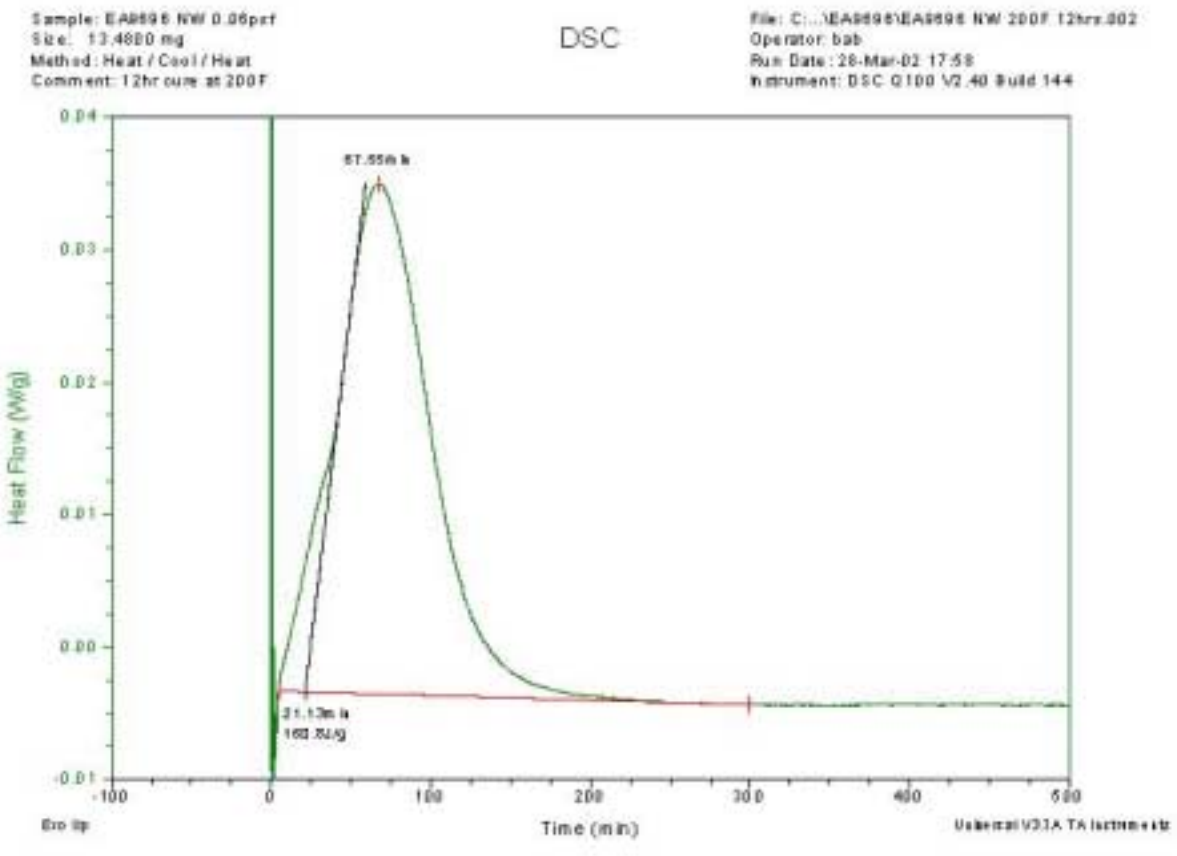

Figure 15: Isothermal Hold at 200°F for EA 9696

The next step was to continue the test by raising the temperature to 300°C. This process yielded the T_g and the residual exothermic heat release ($\Delta H_{residual}$) of the system. The residual exothermic heat release is defined as the remaining exothermic heat release when an uncured material is taken to complete cure. This value is independent of temperature for a particular thermosetting resin [10]. The residual exothermic heat release and T_g graph is important, as it shows the degree of conversion (α), or crosslinking, for the system:

$$\alpha = 1 - \left(\frac{\Delta H_{\mathrm{Re}\,sidual}}{\Delta H_{Total}} \right) \qquad (22).$$

The residual exothermic heat release and T_g determination test results are shown below. Figures 16-18 represent EA 9696 cure cycles; Figures 22-23 represent FM 73M cure cycles.

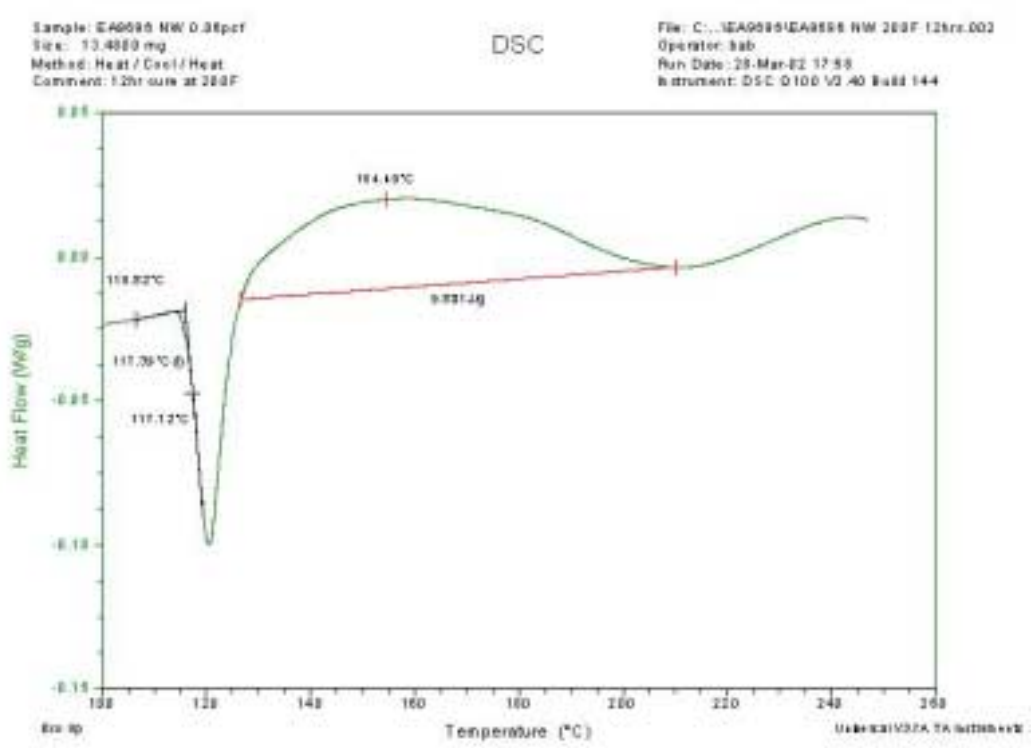

Figure 16: T_g and Residual Exothermic Heat Release Determination for EA 9696 200°F Cure

Figure 16 shows a residual exothermic heat release of 9.801 J/g and a T_g of 117.39°C (243.3°F). The decrease in T_g from the 250°F cure cycle is expected because there is less cross-linking in the adhesive system when cured at a lower temperature. When EA 9696 is cured at 200°F, it yields an eight hour cure cycle and a 95.8% degree of conversion as seen in Equation 23:

$$\alpha = 1 - \left(\frac{9.801}{232.4} \right) = 0.9578 = 95.8\% \qquad (23).$$

This value means that the adhesive system is 95.8% cured; therefore, the selected times and temperatures are acceptable. Figures 17 and 18 show the isothermal hold and residual exothermic heat release graphs for EA 9696 when cured at 220°F.

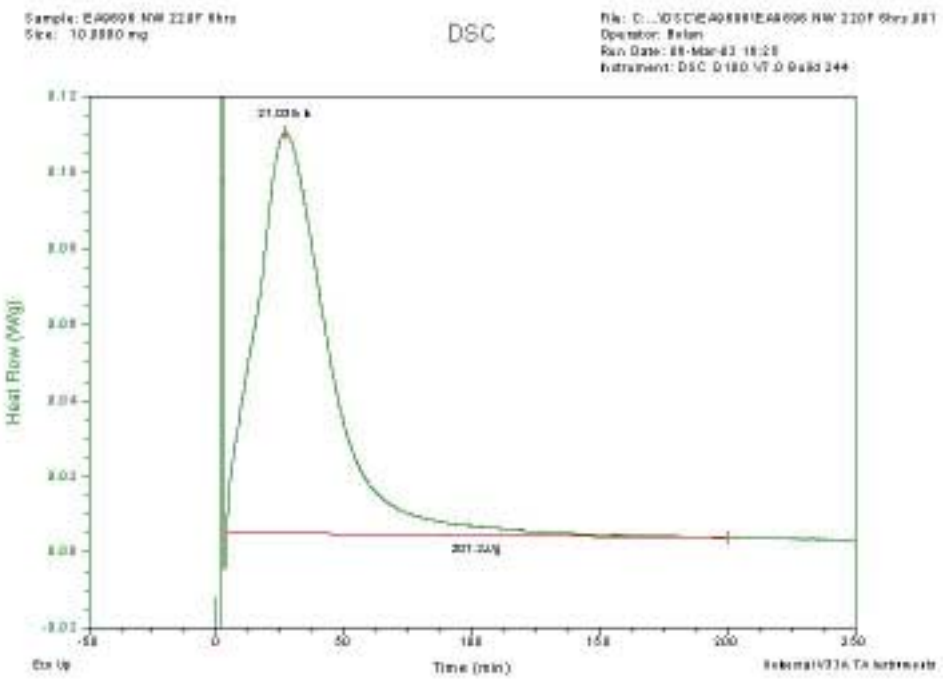

Figure 17: Isothermal Hold for EA 9696 220°F Cure

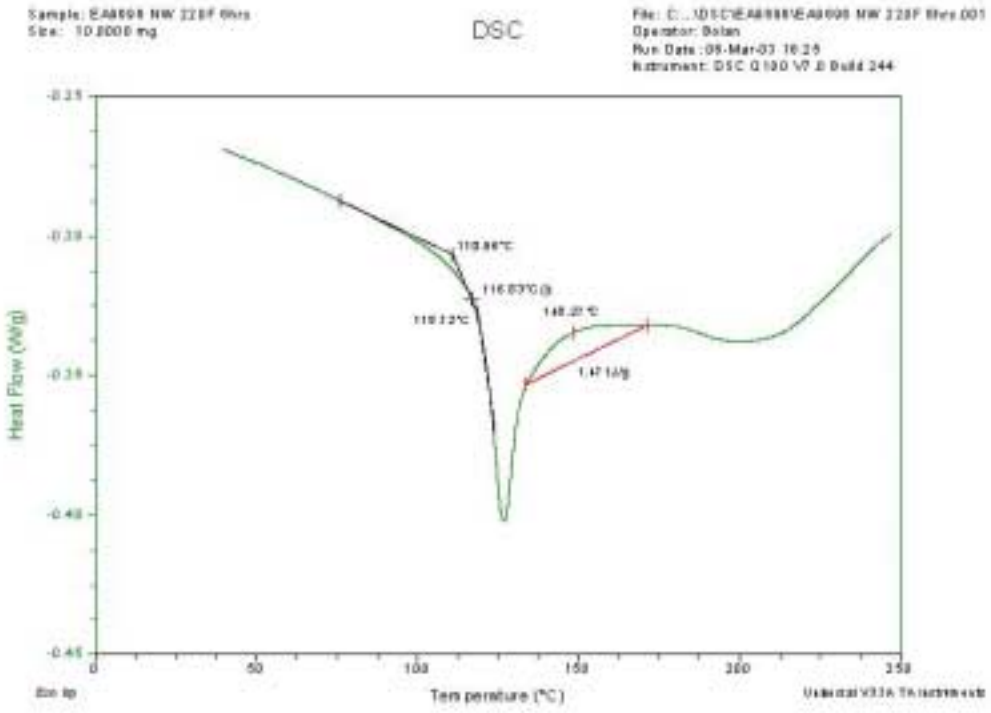

Figure 18: T_g and Residual Exothermic Heat Release Determination for EA 9696 220°F Cure

From the figures above, the isothermal exothermic heat release is 207.2 J/g and the residual exothermic heat release is 1.471 J/g. The decrease in T_g from the 250°F cure cycle is expected because there is less cross-linking in the adhesive system when cured at a lower temperature. This yields a four hour cure cycle and a 99.4% degree of conversion as shown in Equation 24:

$$\alpha = 1 - \left(\frac{1.471}{232.4} \right) = 0.9937 = 99.4\% \qquad (24).$$

For the EA 9696 220°F Cure, the degree of conversion yields an acceptable cure cycle. Figures 19 and 20 show the isothermal and residual exothermic heat releases for FM 73M at 200°F cure.

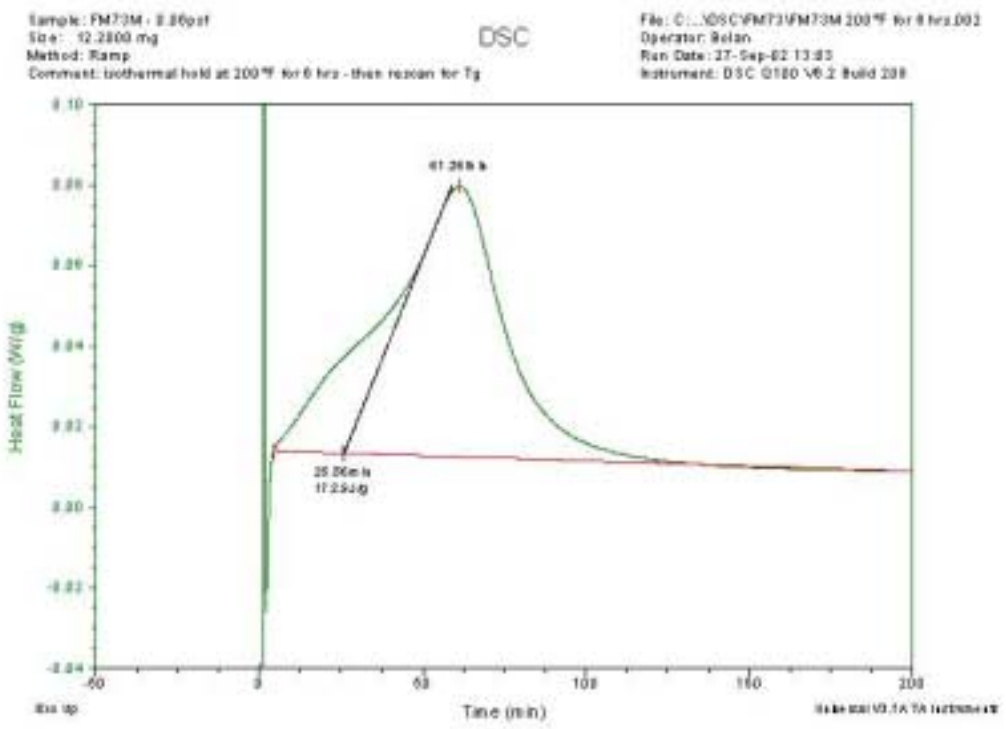

Figure 19: Isothermal Hold for FM 73M at 200°F Cure

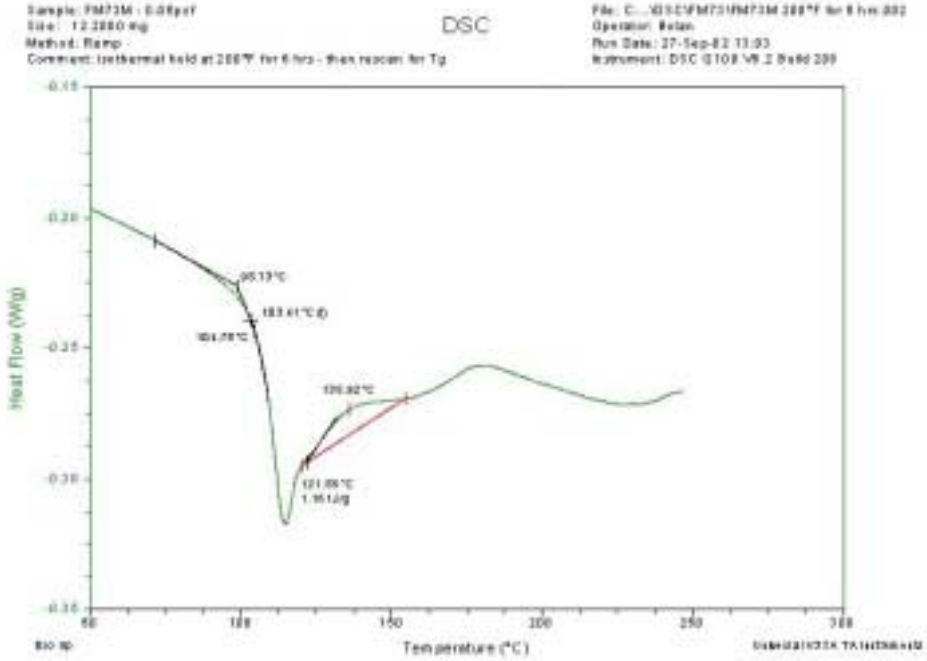

Figure 20: T_g and Residual Exothermic Heat Release Determination for FM 73M at 200°F Cure

The graphs above yield an isothermal and residual exothermic heat release of 172.9 J/g and 1.161 J/g, respectively. This gives an α of 99.4%, as shown in Equation 25.

$$\alpha = 1 - \left(\frac{1.161}{196.2} \right) = 0.9941 = 99.4\% \quad (25).$$

Table 4 below shows the cure systems and their respective DSC results. All three modified cure cycles had an $\alpha > 95\%$; therefore, all selected cure cycles were acceptable. Notice the change in T_g between cure cycles. EA 9696 showed a decrease in T_g when a lower cure temperature was used, while FM 73M showed an increase in T_g. This difference is due to the different material properties within the two cure systems, which is proprietary information belonging to the respective adhesive companies.

Table 4: DSC Results

	EA 9696	**FM 73M**
Baseline Exothermic Heat Release	232.4 J/g	196.2 J/g
Standard Cure T_g	252°F [22]	203°F [12]
Isothermal Exothermic Heat Release 220°F Cure	207.2 J/g	-
Isothermal Exothermic Heat Release 200°F Cure	160.8 J/g	172.9 J/g
Residual Exothermic Heat Release 220°F Cure	1.471 J/g	-
Residual Exothermic Heat Release 200°F Cure	9.801 J/g	1.161 J/g
T_g 220°F Cure	242.3°F	-
T_g 200°F Cure	243.3°F	218.1°F
α 220°F Cure	99.4%	-
α 200°F Cure	95.8%	99.4%

2.3.3 Modified Cure Cycles #1 and #2

The second and third cure cycles investigated were modified from the manufacturers' suggested cycle. Therefore, these cure cycles were modified to run at a lower temperature and for a longer time.

The modified cure cycles for EA 9696 are as follows:

1. Ramp the temperature at 5˚ per minute to 200˚F; hold at 200˚F for eight hours under full vacuum.

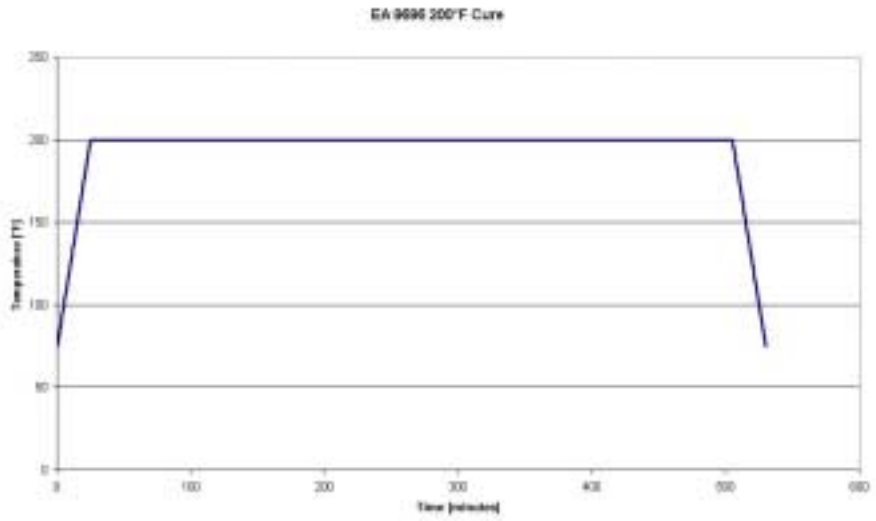

Figure 21: EA 9696 200°F Cure

2. Ramp the temperature at 5˚ per minute to 220˚F; hold at 220˚F for four hours under full vacuum.

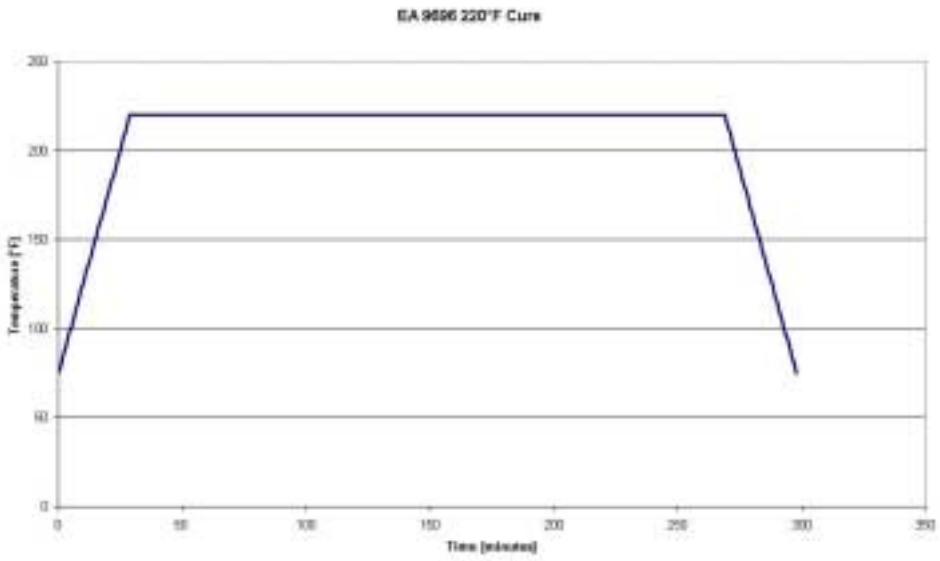

Figure 22: EA 9696 220°F Cure

The modified cure cycle for FM 73M is as follows:

1. Ramp the temperature at 5˚ per minute to 200˚F; hold at 200˚F for four hours under full vacuum.

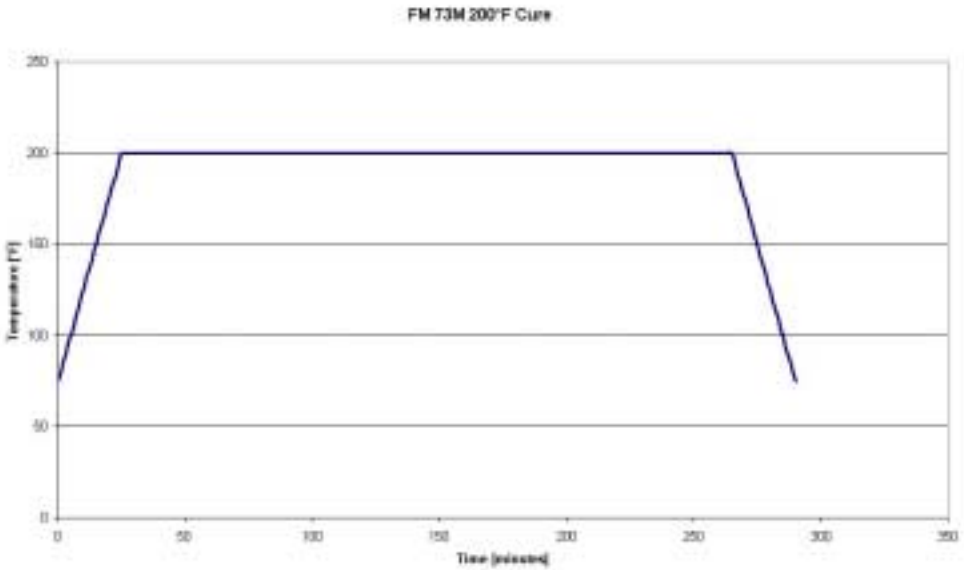

Figure 23: FM 73M 200°F Cure

2.4 Chapter Summary

This chapter discussed the surface preparation, the design of the patches, and the adhesive cycle design. A sol-gel surface preparation was selected and is further discussed in section 3.2. Patches were designed to be used with each adhesive: 4.0 inches x 4.0 inches for EA 9696 and 5.66 inches x 4.0 inches for FM 73M. The adhesive cycles were designed using differential scanning calorimetry and are as follows: EA 9696 250°F for one hour, 220°F for four hours, and 200°F for eight hours; FM 73M 250°F for one hour and 200°F for four hours. The change in T_g from the standard cure cycles to the modified cure cycles was also discussed.

CHAPTER 3: EXPERIMENTAL SETUP AND TEST PROCEDURE

3.1 Materials

This section discusses the specimen design and fabrication, as well as the manufacturing of the patch.

3.1.1 Specimen Design and Fabrication

This section describes the processes used in machining and precracking the aluminum panels.

3.1.1.1 Machining the Aluminum Panels

The University of Dayton Research Institute, under contract F33615-00-D-5600 with the USAF, machined the aluminum panels to the specifications shown in Figure 24. These specifications were chosen to fit the available servo-hydraulic fatigue machine detailed in section 3.1.1.2.

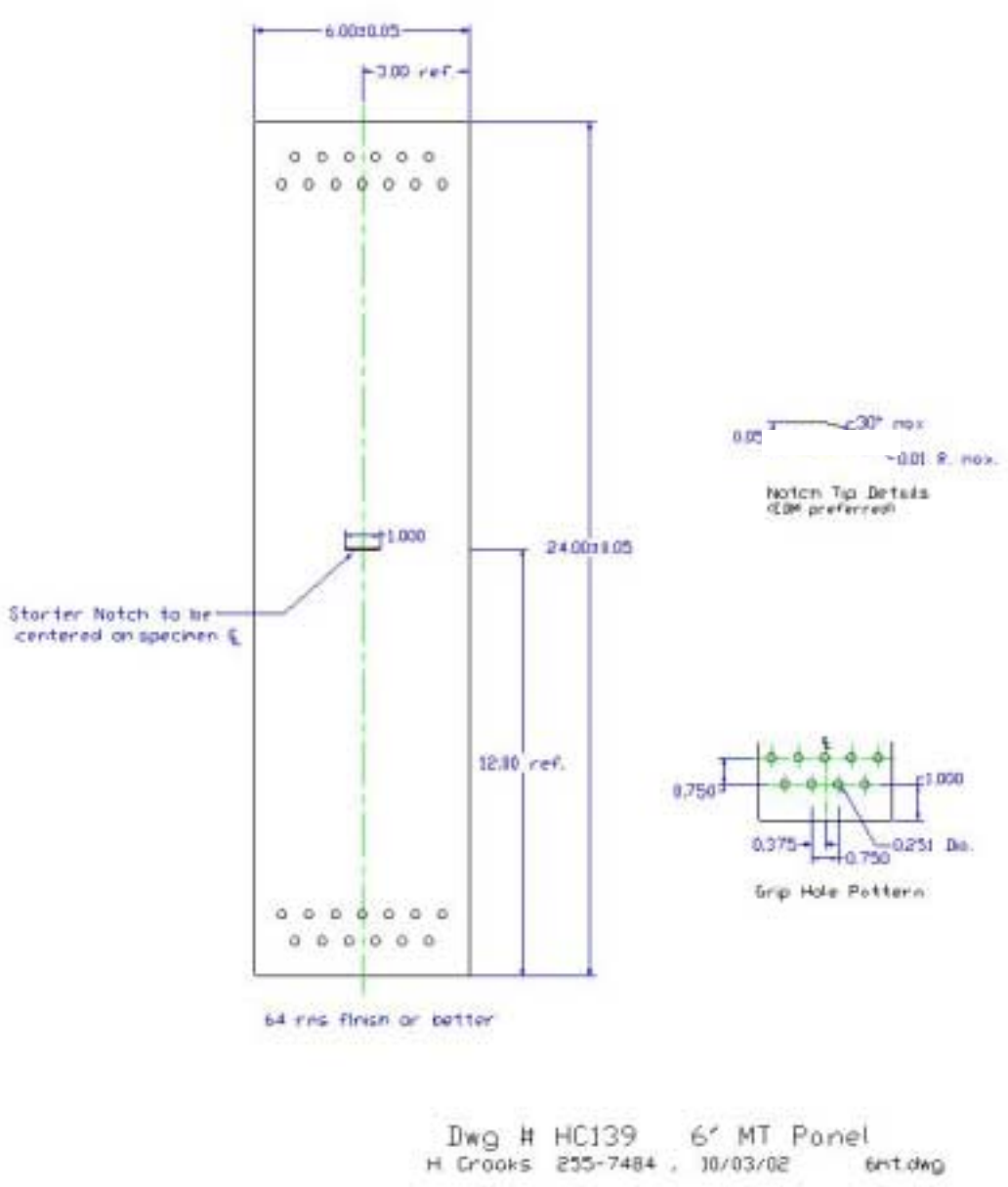

Figure 24: Aluminum Panel Specifications (inches)

3.1.1.2 Precracking the Aluminum Panels

Each panel had a one-inch starter notch electrostatic-discharge-machined (EDM) into its center. Precracking the notch, and subsequent fatigue crack growth rate testing, was

performed in accordance with ASTM E 647: *Standard Test Method for Measurement of Fatigue Crack Growth Rates* [25]. Both the precracking and fatigue testing were conducted in AFRL/MLSC's Materials Test and Evaluation Laboratory using an MTS Systems Corporation (MTS) 200 KIP servo-hydraulic fatigue machine, as shown in Figures 25 and 26.

Figure 25: MTS Machine and Setup

Figure 26: Inspection of Precrack

The precracked notch was grown to a total length of nominally two inches using a K-decreasing (load-shedding) method with a K-gradient (C) of -1.5 in^{-1}. Crack length measurements were made by the compliance technique using an MTS clip-gage attached at the center load-line as shown in Figure 27.

Figure 27: Precracking

Data acquisition and test machine control were performed using a commercially available computer software program. The MTS control panel and the computer control are shown below in Figures 28 and 29.

Figure 28: MTS Control Panel

Figure 29: MTS Computer Control

3.1.2 Manufacture of Patch

The prepreg material used to fabricate the patch plies was cut from a roll of FiberCote graphite unitape, T700 24K/E765 prepreg material. The material was cut into 36 inch x 24 inch sheets; these sheets were then cut to the specific patch dimensions according to the tables shown in section 2.2. All plies were cut as 0° directional plies. The 0° direction was defined as the longitudinal direction on the panel as shown in Figure 6. The lay-up process for T700/E765, as suggested by the manufacturer, is documented below.

Working Environment

All handling and lay-up of prepreg materials shall be conducted in a reasonably clean environment. No tool preparation, drilling, grinding, trimming, sanding, or other process creating particles may be conducted in the same room as the lay-up of prepregs. There shall be no solvents, lubricants, mold release agents, or other potential contaminants used or stored in the same room with prepreg materials.

Unless otherwise validated for the material system in use, the area should be temperature and humidity controlled such that the minimum temperature is 65°F with a corresponding relative humidity not greater than 63 percent. The maximum temperature is 75°F with a corresponding relative humidity not greater than 46 percent. The temperature and relative humidity values between the minimum and maximum acceptable values listed above should form a straight-line relationship.

Lay-up Surface

Each lay-up surface shall be cleaned prior to lay-up, using non-contaminating cleaners, such as Acetone or alcohol.

Cutting and Lay-up

> The cutting and lay-up area shall be kept free of contaminants. Before lay-up, the prepreg material shall be near ambient temperature. Upon removal from storage, the prepreg materials shall be allowed to warm to room temperature inside the sealed moisture-proof bag for at least 3 1/2 hours [26].

Forty patches were layed up in a wedding cake style at 15 plies per patch. This type of lay up places the longest ply on the bottom, the next longest ply centered on the first, etc., until all 15 plies have been placed to form a wedding cake appearance as illustrated in Figures 8 and 9. This design was chosen to smooth the load introduction from the cracked metallic structure to the composite patch material. Uncured and cured patches are shown in Figures 30 and 31. Patch curing procedures are outlined in Appendix A.

Figure 30: Uncured Patches

Figure 31: Cured Patches

After curing, the patches were ultrasonically inspected by AFRL/MLSA's Non-Destructive Inspection (NDI) shop. The C-Scan images generated reveal defects within the patch, such as porosity, voids, and delaminations. All patches were within acceptable standards. C-Scan images for all patches are shown in Appendix B.

3.2 Surface Preparation

Specific surface preparation must be followed in the patch bonding process. Powder free latex gloves are worn at all times to reduce the chance of surface contamination. A brief synopsis of these steps is listed below, while a detailed list of these steps is outlined in Appendix C.

The process started by mixing the sol-gel solution and degreasing the panels as shown in Figure 32 below. After degreasing, deoxidation and solvent wiping were accomplished as shown in Figure 33.

Figure 32: Degreasing

Figure 33: Deoxidation

The next steps were to tape off the area to be grit blasted and complete grit blasting as shown in Figure 34. After grit blasting, the specimens were nitrogen blasted to remove excess grit; then the sol-gel application began as shown in Figure 35.

Figure 34: Grit Blast (in progress)

Figure 35: Sol-Gel Application

After the Sol-Gel application, the specimens were primed with Cytec BR® 6747-1 water-based adhesive bonding primer, as shown below, and heat cured to a cured primer film thickness of 1E-4 – 3E-4 inch.

Figure 36: Priming

3.3 Strain Gauges

A total of eight strain gauges were applied on each specimen: six gauges on the panel and one gauge on each patch. Figures 37-39 below depict the location of each strain gauge; note that the figures are not to scale. Each patch had one strain gauge (either gauge 4 or gauge 8) centered on its top ply, as seen in Figure 37.

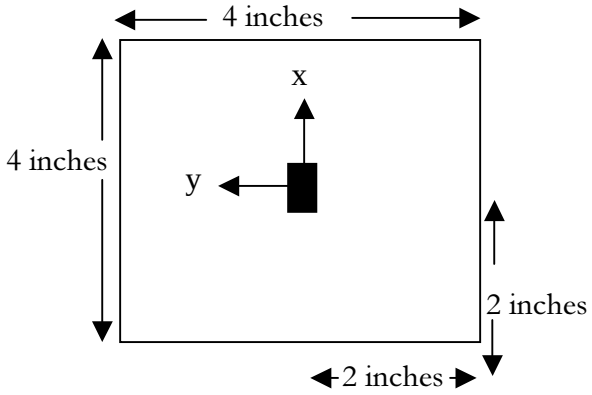

Figure 37: Strain Gauge Location on Patch

Each panel had a total of six strain gauges: three on the top of the panel and three on the bottom of the panel, as seen in Figures 38 and 39 below. All strain gauges were unidirectional gauges and were placed to read the strains in the longitudinal direction of the panel. The origin in these figures is defined as the center of the panel in both the x- and y-directions. Four strain gauges (1, 2, 6, 7) were placed one inch out in the x-direction (loading direction) and 1.5 inch out in the y-direction from the center of the EDM notch. These strain gauges were used to record the strains on the aluminum near the crack tip, under the patch. Two far-field strain gauges (3 and 5) were placed 7.5 inches in the x-direction from the center of the crack. These gauges were used to record the far-field strain on the

aluminum and for comparison to the strains recorded under the patch. The topside of the panel had gauges 1, 2, and 3, while the underside of the panel had gauges 5, 6, and 7.

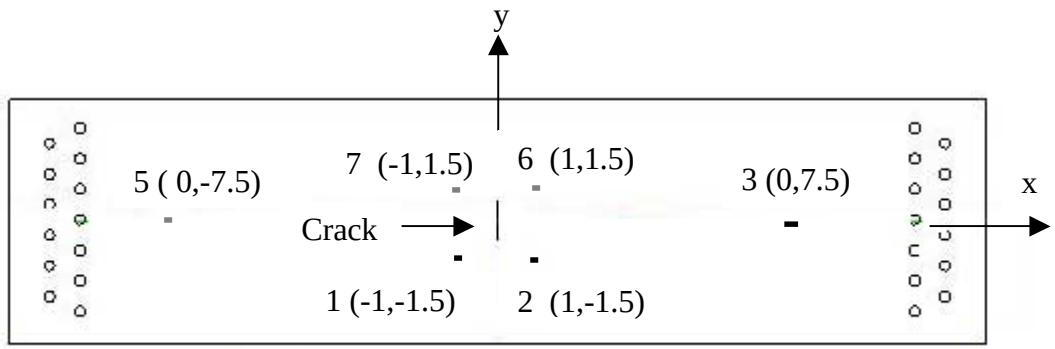

Figure 38: Top View of Strain Gauged Specimen

Figure 39 depicts the specimen from the side.

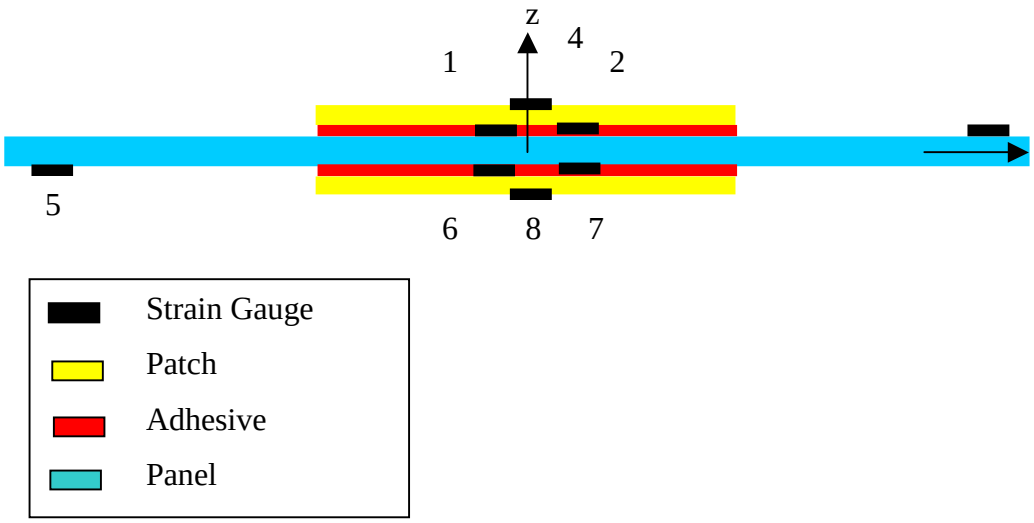

Figure 39: Side View of Entire Specimen With Strain Gauges

3.3.1 Type of Strain Gauges

The strain gauges used were Micro-Measurements CEA-13-250UW-350 (description follows). Micro-Measurements CEA gauges were supplied with a fully encapsulated grid and exposed copper-coated integral solder tab. Because of this fully encapsulated grid, there are no strain effects on the gauge because of the surrounding structure, including the adhesive used to bond the patch to the panel. These gauges were unidirectional gauges and were valid for measurements up to 350°F. This type of gauge however did not allow for strain measurement with varying temperature; however, this was accounted for in the results.

Gauge designation CEA-13-250UW-350 breaks out as follows:

1. CE – Flexible gauge with a cast polyimide backing and encapsulation featuring large, rugged, copper-coated solder tab. This construction provides optimum capability for direct leadwire attachment.
2. A – Constantan alloy in self-temperature-compensated form.
3. 13 – Self-temperature-compensated number; the approximate thermal expansion coefficient in ppm/°F of the structural material on which the gauge is to be located.
4. 250 – Active gauge length in millionths of an inch.
5. UW – Grid and tab geometry
6. 350 – Resistance in Ohms.

3.3.2 Strain Gauge Installation

Micro-Measurements M-Bond 600 was the adhesive used to bond the strain gauges to the specimens. This adhesive is useful in temperatures raging from -452°F to 700°F when properly cured [27]. The following list of materials are needed for strain gauge installation:

- Isopropyl Alcohol
- Silicon-Carbide Paper
- M-Prep Conditioner A
- M- Prep Neutralizer 5A
- Tweezers
- Gauges/gauge boxes
- High temperature terminals: type PF (ployimide film)
- GSP-1 Gauze sponges
- CSP-1 Cotton Applicators
- MJG-2 Mylar® Tape
- TFE-1 Teflon® Flim
- HSC-1 Spring Clamps
- GT-14 Pressure Pads and Backup Plates
- RSK Rosin

Strain gauge installation instructions are outlined in Appendix D. A brief synopsis of the procedures is outlined below.

The surfaces of the panels were prepared for strain gauge installation and the gauges were aligned in the longitudinal 0° direction as shown in Figure 40. The gauges were then cured to the panels and the patches as seen in Figure 41, and wires were soldered to the terminals of all gauges.

Figure 40: Strain Gauge Placement

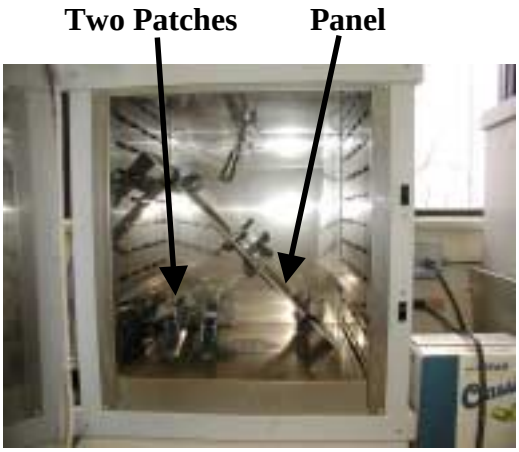

Figure 41: Curing of Strain Gauges

3.4 Patch Bonding Process and Vacuum Bagging Procedures

Once the gauges were cured to the panel and patches, the patches were applied to the aluminum panel. The respective adhesive was cut to the dimensions of the patch plus 1/8 inch on all sides and was centered on the aluminum panel. The patch was then placed on top of the adhesive and taped down to eliminate movement during the vacuum bagging process. The entire specimen was then vacuum bagged according to the procedures outlined in Appendix E.

There was no interference from the patch in the functioning of the strain gauges. All gauges were coated and isolated from the patch. In addition, the backings provided by the manufacturer allow for increased elongation of the material without affecting the strain output of the gauges. Also, the adhesive was specifically designed for use with these strain gauges [27].

3.5 Data Collection

The vacuum bagged specimen was then placed into a Fisher Scientific programmable oven and put under full vacuum for the entire length of the cure cycle as shown in Figure 42. The strain gauge wires were connected to an Optim Electronics MEGADAC data acquisition system as shown below in Figure 43.

Figure 42: Testing Specimen

Figure 43: MEGADAC System

3.6 Testing Procedures

There were two baseline fatigue specimens of 7075-T6 aluminum with a two inch precrack and no patch. These specimens were fatigue crack growth rate tested to failure and the

results averaged. There were also three baselines for each adhesive cured under the manufacturers' suggested cycle. One of these panels was fatigue crack growth rate tested to failure for comparison to modified cure cycles, as well as baseline (no patch) data.

The testing procedure was as follows:

1. All strain gauges were normalized to zero at the beginning of each test.
2. Strain readings were taken every 25 seconds during patch cure and throughout the cool-down phase. Note that the strain readings were not corrected for the CTE mismatch between the gauge and the aluminum. This correction occurred in the determination of thermal residual strains.
3. The strain readings at the end of the cool-down yield the thermal residual strains.
4. One specimen from each cure cycle was fatigue crack growth tested to failure.
5. After the data were collected, the modified cure cycle results for thermal residual strains and fatigue crack growth rate testing were compared with those of the nonpatched specimen and the manufacturers' cure cycle specimen.

The following table depicts the panel number, adhesive utilized, and the type of cure cycle.

Table 5: Panel Identification

Number	Adhesive	Cure Cycle
20	None	-
21	None	-
1	EA 9696	250°F – 1hr
16	EA 9696	250°F – 1hr
17	EA 9696	250°F – 1hr
4	EA 9696	200°F – 8hrs
5	EA 9696	200°F – 8hrs
6	EA 9696	200°F – 8hrs
9	EA 9696	220°F – 4hr
18	EA 9696	220°F – 4hr
19	EA 9696	220°F – 4hr
10	FM 73M	250°F – 1hr
11	FM 73M	250°F – 1hr
12	FM 73M	250°F – 1hr
13	FM 73M	200°F – 4hrs
14	FM 73M	200°F – 4hrs
15	FM 73M	200°F – 4hrs

3.7 Chapter Summary

This chapter talked about the experimental setup and test procedures to be followed. Details of the aluminum panels and the precracking process were outlined, as was the patch manufacturing process. The strain gauge type and installation were discussed including placement of the gauges. Finally, the patch bonding process, vacuum bagging process, and testing procedures were outlined.

CHAPTER 4: RESULTS and DISCUSSIONS

This chapter is divided into two sections. Section 4.1 shows the strain results and discussion of the panels using EA 9696 adhesive, while Section 4.2 shows the results and discussion of the panels using FM 73M adhesive. In both sections, the strain readings were zeroed at the beginning of the test, thus the readings at the beginning of the cure cycle and at the end of the cure cycle are valid strain measurements, as they were readings taken at or near room temperature. The values during the cure cycle, however, are not corrected for strain gauge expansion/contraction due to the gauge's coefficient of thermal expansion and the CTE mismatch of the gauge material and the aluminum panel. The residual strains are calculated as a difference of final strain under the patch and final far-field strain. Because this is a difference of values, the CTE mismatch between the gauge and the panel does not affect the final thermal residual strain determination.

4.1 Panels with EA 9696 Adhesive

There were three cure cycles used with the EA 9696 adhesive: 250°F for one hour, 220°F for four hours, and 200°F for eight hours. The averages of the thermal residual strains for each individual cure cycle are shown in the following sections. Refer to Appendix F for detailed strain data for each individual panel. The residual strain is defined as the difference between the final strain under the patch and the final far-field strain.

Equation 26 describes the strain-temperature relation,

$$\varepsilon = \alpha_T \Delta T \qquad (26),$$

where α_T is the coefficient of thermal expansion. The strains on the panel are directly proportional to the temperature change through the coefficient α_T. Because of the CTE mismatch between the gauge and the aluminum, the strain readings will be proportional to the $\Delta\alpha$ between the aluminum and the gauge material. Equation 26 is valid until the cool-down phase, when the adhesive has locked into its structure and the CTE mismatch becomes visible.

The following criteria apply to Figures 44-46 and 52-53. The dark blue curve represents the average strain recorded under the patch, while the pink curve represents the average strain recorded at the far-field gauges. These two curves overlap until the cool-down phase of the cycle. This overlap occurs because all the gauges are recording strains on aluminum that is freely expanding. However, once the cool-down phase begins and the adhesive is locked into its structure, the aluminum under the patch is not allowed to contract (because of the CTE mismatch between the aluminum and the graphite/epoxy patch) and the strain recordings diverge. The far-field strains should theoretically return to zero when cooled to a room temperature equal to that at the beginning of the test. Any deviation from zero is a result of experimental error. The light blue curve represents the temperature of the panel throughout the curing process. The yellow curve represents the average strain on the patch material. Notice that the strain is compressive when heated and expands when cooled. This

strain does not return to zero, and is not expected to, since there are compressive strains applied to the patch by the contracting aluminum.

4.1.1 250°F Standard Cure Cycle

Panels 1, 16, and 17 were cured using the standard 250°F cure cycle. All three panels were used in averaging the strains. The strain averages for the standard cure cycle are shown in Figure 44.

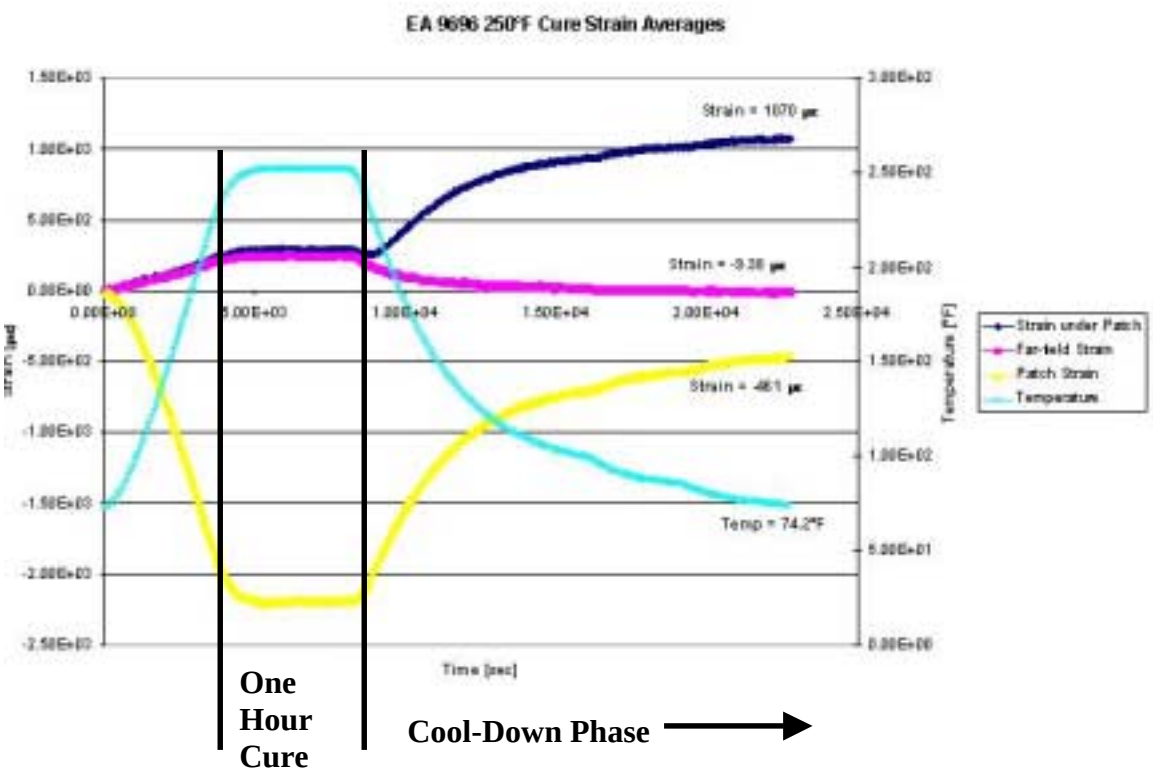

Figure 44: EA 9696 250°F Cure Strain Averages

Notice that the far-field strain and the strain underneath the patch fell on top of each other throughout the cure cycle. It was not until the cool-down phase, when the CTE mismatch

became visible, that these strains diverged. It is the difference in these final strains that gives the thermal residual strains of the aluminum under the patch. The slope of the strains on the aluminum is not the CTE of the aluminum, as it would be expected. Because of the CTE mismatch, this slope represents the $\Delta\alpha$ between the gauge material and the aluminum. The averages for panels 1, 16, and 17 are shown in Table 6 below. The net residual strains under the patches, 1079.38 με, resulted in a comparable stress of 1,079 psi forcing open the crack.

Table 6: Strain Readings of EA 9696 250°F Cure Averages at 74.2°F

Gauge Placement	Strain Reading
Under the Patch	1070 με
Far-Field	-9.38 με
On Top of Patch	-461 με
Final Temperature	74.2°F
Net Residual Strain	1079.38 με

4.1.2 220°F Modified Cure Cycle

Panels 9, 18, and 19 were cured using the 220°F cure cycle. All three panels were used in the following average shown in Figure 45. Note the increase in cure hold time from one hour at 250°F to four hours at 220°F.

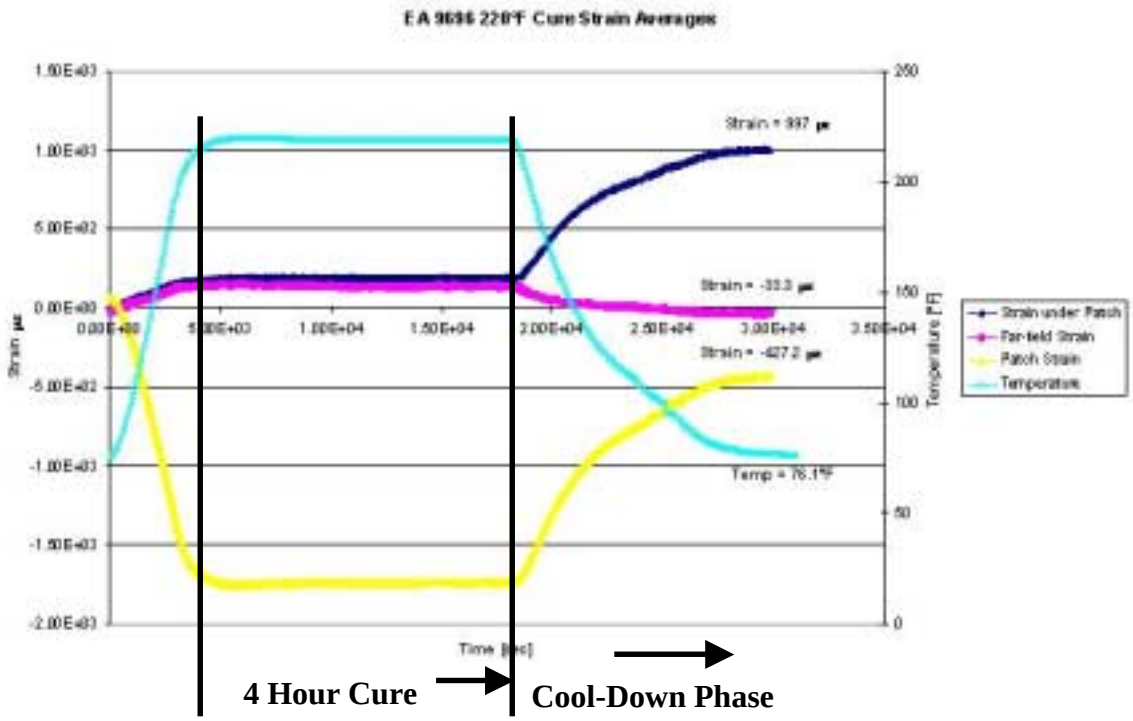

Figure 45: EA 9696 220°F Cure Strain Averages

As with the standard cure cycle, the far-field strain and the strain underneath the patch were equal until the lock in of the adhesive, where the strains diverged. The averages at 76.1°F are shown in Table 7 below. The net strains under the two patches, 1030.3 με, resulted in a crack-opening stress of 1,030 psi.

Table 7: Strain Readings of EA 9696 220°F Cure Averages at 76.1°F

Gauge Placement	Strain Reading
Under the Patch	997 με
Far-Field	-33.3 με
On Top of Patch	-427.2 με
Final Temperature	76.1°F
Net Residual Strain	1030.3 με

4.1.3 200°F Modified Cure Cycle

Panels 4, 5, and 6 were cured using the 200°F cure cycle; all panels were used in the average, and the results are shown in Figure 46 below.

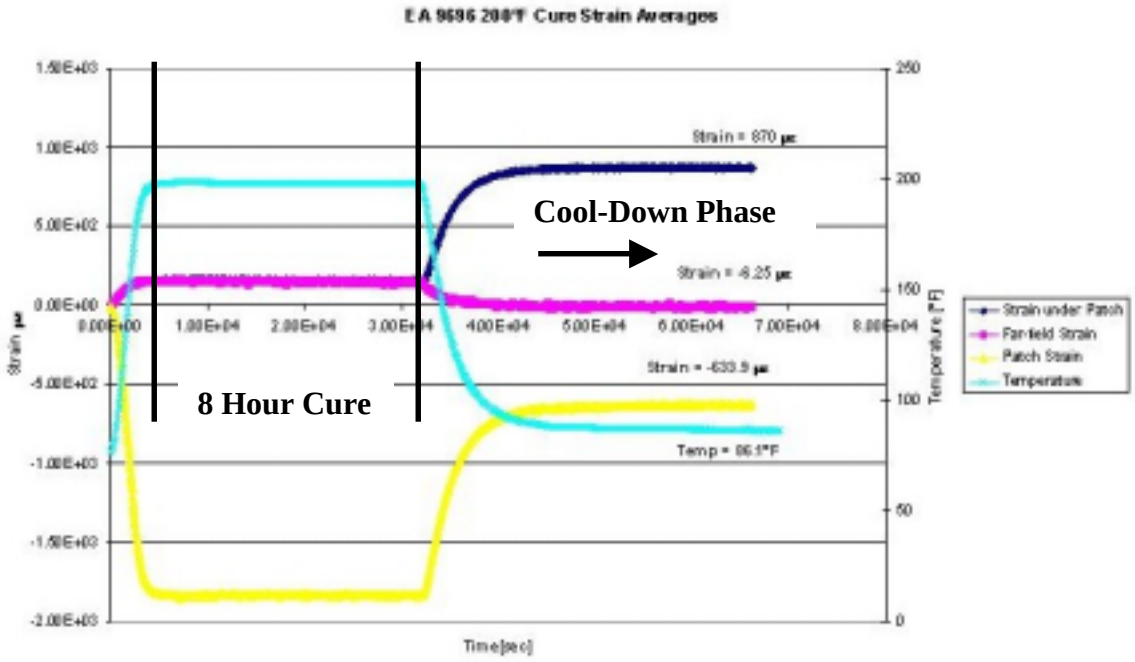

Figure 46: EA 9696 200°F Cure Strain Averages

The results of the strain averages at 86.1°F are shown in Table 8 below. The net residual strains under the two patches, 876.25 με, resulted in a crack-opening stress of 876 psi.

Table 8: Strain Readings of EA 9696 200°F Cure Averages at 86.1°F

Gauge Placement	Strain Reading
Under the Patch	870 με
Far-Field	-6.25 με
On Top of Patch	-633.9 με
Final Temperature	86.1°F
Net Residual Strain	876.25 με

4.1.4 Comparison of 250°F and 220°F Cure Cycles

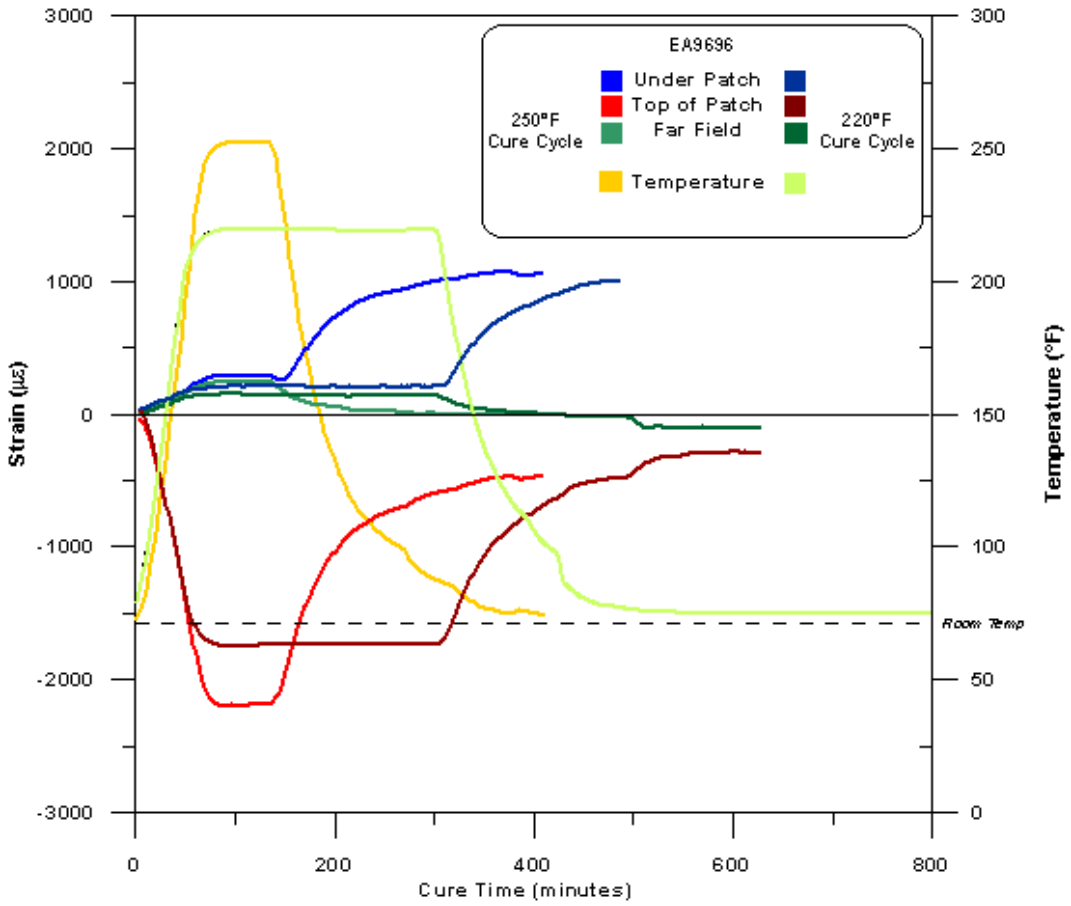

Figure 47: EA 9696 250°F and 220°F Cure Averages Comparison

Figure 47 shows the comparison of two cure cycles (250°F and 220°F) for EA 9696. The purpose of this graph is to show the reduction in thermal residual strains, underneath the

patch, when the lower cure temperature is utilized. These data are compared in Table 9 below.

Table 9: Strain Readings of EA 9696 250°F and 220°F Cure Averages

Gauge Placement	Strain Reading (250°F)	Strain Reading (220°F)	Strain Reduction
Under the Patch	1070 με	997 με	73 με
Far-Field	-9.38 με	-33.3 με	-23.92 με
On Top of Patch	-461 με	-427.2 με	130.72 με
Final Temperature	74.2°F	76.1°F	-
Net Residual Strain	1079.38 με	1030.3 με	49.08 με

4.1.5 Comparison of 250°F and 200°F Cure Cycles

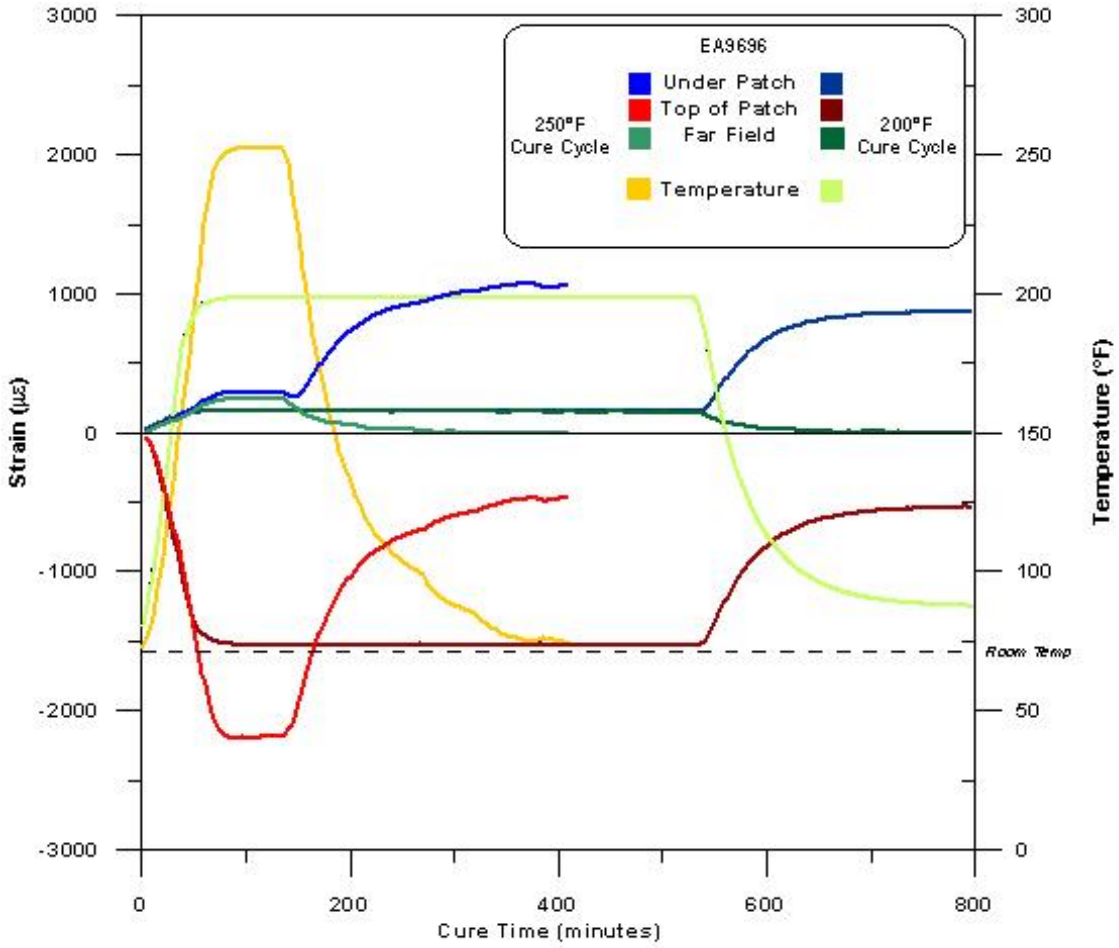

Figure 48: EA 9696 250°F and 200°F Cure Averages Comparison

Figure 48 shows the comparison of two cure cycles (250°F and 200°F) for EA 9696. The purpose of this graph is to show the reduction in thermal residual strains, underneath the patch, when the lower cure temperature is utilized. These data are compared in Table 10 below. Negative signs in the Strain Reduction column indicate an increase, rather than a decrease, in strain.

Table 10: Strain Readings of EA 9696 250°F and 200°F Cure Averages

Gauge Placement	Strain Reading (250°F)	Strain Reading (200°F)	Strain Reduction
Under the Patch	1070 με	870 με	200 με
Far-Field	-9.38 με	-6.25 με	3.13 με
On Top of Patch	-461 με	-633.4 με	-172.4 με
Final Temperature	74.2°F	86.1°F	-
Net Residual Strain	1079.38 με	876.25 με	203.13 με

4.1.6 Determination of Most Beneficial Cure Cycle

The most beneficial cure cycle in this research was the cure cycle that yielded the lowest thermal residual strains. The average data for the EA 9696 cure cycles are shown in Figure 49 below.

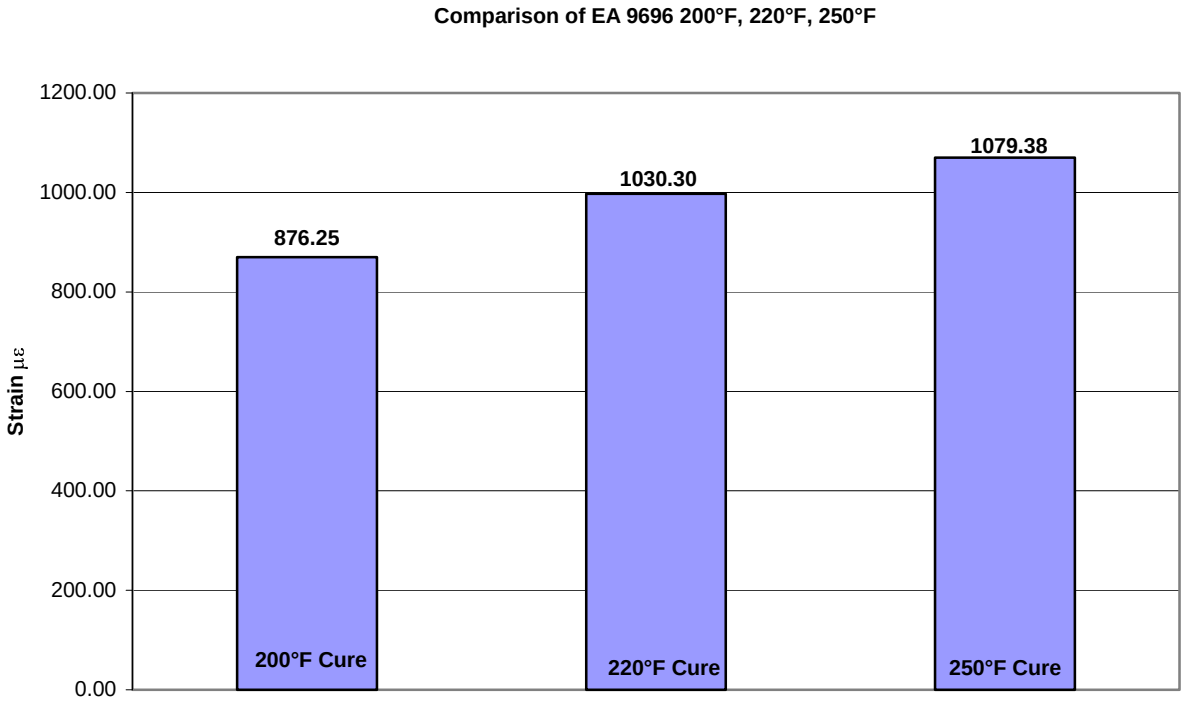

Figure 49: Comparison of EA 9696 200°F, 220°F, and 250°F

As can be seen in Figure 49, the lower the cure cycle temperature, the lower the thermal residual strains under the patch. However, the highest final temperature of the EA 9696 panels was 88.2°F; therefore, all data must be compared at this final temperature to ensure accuracy. Table 11 and Figure 50 below show these data.

Table 11: EA 9696 88.2°F Strain Data

	200°F	220°F	250°F
Under Patch	**859.67** με	**944.33** με	**985.50** με
Far-Field	**-59.17** με	**-28.12** με	**-6.25** με
Top of Patch	**-544.0** με	**-521.0** με	**-620.5** με
Final Temp	**88.20 °F**	**88.20 °F**	**88.20 °F**
Net Residual Strain	**918.84** με	**972.45** με	**991.75** με

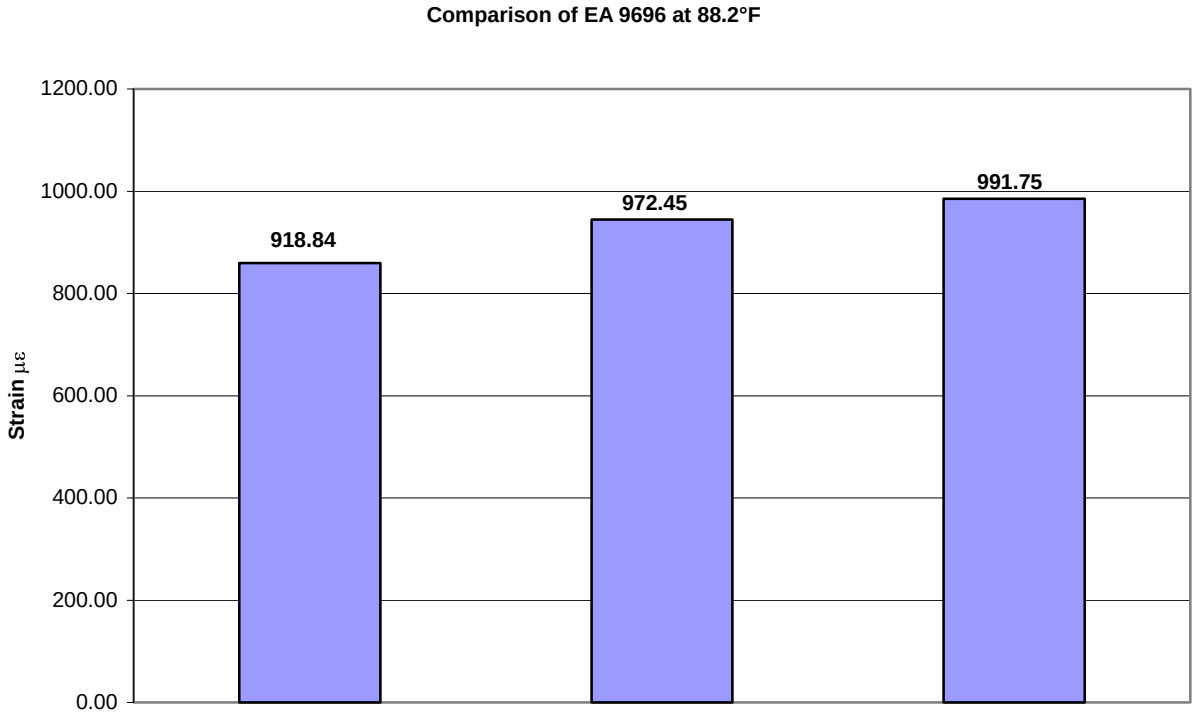

Figure 50: Comparison at 88.2°F

There was a 19.3 με reduction when the 220°F cure cycle was utilized instead of the 250°F cure cycle. This results in a 2% strain reduction and a 19.3 psi reduction in crack-opening stress. When the 200°F cure cycle was utilized in place of the 250°F cure cycle, there was a 7.4% reduction in strain and a 72.9 psi reduction in crack-opening stress.

The temperature versus thermal residual strain data for all EA 9696 cure cycles are shown in the line graph in Figure 51. From this figure it is shown that for cure cycles with lower cure temperatures, there are lower thermal residual strains. The 200°F cycle for EA 9696 shows the lowest thermal residual strain. This was expected, as the cure cycle temperature hold was the lowest for this cure cycle, thus the initial strains were smaller. The "looping" at the peak of the cure temperature, where the strains decrease slightly before increasing, was due to the properties of the adhesive. At the peak of the cure temperature, the adhesive was still free-flowing and had not yet locked into its structure. As the temperature began to cool, the adhesive began to set and lock in; this point was the onset of the thermal residual strains.

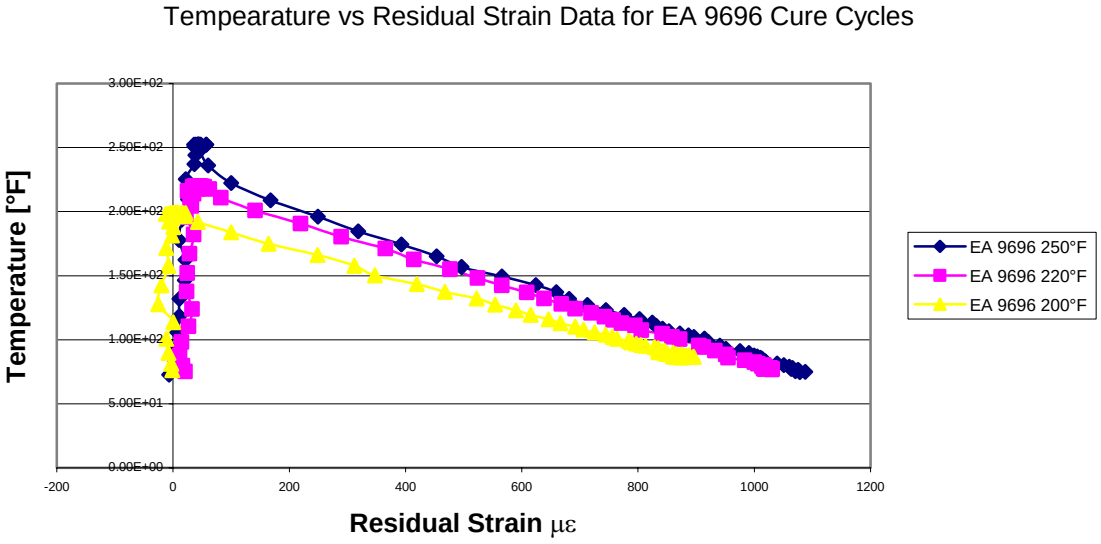

Figure 51: Temperature vs Strain Data for EA 9696 Cure Cycles

An empirical formula can be formed using the previous data. This formula can theoretically be applied to the EA 9696 adhesive with cure cycles between 200°F and 250°F, and extrapolated to include lower cure temperatures than 200°F, to find the thermal residual strains for a given cure temperature after a cool down to 88.2°F. In the following equation, 'x' refers to the cure cycle temperature and 'y' refers to the resulting thermal residual strain,

$$y = -0.0407x^2 + 19.73x - 1410 \quad (27).$$

4.2 Panels with FM 73M Adhesive

There were two adhesive cycles used with the FM 73M adhesive: 250°F for one hour and 200°F for four hours. The averages for each of these cure cycles are shown in the following sections. Refer to Appendix F for strains on each individual panel.

4.2.1 250°F Standard Cure Cycle

Panels 10, 11, and 12 were cured using the standard 250°F cure cycle. Only panels 10 and 12 were used in the following average due to an error in data recording for panel 11. These data are shown in Figure 52 below.

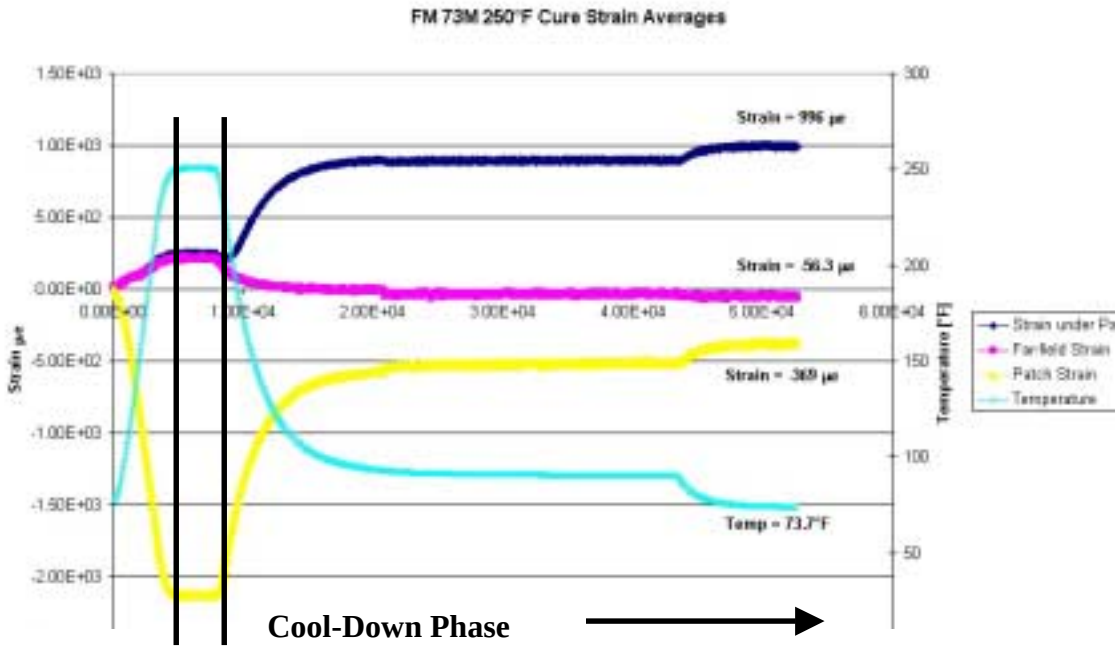

Figure 52: FM 73M 250°F Cure Averages

Note that, once again, the far-field strain and the strain under the patch are equal during the ramp and cure hold phases of the cure cycle. The results of this average are shown in Table 12 below. The net residual strains under the two patches, 1052.3 με, resulted in a comparable stress of 1,052 psi. This tensile stress was opening the crack on the structure.

Table 12: Strain Readings of FM 73M 250°F Cure Averages at 73.7°F

Gauge Placement	Strain Reading
Under the Patch	996 με
Far-Field	-56.3 με
On Top of Patch	-369 με
Final Temperature	73.7°F
Net Residual Strain	1052.3 με

4.2.2 200°F Alternate Cure Cycle

Panels 13, 14, and 15 were cured using the 200°F cure cycle; all panels were used in the following average as shown in Figure 53.

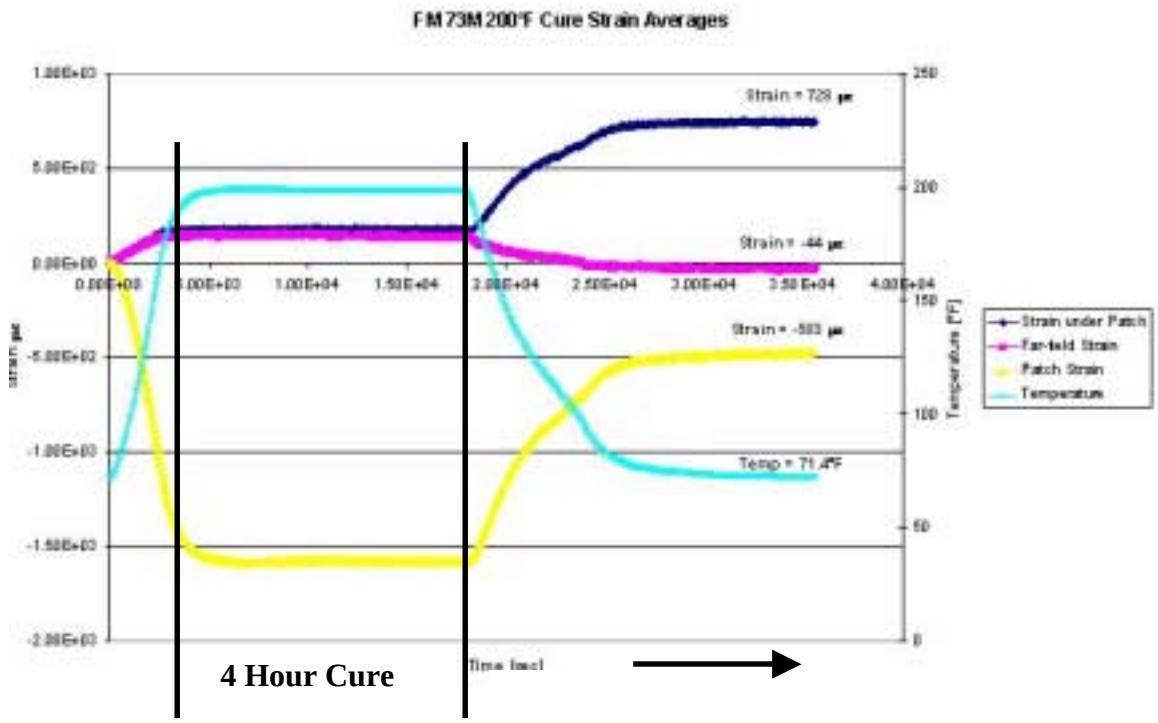

Figure 53: FM 73M 200°F Cure Averages

The results of this average are shown in Table 13 below. The net residual strains under the two patches, 772 με, resulted in a comparable stress of 772 psi.

Table 13: Strain Readings of FM 73M 200°F Cure Averages at 71.4°F

Gauge Placement	Strain Reading
Under the Patch	728 με
Far-Field	-44 με
On Top of Patch	-503 με
Final Temperature	71.4°F
Net Residual Strain	772 με

4.2.3 Comparison of 250°F and 200°F Cure Cycles

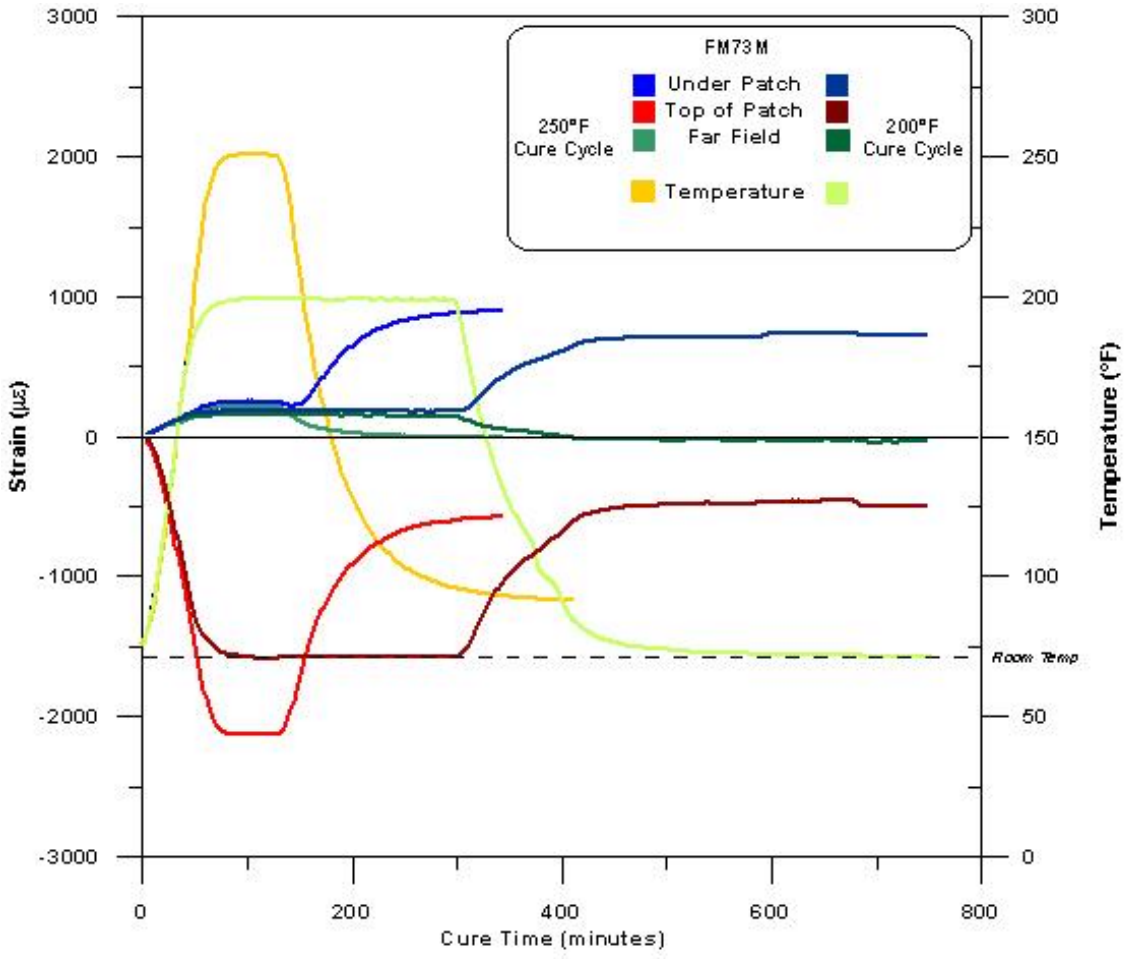

Figure 54: FM 73M 250°F and 200°F Cure Averages Comparison

Figure 54 shows the comparison of two cure cycles for FM 73M. The purpose of this graph is to show the reduction in thermal residual strains, underneath the patch, when the lower cure temperature is utilized. These data are compared in Table 14 below.

Table 14: Strain Readings of FM 73M 250°F and 200°F Cure Averages

Gauge Placement	Strain Reading (250°F)	Strain Reading (200°F)	Strain Reduction
Under the Patch	996 με	728 με	268 με
Far-Field	-56.3 με	-44 με	12.3 με
On Top of Patch	-369 με	-503 με	-134 με
Final Temperature	73.7°F	71.4°F	-
Net Residual Strain	1052.3 με	772 με	280.3 με

4.2.4 Determination of Most Beneficial Cure Cycle

The raw data for FM 73M cure cycles are shown below in Figure 55.

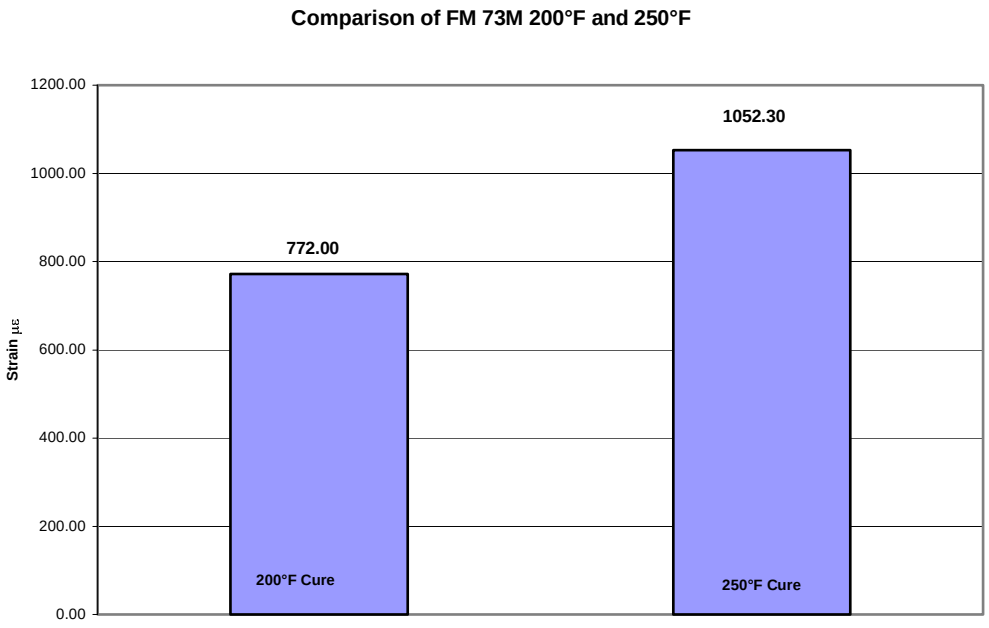

Figure 55: Bar Graph Comparison of 200°F and 250°F Cures

According to these data, the 200°F cure cycle reduced the thermal residual strains by 26.7% from 1052.3 με to 772.00 με. However, the highest final temperature for FM 73M panels was 93.3°F. Therefore, data must be compared at that temperature. Table 15 depicts these values and Figure 56 shows the bar graphs. (Negative signs indicate an increase in strain, rather than a reduction.)

Table 15: FM 73M 93.30°F Data

	Strain Reading (200°F)	Strain Reading (250°F)	Strain Reduction
Under Patch	**662.81** με	**896.50** με	**233.69** με
Far-Field	**-2.10** με	**-7.85** με	**5.75** με
Top of Patch	**-676.33** με	**-575.20** με	**-101.13** με
Final Temperature	**93.30 °F**	**93.30 °F**	**-**
Net Residual Strain	**664.91** με	**904.35** με	**239.44** με

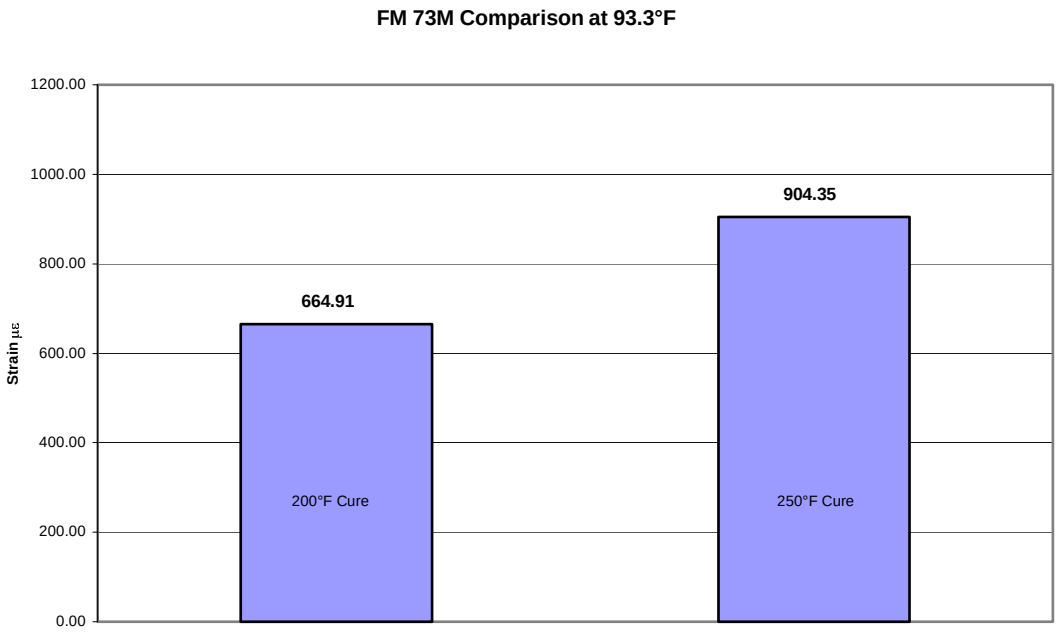

Figure 56: 93.3°F Final Temperature Strain Data

As seen from these data, the thermal residual strains were reduced by 26.5% from 904.35 με to 664.91με. Once again, it can be seen that the modified cure cycle resulted in a lower thermal residual strain under the patch. Also, there was a decrease of 239 psi in the crack opening stress.

The temperature versus strain data for all FM 73M cure cycles are shown in the line graph in Figure 57. From this figure it is shown that for the cure cycle with the lower cure temperature, there are lower thermal residual strains. The 200°F cycle for FM 73M shows these lower thermal residual strains. This was expected, as the cure cycle temperature hold was the lower for this cure cycle, thus the initial strains were smaller. The "looping" at the peak of the cure temperature, where the strains decrease slightly before increasing, was due to the properties of the adhesive. At the peak of the cure temperature, the adhesive was still free-flowing and had not yet locked into its structure. As the temperature began to cool, the adhesive began to set and lock in; this point was the onset of the thermal residual strains.

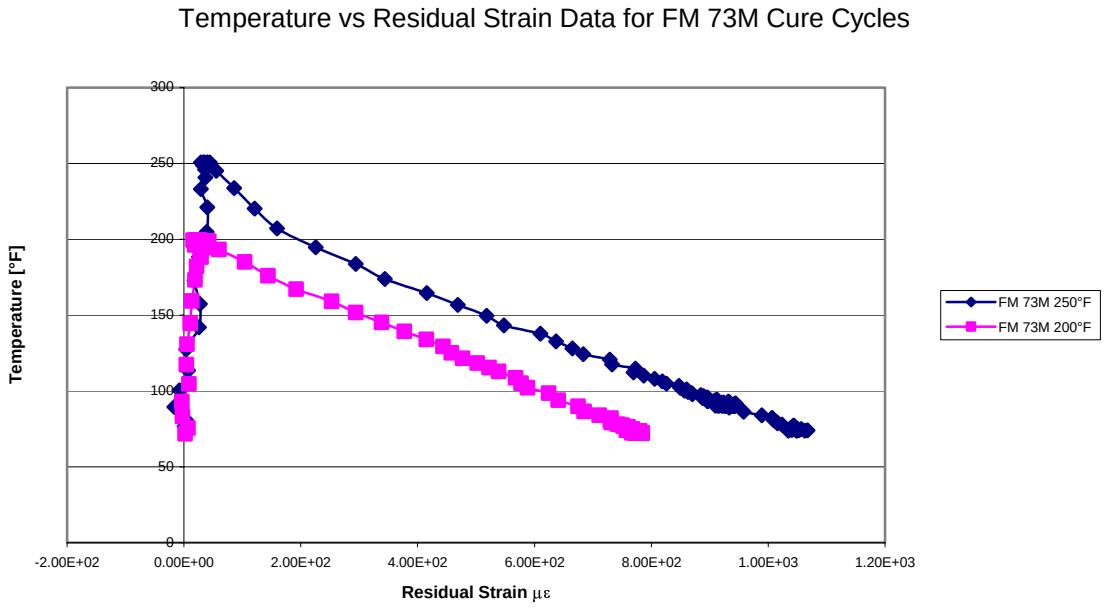

Figure 57: Temperature versus Strain Data for FM 73M Cure Cycles

An empirical formula can be formed using the previous data. This formula can theoretically be applied to the FM 73M adhesive with cure cycles between 200°F and 250°F to find the thermal residual strains at for given cure temperature after a cool down to 93.3°F. In the following equation, 'x' refers to the cure temperature and 'y' refers to the resulting thermal residual strain,

$$y = 4.7888x - 292.85 \quad (28).$$

Table 16 below shows the percent reduction of the thermal residual strains and the corresponding stress reduction under the patch for both cure systems. There was a 2% reduction in strain, equating to a 19.3 psi stress reduction, under the patch when utilizing the 220°F cure cycle as opposed to the 250°F cure cycle for EA 9696. When the 200°F cure

cycle for EA 9696 was utilized, there was a 7.4% reduction in strain, equating to a 72.9 psi stress reduction, from the 250°F cure cycle. For FM 73M, there was a considerable strain reduction of 26.5%, 239.4 psi stress reduction, when the 200°F cure cycle was utilized in place of the 250°F cure cycle. The reduction in the strains, and subsequently the stresses, under the patch theoretically yield an increased lifetime of the repair due to the reduced crack-opening forces. This was tested in the next section through fatigue crack growth rate testing.

Table 16: Percent Reduction of Thermal Residual Strains

Cure System	Strain 1	Strain 2	% Reduction	Stress Reduction
EA 9696 250°F vs 220°F	991.75 με	972.45 με	2%	19.3 psi
EA 9696 250°F vs 200°F	991.75 με	918.84 με	7.4%	72.9 psi
FM 73M 250°F vs 200°F	904.35 με	664.91 με	26.5%	239.4 psi

4.3 Fatigue Testing

This section outlines the fatigue testing of five panels, one from each cure cycle group. Baseline testing on unpatched panels is discussed, as is testing on each of the five patched panels.

4.3.1 Baseline Testing

Two unpatched panels were fatigue crack growth rate tested to failure. The testing was performed in accordance with ASTM E 647 [25] in an ambient laboratory environment. The

stress ratio (minimum stress/maximum stress), R, used for these tests was 0.1 and the frequency was 5 Hz. The value of R used in this program was based on a typical value used for testing of aluminum. The frequency was based on machine limitations. The results are shown in Figure 58. Initially (for precracking), the tests were performed in a K-decreasing (load-shedding) condition. It can be seen from Figure 58 that the two specimens have nearly identical Region II crack growth. Region II is the area of the fatigue crack growth rate curve that is essentially linear. The maximum stress intensity factor (ΔK) seen in this testing was approximately 20 ksi$\sqrt{in}$.

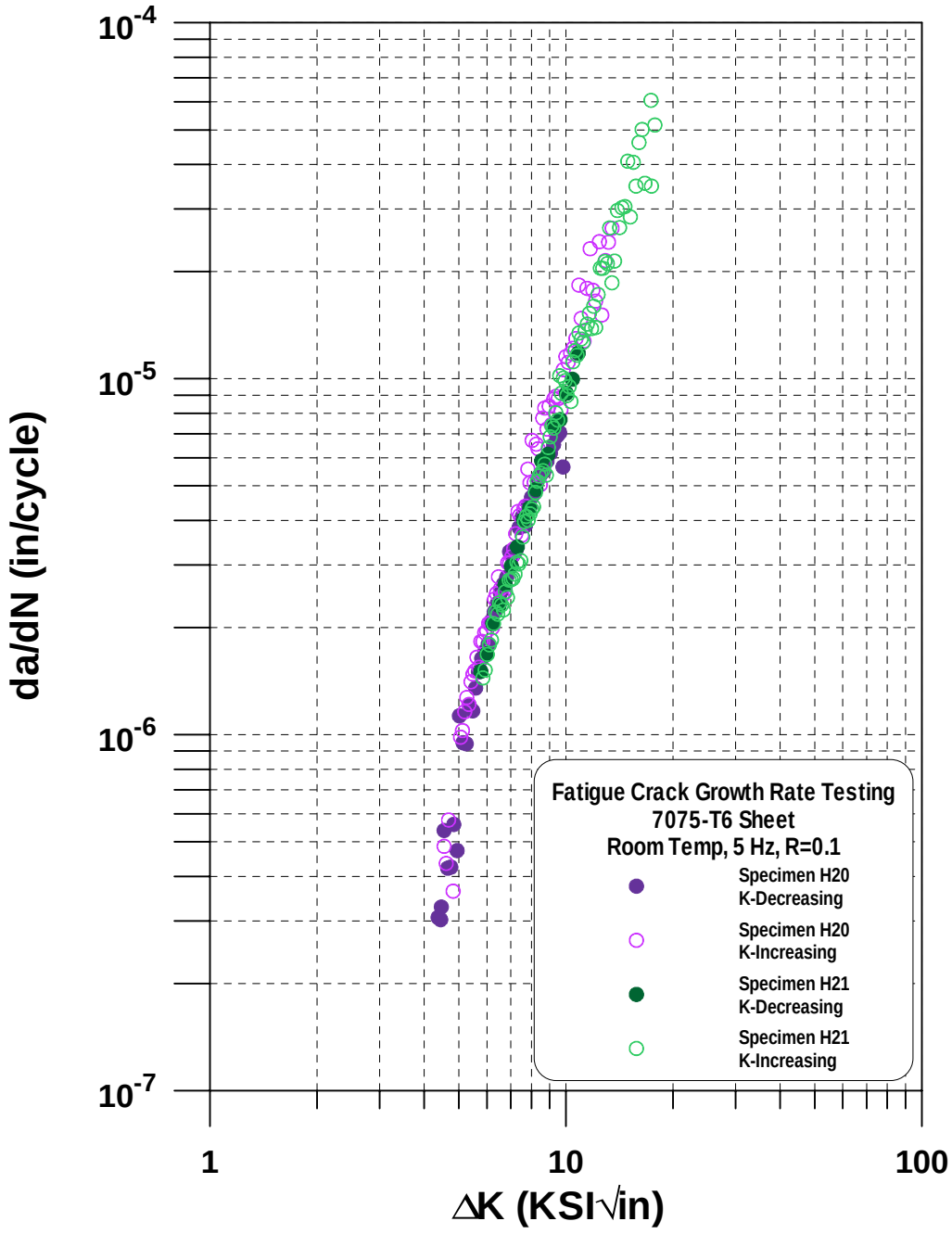

Figure 58: Fatigue Crack Growth Rate Testing on Panels 20 and 21

4.3.2 Patched Specimen Testing

Comparing the results in Figure 58 with the precracking results of the remaining specimens helped direct the selection of loads for the patched panels. (The final precracking stress intensity factor was approximately ΔK=5.4 ksi$\sqrt{in}$ (K_{max}=6 ksi$\sqrt{in}$).) It was expected that any crack growth found after patching would be significantly slower than that shown in Figure 58. (The stress intensity factor, K, values noted for patched panels in this investigation are assumed to be those values in the aluminum panel and do not account for any contributions from the patch. The K values are to be used for reference purposes only in comparisons to testing performed on unpatched specimens [9].)

Each panel was cycled for two million cycles; the panel was then ultrasonically inspected to determine crack length. Once this was determined, the applied ΔK values were back calculated from the length of the crack after the load step and the load applied at that load step. The panel was then cycled for another two million cycles at a higher load. This process was repeated until failure of the panel. The results of the crack growth rate testing on the patched specimens are shown in Figure 59. The curves shown in this figure are power-law fits to the data collected. These are shown only to display the location and general trend of the data and should not be used to model the actual fatigue crack growth rate for that panel. In two cases, there was only enough data to show one point. Figure 59 shows that the crack growth rates for the 250°F EA 9696 and FM 73M cure cycles are much less than that of the unpatched specimen. This means that for an applied ΔK value, the crack growth rate is slower for the patched specimen than the unpatched specimen.

Therefore, for a given cyclic load on the structure, you will have a decrease in fatigue crack growth rate, thus an increase in life, when the crack is patched.

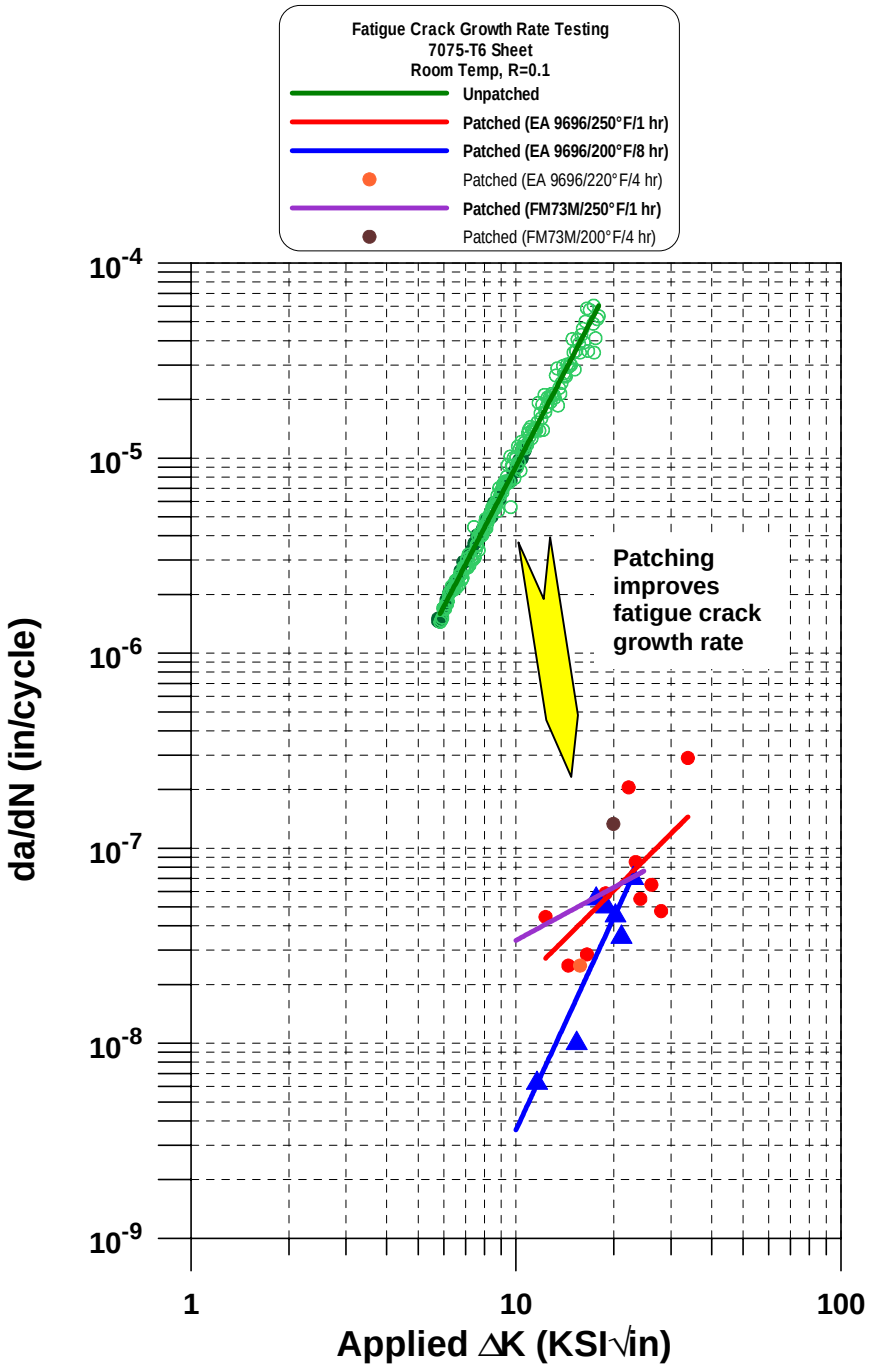

Figure 59: Comparison of Fatigue Crack Growth Rate Testing on Patched and Unpatched Specimens

4.3.2.1 Panel 1 Fatigue Results

Panel 1, cured at 250°F with EA 9696, failed after 10,500,000 cycles at a P_{max} of 8000 (lbs) and a ΔK of 33.79(ksi$\sqrt{in}$). When the aluminum failed, the patch continued to carry the load; therefore, the specimen was pulled in tension until the patch failed as well. This type of failure indicates that the patch has the ability to continue to carry the load even after the structure has failed.

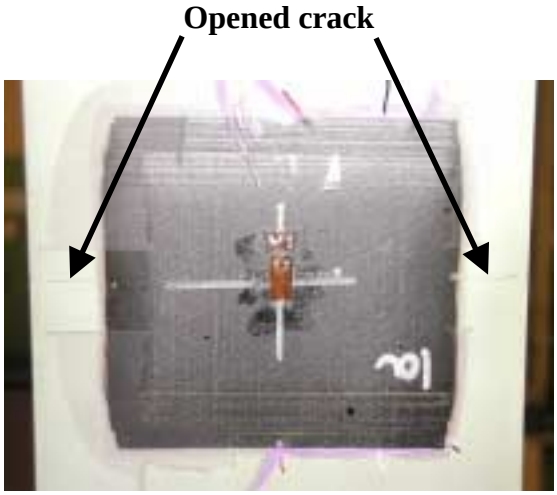

Figure 60: Failed Aluminum, Intact Patch


Figure 61: Failed Patch

Figures 60 and 61 show the panel after the aluminum failed and also after the patch failed. Table 17 represents the load history of this panel. A ΔK of 19 (ksi$\sqrt{in}$) was randomly chosen for comparison purposes only. As shown in Figure 59, when ΔK = 19 (ksi$\sqrt{in}$), da/dN = 5.1E-8 (in/cycle). This is a decrease of a factor of 1000 in fatigue crack growth rate, which was expected, as the structure near the crack has been reinforced with high strength composite material.

Table 17: Load History of Panel 1

ΔK (ksi*in$^{0.5}$)	Pmax (lbs)	Total Cycles	Total Crack Length
8.45	3500	100,000	2.19”
10.62	4400	1,275,000	2.19”
12.33	5075	1,500,000	2.21”
14.48	5925	1,900,000	2.23”
16.53	6680	2,600,000	2.27”
18.88	7400	3,450,000	2.37”
22.21	7700	4,450,000	2.78”
23.36	7700	5,450,000	2.95”
24.13	7700	6,450,000	3.06”
26.10	7700	8,450,000	3.32”
27.96	8000	9,500,000	3.42”
33.79	8000	10,500,00	Failure

4.3.2.2 Panel 9 Fatigue Results

Panel 9, cured at 220°F with EA 9696, could not be tested to failure. The panel broke in the grips due to fretting. However, results obtained prior to this failure show a slight decrease in fatigue crack growth rate when compared to that of the 250°F specimen. In the load step sequence before grip failure, the specimen was at 7,750,000 cycles, a crack length of 2.11”, a P_{max} of 8000(lbs), and a ΔK of 16.00 (ksi$\sqrt{in}$).

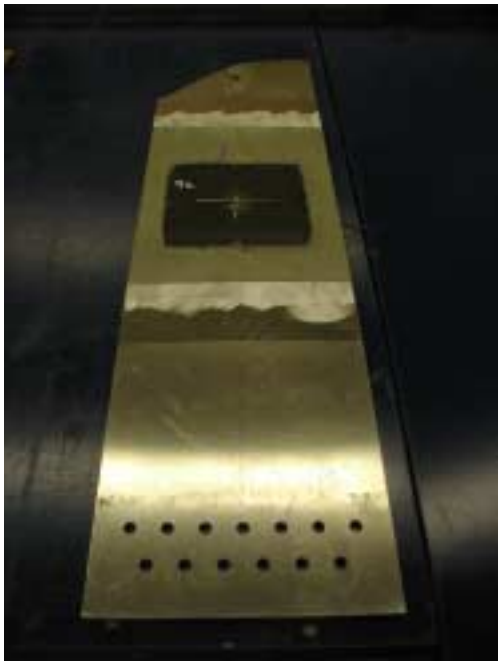

Figure 62: Panel 9 Grip Failure

Table 18: Load History of Panel 9

ΔK (ksi*in$^{0.5}$)	Pmax (lbs)	Total Cycles	Total Crack Length
10.0	4700	2,750,000	1.86”
16.0	6680	7,750,000	2.11”
18.0	8000	8,476,511	2.12”

4.3.2.3 Panel 4 Results

Panel 4, cured at 200°F with EA 9696, showed a significant decrease in fatigue crack growth rate at the selected ΔK value. As shown on Figure 59, when ΔK = 19 (ksi$\sqrt{in}$), da/dN = 4E-8 (in/cycle). This is a decrease of a factor of 1.3 (22%) in fatigue crack growth rate from the EA 9696 250°F specimen. Figures 63 and 64 below show specimen 4.

Figure 63: Specimen 4

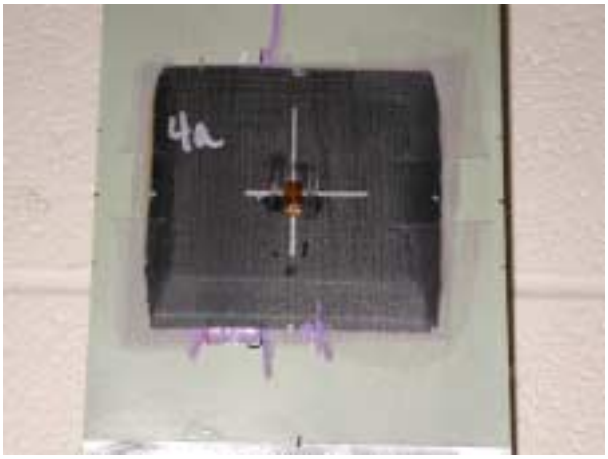

Figure 64: Patch 4a

Table 19: Load History of Panel 4

ΔK (ksi*in$^{0.5}$)	Pmax (lbs)	Total Cycles	Total Crack Length
10.0	4400	1,000,000	1.97”
11.60	5075	2,600,000	1.99”
15.37	6680	3,600,000	2.01”
17.64	7400	4,600,000	2.12”
18.94	7700	5,600,000	2.22”
20.23	8000	6,600,000	2.31”
21.11	8000	8,600,000	2.45”
22.95	8000	10,600,000	2.73”

The 200°F EA 9696 cure cycle shows a slower crack growth rate than the 250°F cure cycle. Data show that the 200°F cure cycle, when compared to the 250°F cure cycle, yield a 7.4% decrease in strain under the repair, a 72.9 psi decrease in stress under the repair, and a 22% slower fatigue crack growth rate. Therefore, it can be concluded that the 200°F cure cycle reduces the thermal residual strains and that the reduction in cure cycle temperature does not have a detrimental effect on the fatigue crack growth rate.

4.3.2.4 Panel 10 Results

Panel 10, cured at 250°F with FM 73M, also shows a significant decreased fatigue crack growth rate. As shown on Figure 59, when ΔK = 19 (ksi$\sqrt{in}$), da/dN = 6.2E-8 (in/cycle). This is a decrease of a factor of 1000 times in fatigue crack growth rate from the unpatched specimen. Figures 65 and 66 below show specimen 10.

Figure 65: Specimen 10

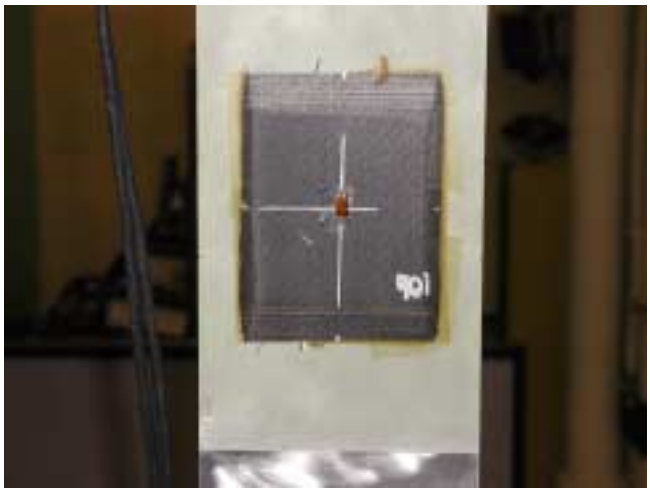

Figure 66: Patch 10b

Table 20: Load History of Panel 10

ΔK (ksi*in$^{0.5}$)	Pmax (lbs)	Total Cycles	Total Crack Length
10.02	4400	2,750,000	2.00”
16.72	6680	5,750,000	2.30”
20.18	7700	6,750,000	2.45”
22.66	8000	8,750,000	2.70”
24.77	8000	10,750,000	3.10”

4.3.2.5 Panel 13 Results

Panel 13, cured at 200°F with FM 73M, could not be tested to failure. The panel broke in the grips due to fretting. In the load step sequence before the grip failure, the specimen was at 5,250,000 cycles, a crack length of 2.875", a P_{max} of 8000 (lbs), and a ΔK of 19.94(ksi$\sqrt{in}$). The data point obtained from testing does not show an improvement in fatigue crack growth when compared to the 250°F cure cycle.

Figure 67: Grip Failure on Panel 13

Table 21: Load History of Panel 13

ΔK (ksi*in$^{0.5}$)	Pmax (lbs)	Total Cycles	Total Crack Length
10.75	4400	2,750,000	2.21"
19.94	6680	5,250,000	2.875"

4.4 Chapter Summary

This chapter discussed the results of both the thermal residual strain testing and the fatigue crack growth rate testing. The summary and conclusions of these results are listed in Chapter 5.

CHAPTER 5: SUMMARY and CONCLUSIONS

5.1 Summary

The purpose of this research was to determine if reducing the cure cycle temperature of the patch bonding process would decrease the thermal residual strains underneath the patch and whether this repair process would have a beneficial effect on the fatigue crack growth rate of the structure. Panels were machined from 7075-T6 aluminum to 24 inches x 6 inches x 0.125 inch. Each of these panels then had a one inch starter notch machined into its center. Two of these panels were fatigue crack growth rate tested to failure, while the remaining nineteen were precracked to two inches.

Two adhesive systems were utilized: Loctite's Hysol EA 9696 and Cytec FM 73M, both modified epoxy film adhesives. Standard cure cycle times and temperatures were used as baseline studies. Both systems have a standard cure cycle of one hour at 250°F. Differential scanning calorimetry was used to determine modified cure cycle times. For EA 9696, the modified cure cycles were four hours at 220°F and eight hours at 200°F. For FM 73M, the modified cure cycle was four hours at 200°F.

The patch material chosen was FiberCote T700/E765 graphite/epoxy prepreg. Patches were manufactured to fifteen plies thickness with dimensions of 4 inches x 4 inches and 5.66 inches x 4 inches. The panels were prepared using a grit-blast/sol-gel procedure. Eight 350 Ohm strain gauges were applied to the test specimen: four under the patches, two far-field,

and one on top of each patch. The panels were then patched on both sides, centered on the crack. The entire specimen was vacuum bagged and cured at the appropriate cure cycle time and temperature. Strain readings were taken throughout the cure process, and one panel from each cure set was fatigue crack growth rate tested to failure.

5.1.1 EA 9696 Data Summary

Using the EA 9696 adhesive system, the manufacturer's suggest cure cycle (when cooled to 88.2°F) yields a tensile stress equal to 992 psi. This tensile stress is exerting a force against the patch and could potentially have the effect of opening the crack. When the cure cycle is reduced by 30°F to 220°F, the thermal residual strains decrease by 2% (19.3 με). This is equivalent to reducing the tensile stress on the crack by 19.3 psi. When the 200°F cure cycle is used in place of the 250°F cure cycle, the thermal residual strains decrease by 7.4%, resulting in a decrease in tensile stress of 72.9 psi. Strictly looking at reductions in thermal residual strain and induced tensile stress, it can be concluded that the 200°F modified cure cycle is slightly improved compared to the manufacturer's suggested cure cycle and the 220°F modified cure cycle.

When analyzing the fatigue crack growth rate data of the EA 9696 panels, it is shown that the 220°F cure cycle shows a slightly slower crack growth rate than the 250°F cure cycle. Data show that the 220°F cure cycle, when compared to the 250°F cure cycle, yield a 2% decrease in strain under the repair, a 19.3 psi decrease in stress under the repair. Based on the limited data trends as shown in Figure 64, there was not a detrimental effect on the

fatigue crack growth rate due to the patching processes. No comparison should be made, however, between the 220°F and 250°F processes due to the limited amount of data generated for the 220°F cure cycle.

When analyzing the fatigue crack growth rate data of the EA 9696 panels, it is shown that the 200°F cure cycle shows a slower crack growth rate than the 250°F cure cycle by 22%. Data show that the 200°F cure cycle, when compared to the 250°F cure cycle, yield a 7.4% decrease in strain under the repair, a 72.9 psi decrease in stress under the repair, and a similar fatigue crack growth rate. Therefore, it can be concluded that not only does the 200°F cure cycle meet the strain, stress, and fatigue crack growth rates of the 250°F cure cycle, it actually reduces the strain, stress, and fatigue crack growth rates of the standard cycle.

5.1.2 FM 73M Data Summary

Using the FM 73M adhesive system, the manufacturer's suggested cure cycle (when cooled to 93.3°F) yields a tensile stress equal to 904 psi. This tensile stress is exerting force against the patch and actually opening the crack. When the 200°F cure cycle is used in place of the 250°F cure cycle, the thermal residual strains decrease by 26.5%, resulting in a decrease in tensile stress of 239 psi. Strictly looking at reductions in thermal residual strain and induced tensile stress, it can be concluded that the 200°F modified cure cycle is superior to the manufacturer's suggested cure cycle.

When analyzing the fatigue crack growth rate data of the FM 73 panels, it is shown that the 200°F cure cycle shows a slightly slower crack growth rate than the 250°F cure cycle. Data

show that the 200°F cure cycle, when compared to the 250°F cure cycle, yield a 26.5% decrease in strain under the repair, a 239 psi decrease in stress under the repair, and a slightly slower fatigue crack growth rate. Based on the limited data trends as shown in Figure 64, there was a definitive improvement in fatigue crack growth rate due to the patching processes, as was expected. No comparison should be made, however, between the 200°F and 250°F processes due to the limited amount of data generated for the 200°F cure cycle.

5.2 Conclusions

The following conclusions can be made:

- For EA 9696 adhesive, when the cure cycle temperature is reduced from 250°F to 220°F, there is an additional 5 hours cure cycle time, yet a reduction in thermal residual strain of 2%
- For EA 9696 adhesive, when the cure cycle temperature is reduced from 250°F to 200°F, there is an additional 7 hours cure cycle time, yet there is a reduction in thermal residual strain of 7.4%
- For FM 73 adhesive, when the cure cycle temperature is reduced from 250°F to 200°F, there is an additional 3 hours cure cycle time, yet there is a reduction in thermal residual strain of 26.5%
- For EA 9696 250°F, there was a reduction in fatigue crack growth rate by a factor of 1000 from the unpatched specimen.

- For the adhesive EA 9696 at 250°F vs 200°F, there was a decrease in fatigue crack growth rate of 22% when the 200°F cure cycle was used in place of the 250°F cure cycle.
- When the FM 73M 250°F is compared to the EA 9696 250°F, there was a decrease by a factor of 1.2 in fatigue crack growth rate when the EA 9696 250°F cure cycle was utilized.
- At a $\Delta K = 19$ (ksi$\sqrt{in}$), both EA 9696 and FM 73M 250°F standard cure cycle show an almost identical fatigue crack growth rate.
- This research concludes that reducing the cure cycle temperature reduces the thermal residual strains and that there is not a detrimental effect on the fatigue crack growth rate of the modified cure cycles when compared to the manufacturers' standard cure cycle.

Appendix A: Patch Curing Procedures

1. Place two sheets of Airtech nonporous Teflon on the base of the portable autoclave
2. Place all patches on top of nonporous Teflon
3. Cover patches with one sheet of Airtech porous Teflon and place one ply of Airtech Super A bleeder material on top of porous Teflon.
4. Cover bleeder ply with one sheet of nonporous Teflon; cover entire area with one piece of Airtech Airweave N10 breather material.
5. Apply full vacuum for one hour – this is the debulking process, which removes the entrapped air within the patch
6. Apply both 40 psi and full vacuum for 5 minutes
7. Vent the vacuum and apply only 40 psi throughout the remainder of the cure cycle
8. Ramp the portable autoclave at 3°F per minute to 180°F
9. Hold at 180°F for one hour
10. Ramp at 3°F per minute to 270°F
11. Hold at 270°F for two hours
12. Cool to room temperature and remove patches.

The pictures below show the portable autoclaves, bleeder ply, and cured patches.

Figure 68: Portable autoclaves

Figure 69: Bleeder Ply After Cure

Appendix B: C-Scan Images of Patches

The following figures are the C-Scan images of the patches. Once again, these C-Scans would show any delaminations within the patch.

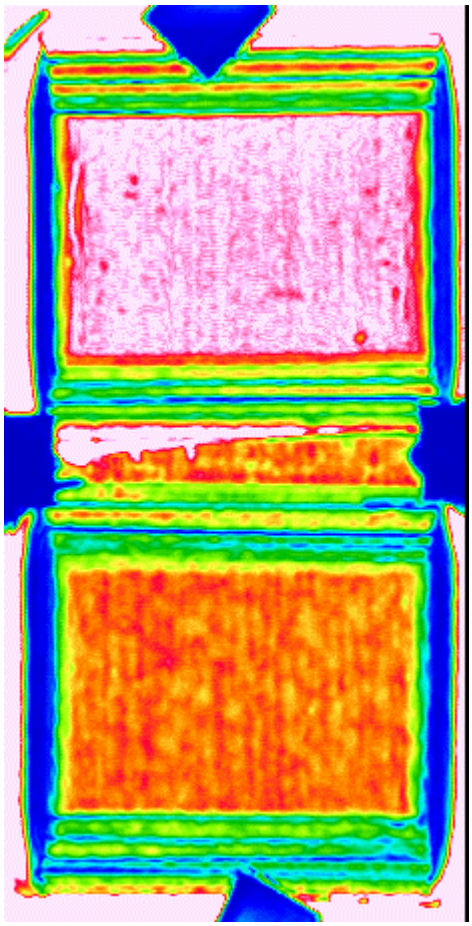

Figure 70: Patches 1a and 1b:

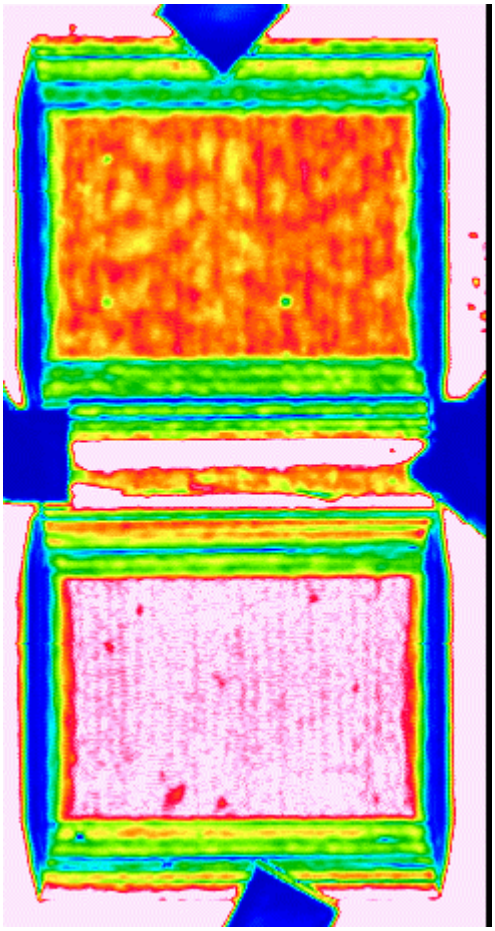

Figure 71: Patches 2a and 2b:

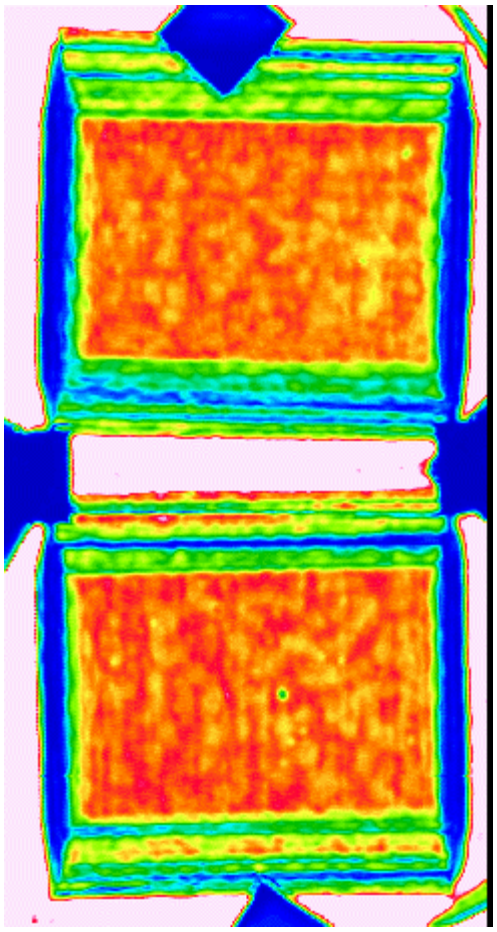

Figure 72: Patches 3a and 3b

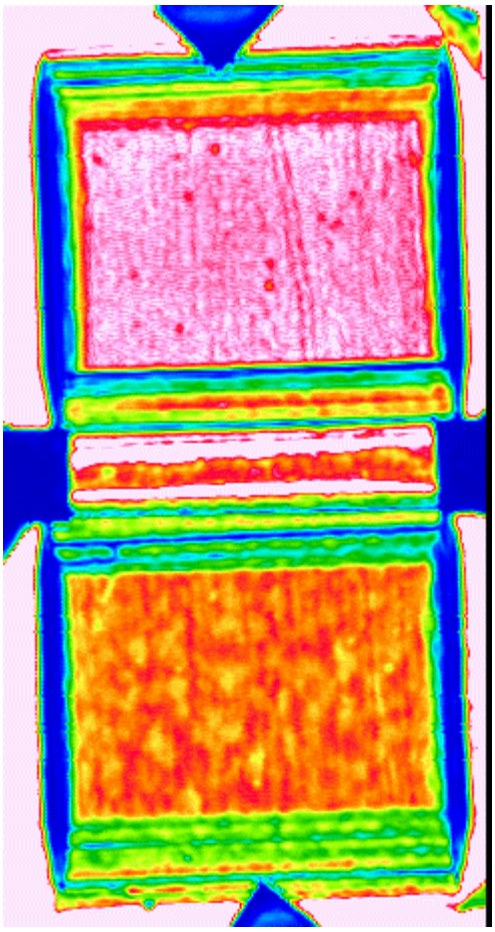

Figure 73: Patches 4a and 4b

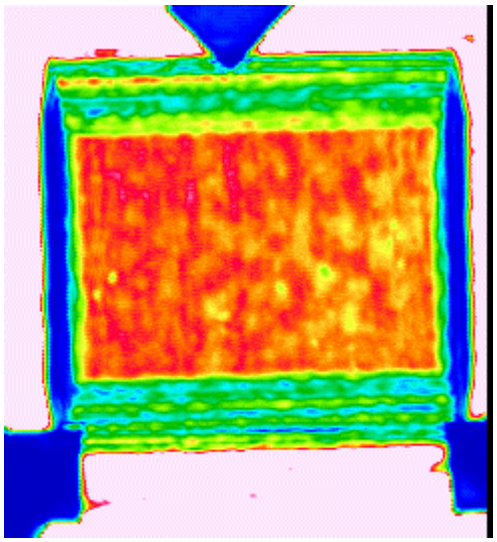

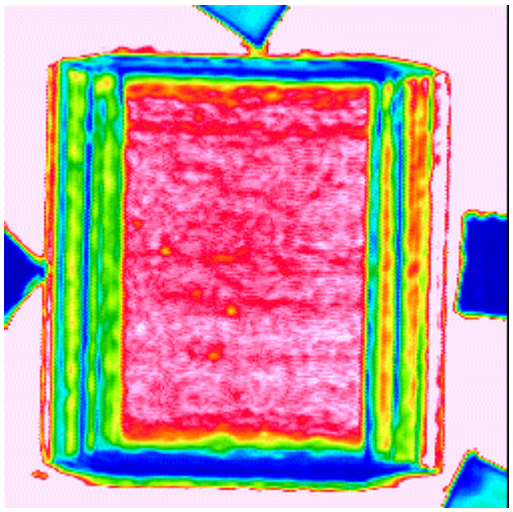

Figure 74: Patches 5a and 5b

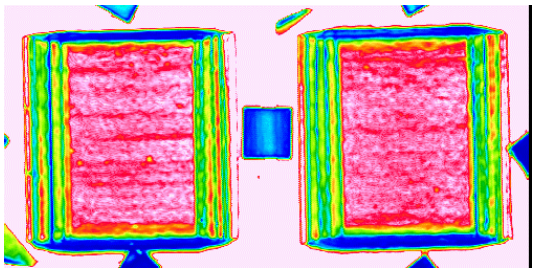

Figure 75: Patches 6a and 6b

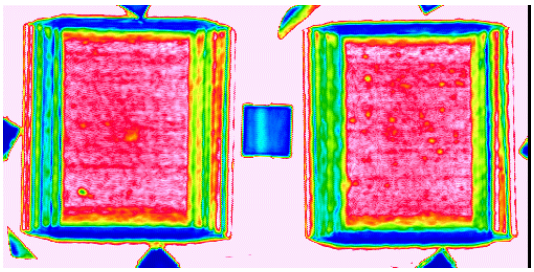

Figure 76: Patches 7a and 7b

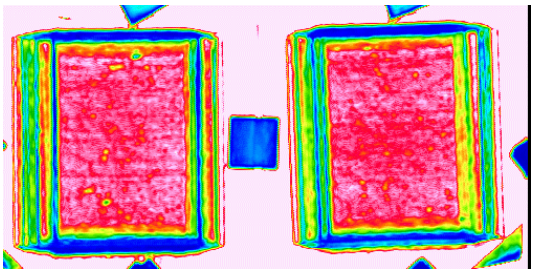

Figure 77: Patches 8a and 8b

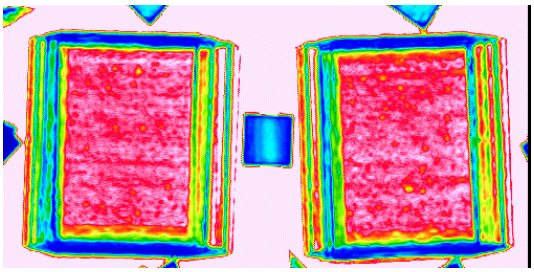

Figure 78: Patches 9a and 9b

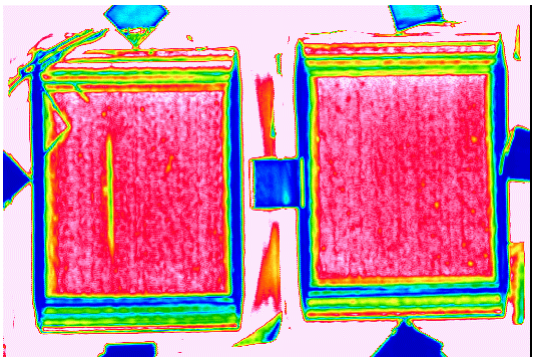

Figure 79: Patches 10a and 10b

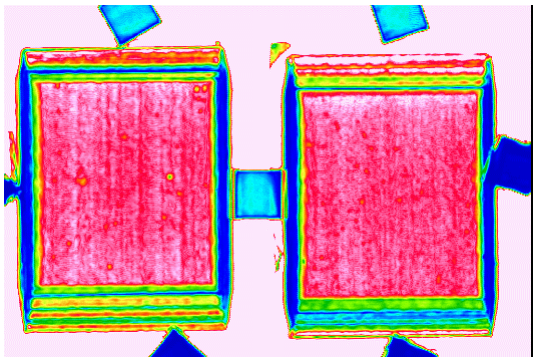

Figure 80: Patches 11a and 11b

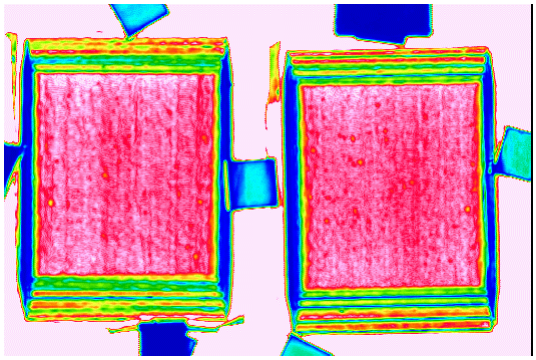

Figure 81: Patches 12a and 12b

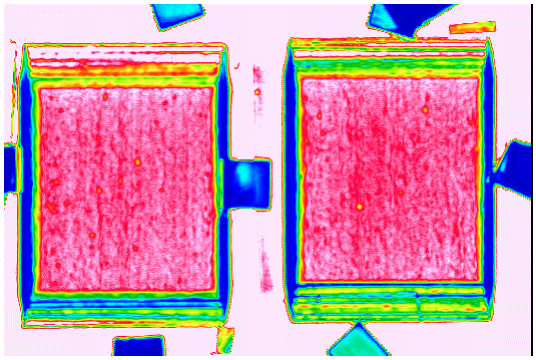

Figure 82: Patches 13a and 13b

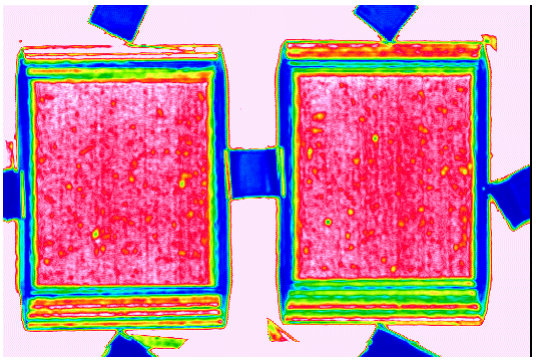

Figure 83: Patches 14a and 14b

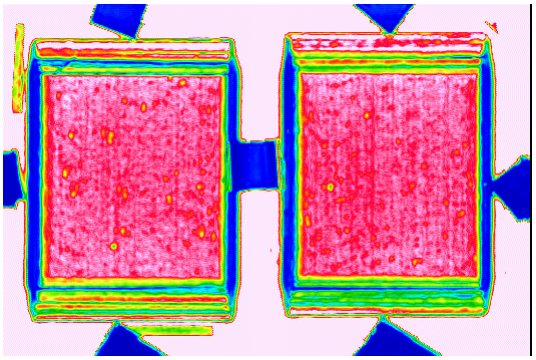

Figure 84: Patches 15a and 15b

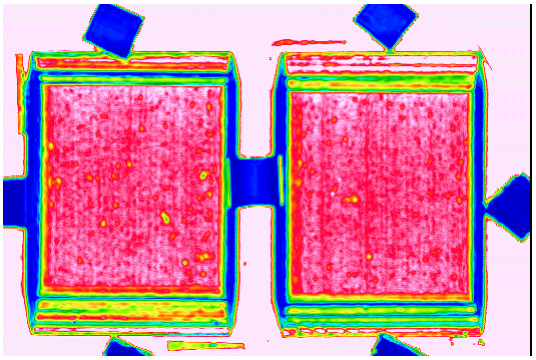

Figure 85: Patches 16a and 16b

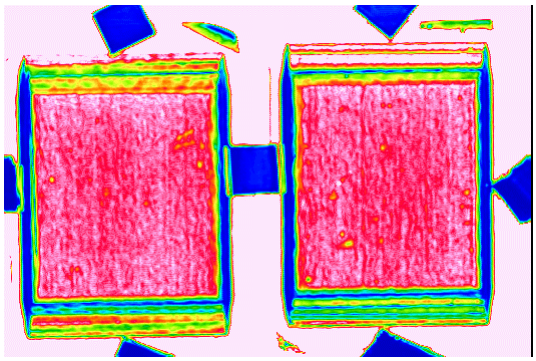

Figure 86: Patches 17a and 17b

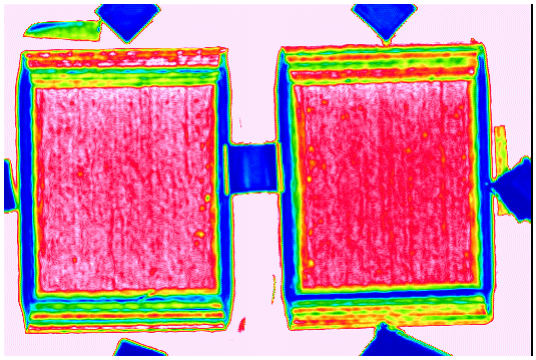

Figure 87: Patches 18a and 18b

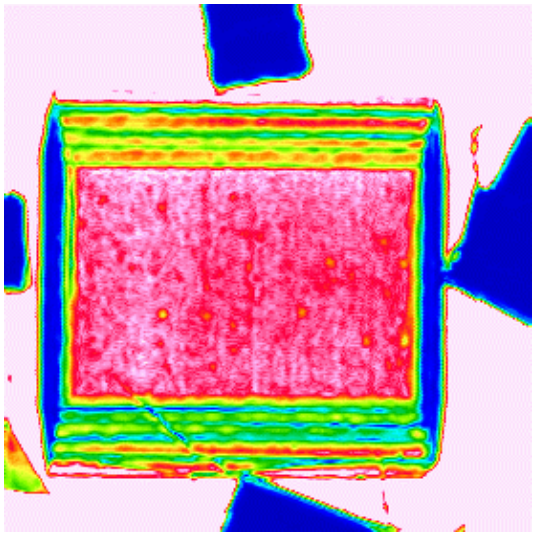

Figure 88: Patch X-1

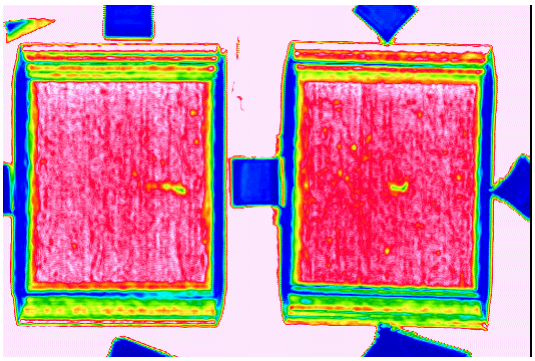

Figure 89: Patches X-2 and X-3

Appendix C: Surface Preparation

1. Mixing of sol-gel – The sol-gel solution is mixed according to the following steps:
    a. Dispense Syringe B1 (Acetic Acid) into Vial B.
    b. Dispense Syringe B2 (Zirconium n-Propoxide) into Vial B. Gently swirl mixture for a minimum of 15 seconds.
    c. Dispense Syringe A1 ((Glycidoxypropyl)trimethoxysilane) into Container A (distilled water). Shake, agitate, or stir for 15 seconds.
    d. Pour Vial B into Container A. Shake vigorously for 15 seconds.
    e. Allow the solution in Container A to sit at room temperature for a minimum of 30 minutes before use.
    f. Shake Container A for 2 to 5 minutes immediately prior to application [27].
2. Solvent Wipe – This step degreases the panel and removes gross contaminants. The panel is wiped with acetone (using Duralace 9404 wipes) until no contaminant is left on the wipe. From this point on, the panel is transported by the edges only.

Figure 90: Solvent Wipe

3. Deoxidation – This step is accomplished by hand sanding with a grinder (driven by 70psi of nitrogen) with 3M Scotch-Brite™ Roloc™ surface condition discs in very fine grain. The repair area is abraded to a uniform surface. After one side of the panel is deoxidized, that side is then placed face down on a Chicopee® Duralace® 9404 Solvent Wipe. The other side is then deoxidized.

Figure 91: Deoxidation

4. Solvent Wipe – After the deoxidation, the contaminants must be removed. This is accomplished with acetone and follows the same procedure as step 1. Time between steps 4 and 6 should not exceed 60 minutes.

5. Tape – The next step is to tape off the areas that will be grit blasted. These areas are at least 3 inches above and below the crack, including the entire width.

6. Grit Blast – The sixth step in the surface preparation process is to grit blast. Both sides were grit blasted with 50 micron nominal size aluminum oxide grit using 40 psi oil-free nitrogen pressure. The area was blasted in overlapping passes until a uniform, fine matte finish was attained. Care was taken to transport only by the edges of the panels.

Figure 92: Panels After Grit Blast

7. Nitrogen Blast – Excess grit was removed by blowing off with dry, oil-free nitrogen. The time between steps 6 and 8 should not exceed 120 minutes.
8. Sol-Gel – The next step is the application of sol-gel. The entire surface of the grit-blasted area must first be wetted with the solution. After this occurs, the area must be kept entirely wetted for three minutes. The sol-gel then drips off the panels, and the panels are then allowed to dry for at least 30 minutes and at most 120 minutes at ambient conditions (~70°F).

Figure 93: Sol-Gel Application

9. Primer – Once the sol-gel has dried for 30 minutes, Cytec BR® 6747-1 (water-based adhesive bonding) primer is then applied. BR® 6747-1, a corrosion inhibiting primer, is a one-part, chromate-containing, modified epoxy primer. This step is hazardous, and health precautions must be taken; a 3M half-face respirator is worn during the priming process, which occurs in a paint booth with

a powerful hood. The primer is applied with a spray gun to obtain a cure film thickness of 0.0001 to 0.0003 inch (0.1 to 0.3 mil), which is verified via color standards. The panels are then allowed to dry at ambient conditions for a minimum of 30 minutes and a maximum of 60 minutes prior to heat cure.

Figure 94: Priming

10. Heat Cure – The last step in the surface preparation is to cure the primer for 60 ± 5 minutes at 250°F ± 5°F [28].

Appendix D: Strain Gauge Process

Mixing Instructions for Adhesive

The following is taken directly from Vishay Measurements Group Instruction Bulletin B-130-15.

1. Resin and curing agent bottles must be at room temperature before opening.
2. Using the disposable plastic funnel, empty contents of bottle labeled "Curing Agent" into bottle of resin labeled "Adhesive". Discard funnel.
3. After tightening the brush cap (included separately), thoroughly mix contents of this "Adhesive" bottle by vigorously shaking it for 10 seconds.
4. Mark bottle with date mixed in space provided on the label.
5. Allow this freshly mixed adhesive to stand for at least one hour before using [29].

Strain Gauge Installation Instructions

The following steps were followed when adhering the strain gauge to the panel/patch.

1. Degrease with isopropyl alcohol
2. Abrade with 220- or 320-grit silicon-carbide paper
3. Apply alignment marks with 4H pencil or a ballpoint pen

4. Apply Conditioner A and scrub with cotton-tipped applicator
5. With a single, slow, wiping motion of a gauze sponge, carefully dry the surface
6. Apply M-Prep Neutralizer 5A and scrub with cotton-tipped applicator
7. With a single, slow, wiping motion of a gauze sponge, carefully dry the surface
8. Remove a gauge with tweezers and place on a chemically clean empty gauge box
9. Position solder terminal below the gauge and secure with Mylar® tape
10. Transfer gauge, terminal, and tape to specimen, carefully placing with alignment marks as shown in Figure 95

Figure 95: Strain Gauge Placement

11. Peel back one end of the tape to raise both gauge and terminal
12. Coat the gauge backing, terminal, and specimen surface with a thin layer of adhesive as seen in Figure 96.

Figure 96: Adhesive Application

13. Let air dry for 5 to 30 minutes at 75°F and 50% relative humidity
14. Return gauge and terminal to the original position on the specimen and apply gentle pressure to allow assembly to be tacked down
15. Overlay area with a thin piece of Teflon sheet and anchor with Mylar® tape
16. Cut a 3/32 in thick silicone gum pad and a metal backup plate slightly larger than gauge/terminal area
17. Center pad and plate and secure with spring clamps or dead weight
18. Place specimen into cool oven and cure as follows: ramp 5°F/minute to 250°F and hold for 3 hours

Figure 97: Curing of Strain Gauges

19. Allow to cool to 100°F before removing the specimen
20. Remove clamps and tape and wash off entire gauge area with either RSK Rosin Solvent or toluene
21. Blot dry with gauze sponge
22. Solder wires to gauge terminals.

APPENDIX E: Patch Bonding Process and Vacuum Bagging Procedures

1. Wipe both sides of the panel with MEK to clean the area.
2. Cut desired adhesive to patch size plus approximately 1/8 inch on all sides.
3. Remove resin rich peel ply from patch and place on adhesive.
4. Place adhesive/patch configuration onto the panel, centered over the crack.
5. Tape down with flash breaker tape to ensure the patch does not shift during the vacuum bagging process.
6. Tape down one thermocouple (per side) on the panel next to the patch.
7. Place one piece of Airtech porous Teflon on top of the entire patch area.
8. Place one ply of Airtech Super A bleeder material on top of the porous Teflon.
9. Place one piece of Airtech nonporous Teflon on top of the bleeder material. Be sure to cover the patch area, but do not completely cover the bleeder, as shown in Figure 98.

Figure 98: Vacuum Bag Lay-up

Vacuum Bagging Procedures

1. Cover the edge of the specimen where the wires will emerge with Airtech Airweave N10 breather material.
2. Cover the entire specimen with breather material.
3. Lay specimen in the center of Airtech Stretchlon 800 vacuum bagging material.
4. Run bag sealing tape along the three edges of the bagging material.
5. Place base of vacuum port on top of a section of the breather, taking care not to place the base on top of the specimen.
6. Cover the specimen with remaining bagging material and secure with tacky tape.
7. Cut a small slit in the bagging material, directly above the base.
8. Attach vacuum port to base and pull full vacuum on the specimen.
9. Check for leaks and ensure that the bag will hold the vacuum when the source is cut off. Refer to figure 99 below.

Figure 99: Vacuum Bagged Specimen

Appendix F: Panel Strains

EA-9696 250°F Cure

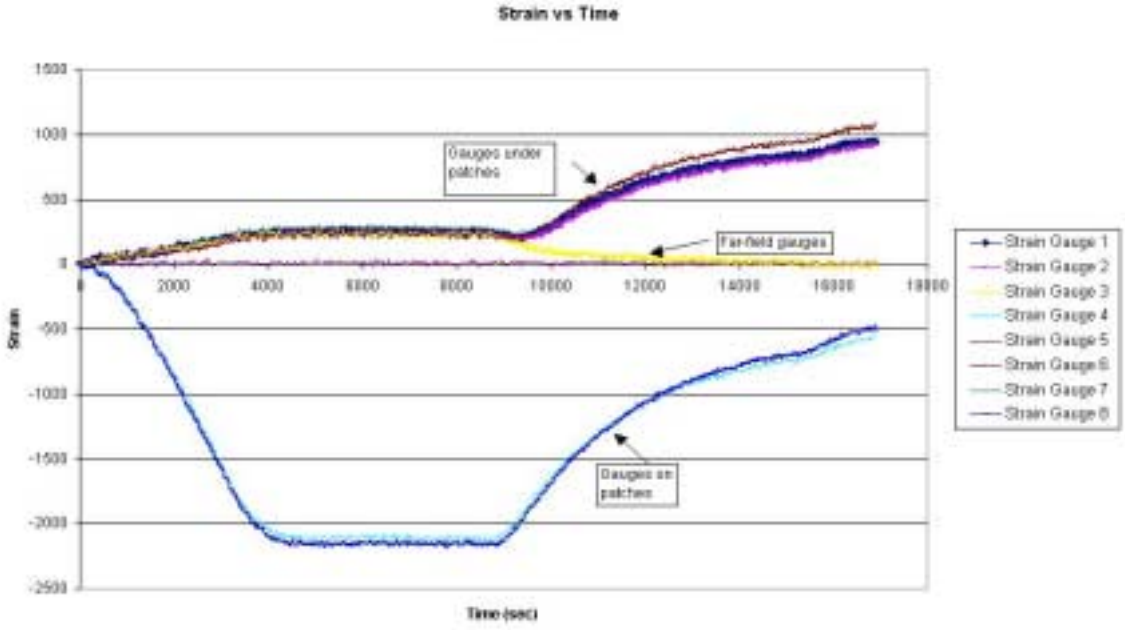

Figure 100: Panel 1 Strains

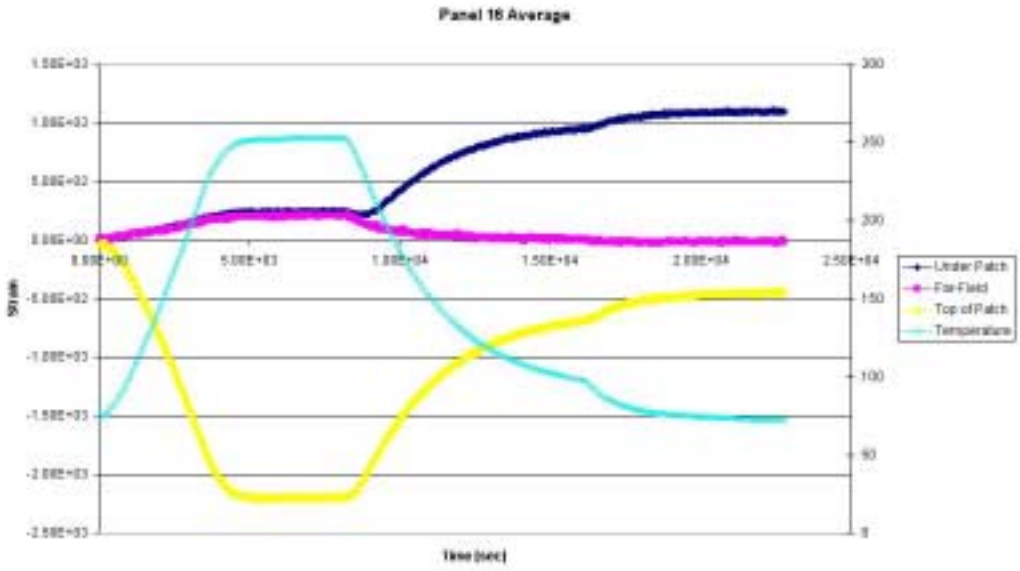

Figure 101: Panel 16 Strains

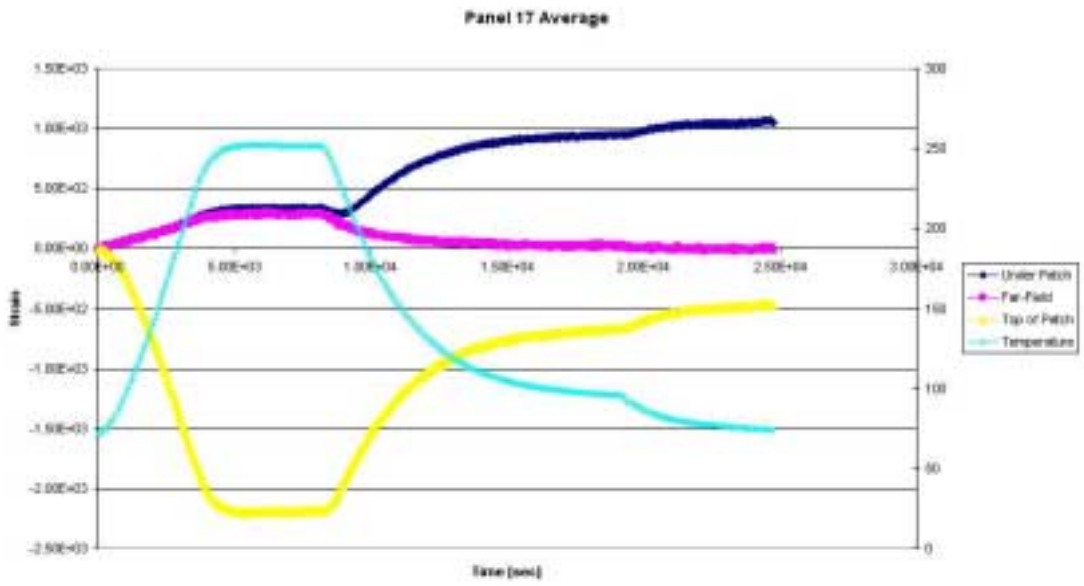

Figure 102: Panel 17 Strains

EA-9696 220°F Cure

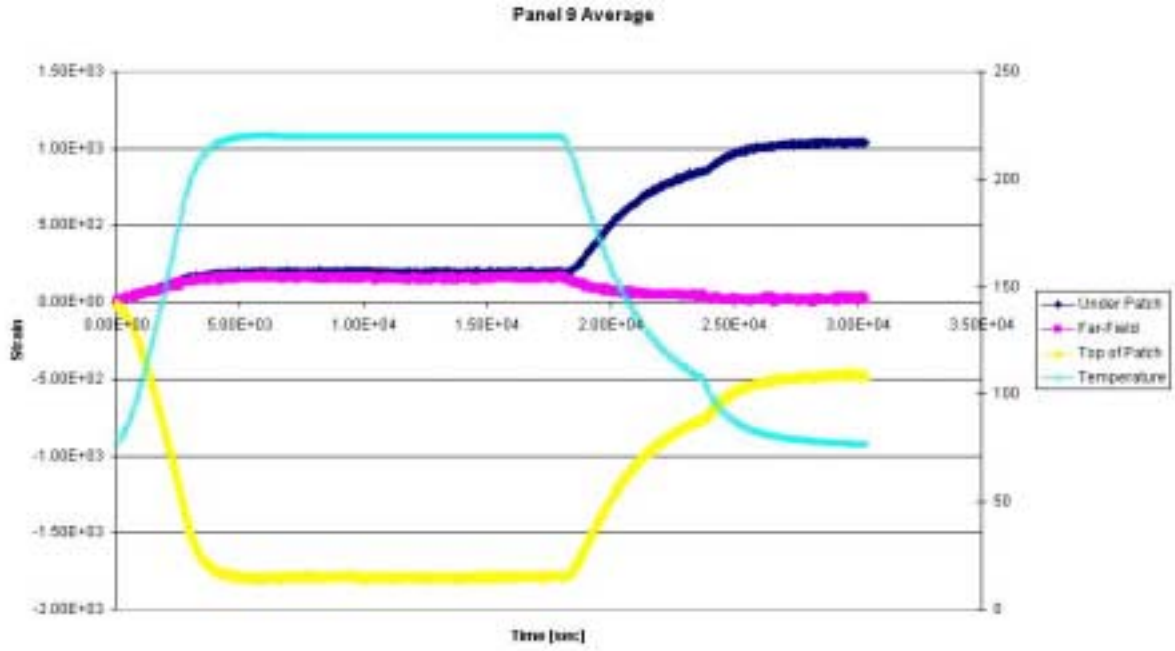

Figure 103: Panel 9 Strains

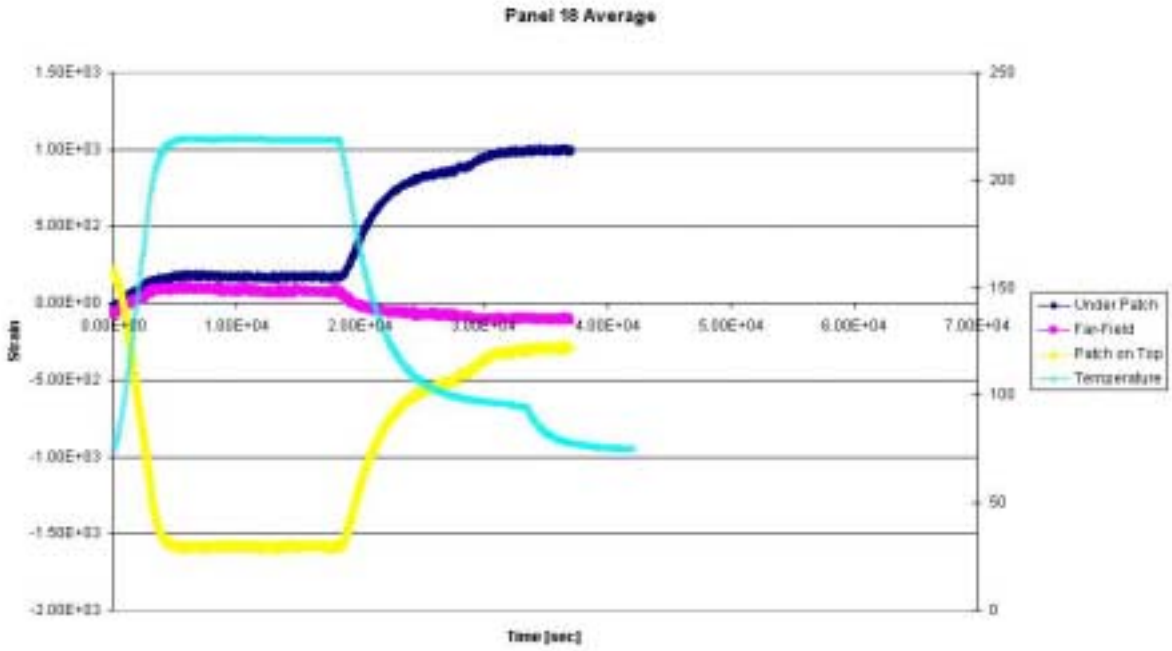

Figure 104: Panel 18 Strains

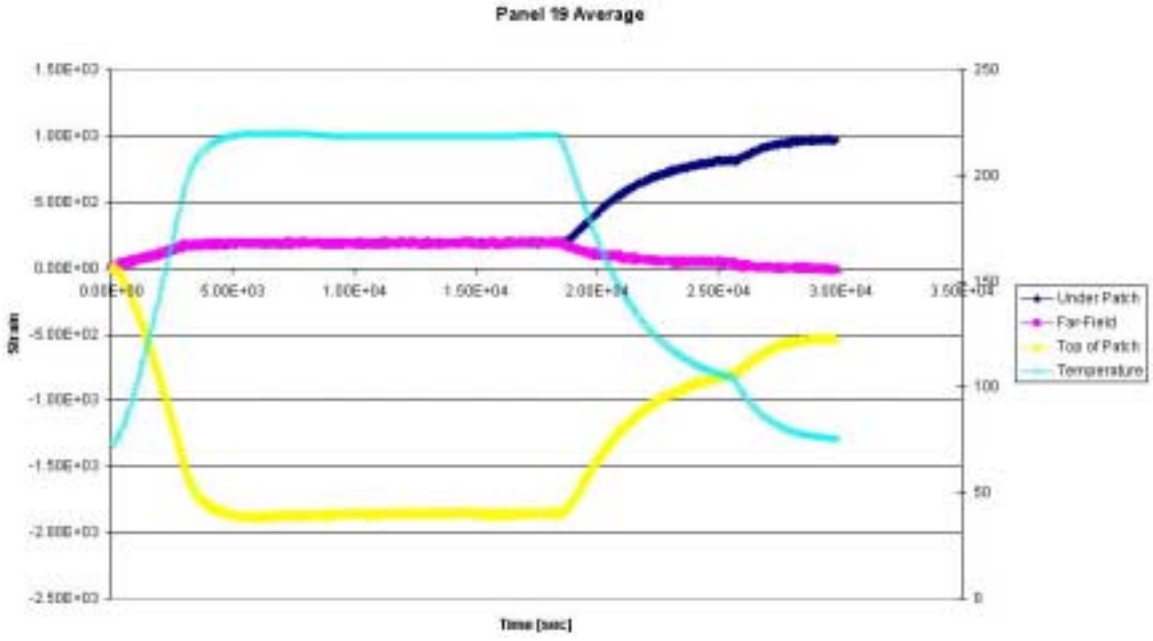

Figure 105: Panel 19 Strains

EA-9696 200°F Cure

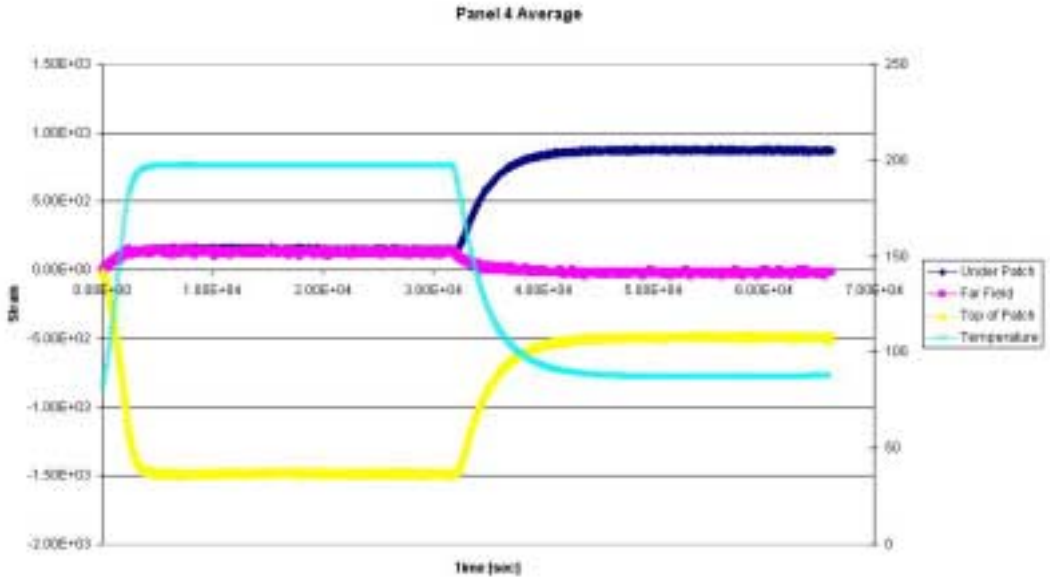

Figure 106: Panel 4 Strains

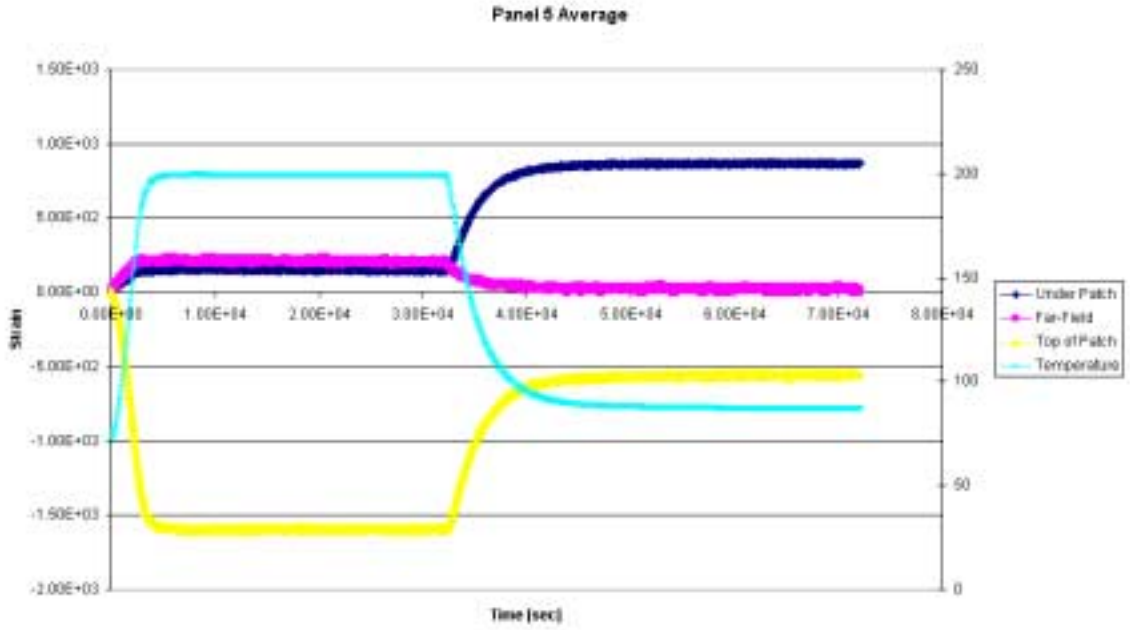

Figure 107: Panel 5 Strains

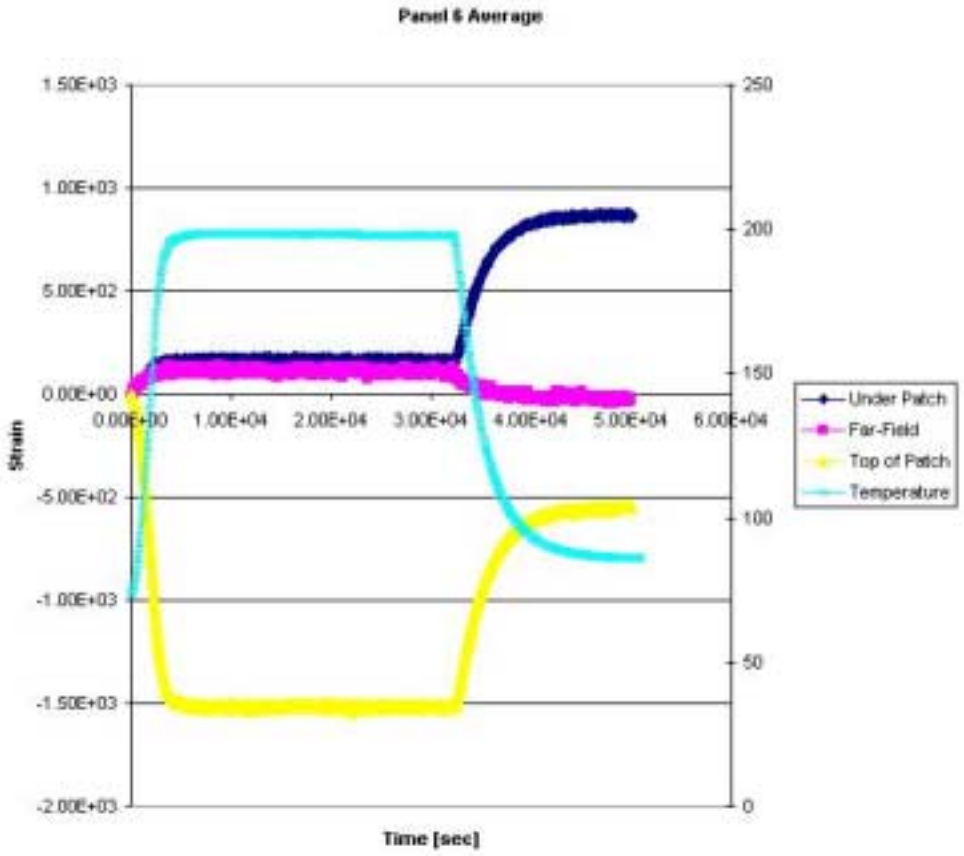

Figure 108: Panel 6 Strains

FM-73M 250°F Cure

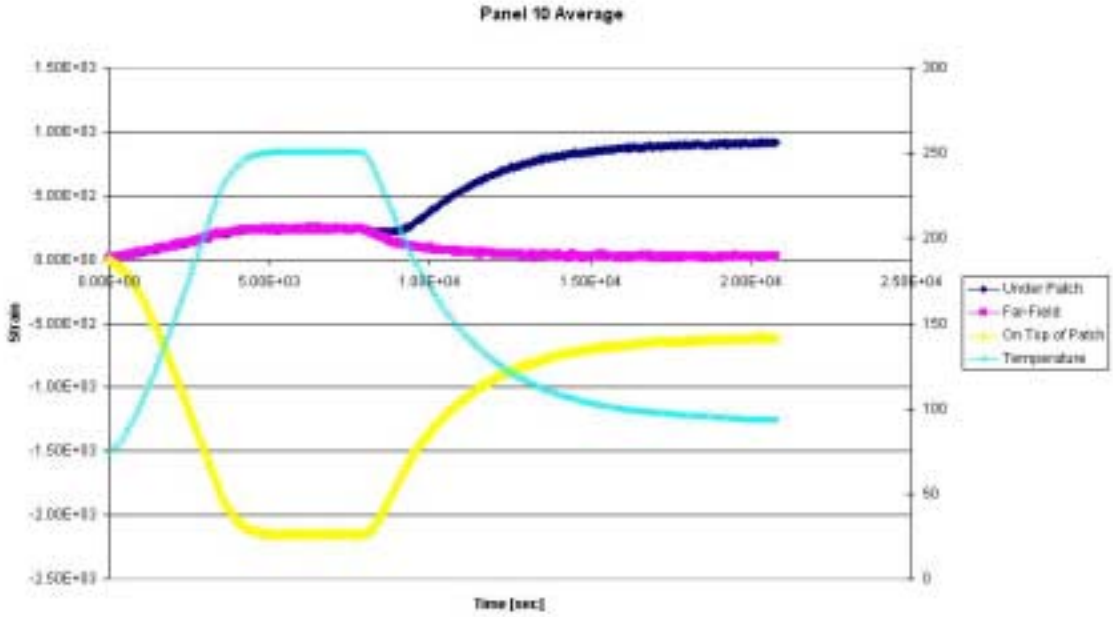

Figure 109: Panel 10 Strains

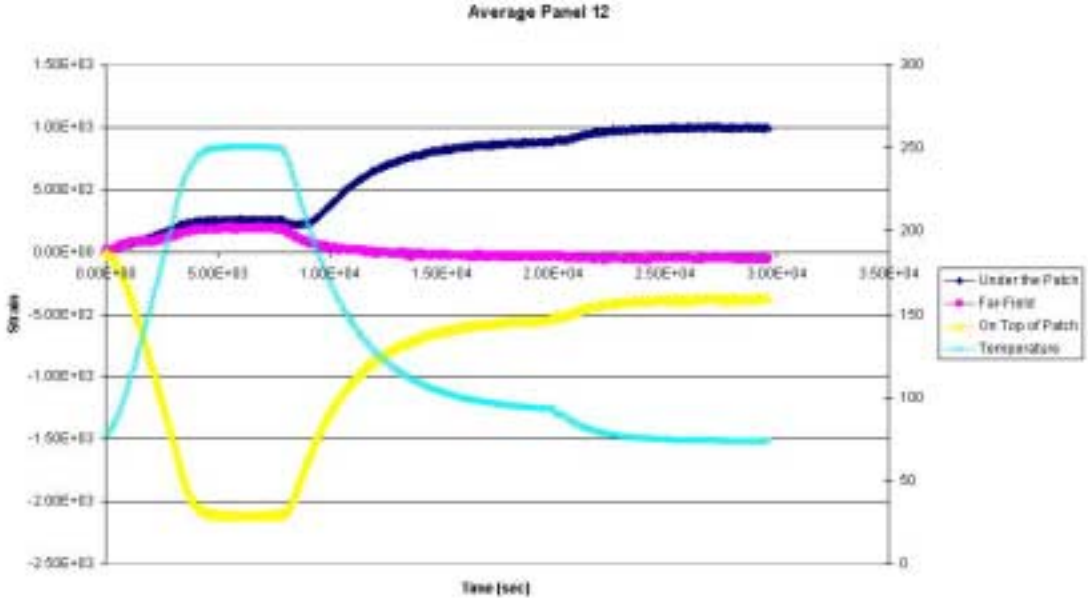

Figure 110: Panel 12 Strains

FM-73M 200°F Cure

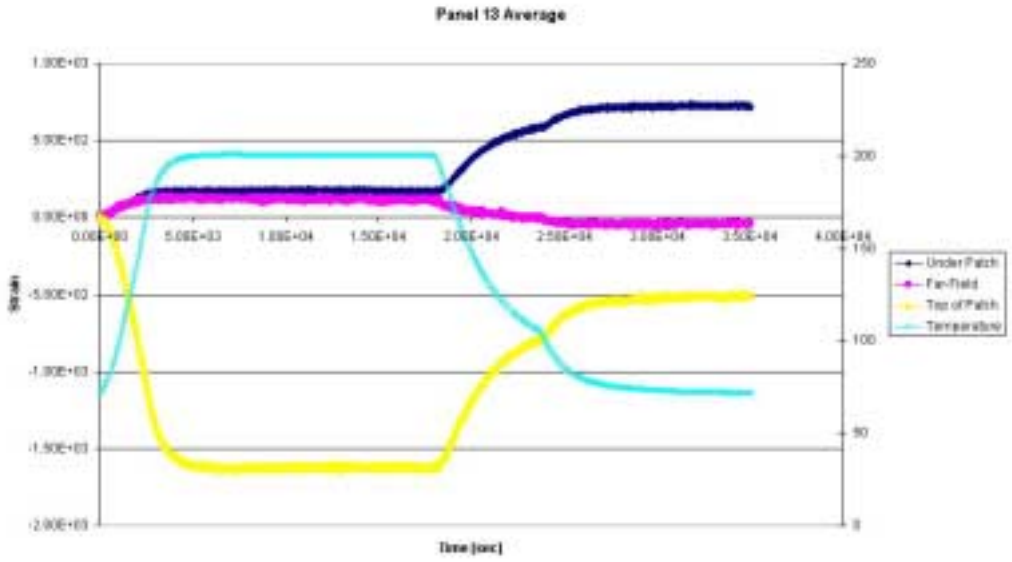

Figure 111: Panel 13 Strains

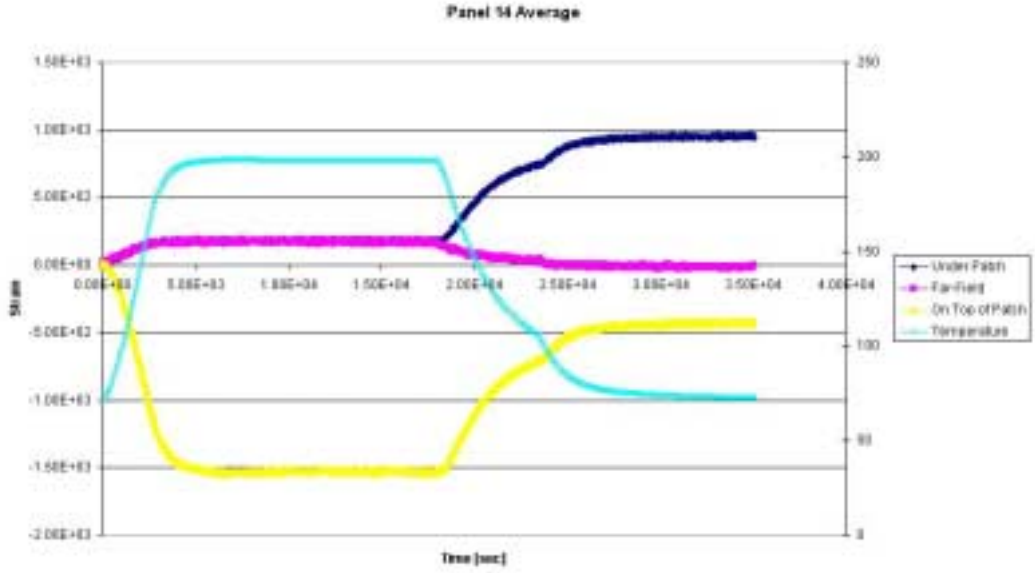

Figure 112: Panel 14 Strains

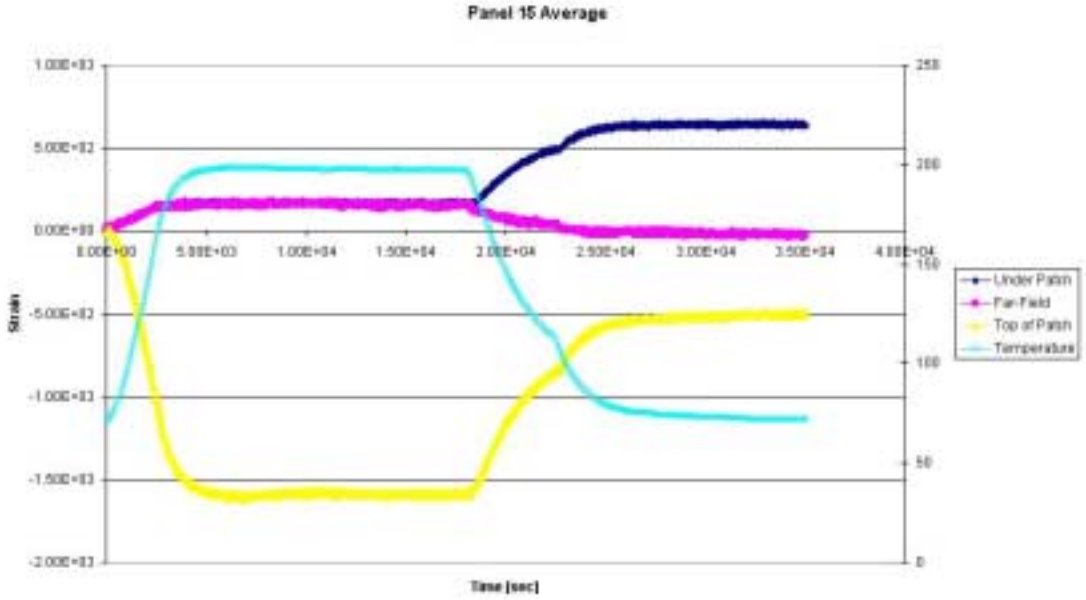

Figure 113: Panel 15 Strains

BIBLIOGRAPHY

1. Wescott, L., and P. Degen. *Wind and Sand.* New York: H.N. Abrams, Inc., 1983.

2. Conley, D.S. *Fatigue Response of Repaired Thick Aluminum Panels with Bondline Flaws.* MS Thesis, AFIT/GAE/ENY/99M-03. Graduate School of Engineering, Air Force Institute of Technology, (AU), Wright-Patterson AFB, 1999.

3. Schweinberg, W.H., Fiebig J.W. *Advanced Composite Repairs of USAF C-141 and C-130 Aircraft.* 1996.

4. Mazza, J. J., Forte, M.S., Cramer, B.D. *F-16 Fuel Vent Hole Bonded Repair Update.* Air Force 4th Aging Aircraft Conference, United States Air Force Academy. July 1996.

5. Caruso, R.P. "Boron/Epoxy Composites for Aircraft Structural Repair," Composite Polymers, 4.

6. Baker, A.A., Jones, R. Bonded Repair of Aircraft Structures *Crack Patching: Experimental Studies, Practical Applications.* Martinus Nijhoff Publisher, Dordrecht. 1988.

7. "Air Force Link." http://www.af.mil/. Last accessed April 2003.

8. Avram, J.B. *Fatigue Response of Thin Stiffened Aluminum Cracked Panels Repaired with Bonded Composite Patches.* MS Thesis, AFIT/GMS/ENY/01M-01. Graduate School of Engineering, Air Force Institute of Technology, (AU), Wright-Patterson AFB, 2001.

9. Thompson, Steven, Private Communication, 2002.

10. Turi, Edith A. Thermal Characterization of Polymeric Materials. Academic Press, California, 1997.

11. Daverschot, D.R. *Thermal Residual Stresses in Bonded Repairs.* MS Thesis. Delft University of Technology, The Netherlands, 2000.

12. Cho, J.; Sun, C.T.; "Lowering Thermal Residual Stresses in Composite Patch Repairs in Metallic Aircraft Structure", January 2001.

13. Green, Robert E. *25th Edition Machinery's Handbook.* New York: Industrial Press, Inc. 1996.

14. Tauriello, John. Private Communication. April 2003.

15. "Aircraft Structural Design." http://adg.stanford.edu/aa241/structures/structuraldesign.html. Last accessed April 2003.

16. McCray, Daniel B., Huff James M., Smith, Jeffrey A., and Mazza, James J. *An Ambient Temperature Adhesive Bonded Repair for Aluminum Alloys.* University of Dayton Research Institute under contract to Air Force Research Laboratory Materials and Manufacturing Directorate. 2001.

17. Blohowiak, K.Y. *Sol-Gel Technology for Space Applications*. The Boeing Company, Phantom Works. Seattle, WA. November 2002.

18. *Composite Repair of Aircraft Structures (CRAS) Design Manual.* Produced by The Boeing Company under USAF contract F33615-97-2-3220, December 2001.

19. Davis, M.J. *Composite Materials and Adhesive Bonded Repairs.* RAAF Standard Engineering C5033. September 1995.

20. FiberCote Industries, Inc. *Certificate of Conformance.* November 2002.

21. Askins, D.R. *Effect of Surface Preparation on Fatigue Durability of Bonded Composite Repair Patches.* AFRL-ML-WP-TR-2000-4154. November 1999.

22. *HYSOL EA 9696.* Product Information. Dexter Aerospace Materials Division. 1997.

23. *FM®73 Film Adhesive: Toughened Epoxy Film.* Product Information. Cytec Engineered Materials, Inc. 1995.

24. "Differential Scanning Calorimetry." http://www.psrc.usm.edy/macrog/dsc.htm. Last accessed March 2003.

25. ASTM E647 *Standard Test Method for Measurement of Fatigue Crack Growth Rates*

26. Tomblin, J., McKenna, J., Ng, Y., Raju, S. *Basic Design Allowables for Epoxy-Based Prepreg: FiberCote Graphite Unitape T700 24K/E765.* National Institute for Aviation Research, Wichita State University. March 1999.

27. *AC-130 100mL Kit Mixing Instructions.* Advanced Chemistry and Technology. Revised May 16, 2002.

28. *AFRL/MLSA Adhesives, Composites, and Elastomers Team Grit-Blast Sol-Gel Procedures.* AFRL/MLSA. Revised June 28, 2000.

29. *Strain Gauge Installations with M-Bond 43-B, 600, 610 Adhesive Systems.* Instruction Bulletin B-130-15. Vishay Measurements Group. July 2002.

Vita

First Lieutenant Heather R. Crooks graduated from Henderson County Senior High School in Henderson, Kentucky, in 1996. She entered undergraduate studies at the Massachusetts Institute of Technology in Cambridge, Massachusetts, where she graduated with a Bachelor of Science degree in Mechanical Engineering in June 2000. She was commissioned through AFROTC Detachment 365 at MIT.

Her first assignment was to Wright-Patterson AFB as a program manager in the Aeronautical Systems Center in July 2000. In October 2000, she entered the Graduate School of Engineering and Management, Air Force Institute of Technology, as a part-time student. In July 2001, she PCA'd to the Air Force Research Laboratory's Materials and Manufacturing Directorate to serve as a research and development engineer. Upon completion of her first assignment in July 2003, she will be assigned to the 412th TW at Edwards AFB.

REPORT DOCUMENTATION PAGE

Form Approved
OMB No. 074-0188

1. REPORT DATE *(DD-MM-YYYY)*	**2. REPORT TYPE**	**3. DATES COVERED** *(From – To)*
27-06-2003 (Grad Date)	**Master's Thesis**	Oct 2000 – Jun 2003

4. TITLE AND SUBTITLE

REDUCTION OF THERMAL RESIDUAL STRAINS IN ADHESIVELY BONDED COMPOSITE REPAIRS

5a. CONTRACT NUMBER
F33615-00-D-5600

5b. GRANT NUMBER

5c. PROGRAM ELEMENT NUMBER

6. AUTHOR(S)

Crooks, Heather R., First Lieutenant, USAF

5d. PROJECT NUMBER

5e. TASK NUMBER

5f. WORK UNIT NUMBER

7. PERFORMING ORGANIZATION NAMES(S) AND ADDRESS(S)
Air Force Institute of Technology
Graduate School of Engineering and Management (AFIT/EN)
2950 Hobson Way
WPAFB OH 45433-7765

8. PERFORMING ORGANIZATION REPORT NUMBER

AFIT/GAE/ENY/03-11J

9. SPONSORING/MONITORING AGENCY NAME(S) AND ADDRESS(ES)
AFRL/MLSA
Attn: Mr. James J. Mazza
2179 12th Street, Bldg 652, Rm 122 DSN: 785-7778
WPAFB OH 45433-7718 e-mail: James.Mazza@wpafb.af.mil

10. SPONSOR/MONITOR'S ACRONYM(S)

11. SPONSOR/MONITOR'S REPORT NUMBER(S)

12. DISTRIBUTION/AVAILABILITY STATEMENT

APPROVED FOR PUBLIC RELEASE; DISTRIBUTION UNLIMITED.

13. SUPPLEMENTARY NOTES

14. ABSTRACT

Many military and commercial aircraft are being called upon to fly well beyond their original intended service lives. This has forced the United States Air Force (USAF) to increasingly rely on structural repairs to address fatigue induced damage and to extend aircraft useful life. The focus of this research is the use of a high-strength composite patch technique to repair a fatigue crack on an aluminum aircraft structure. This study investigates the thermal residual strains that occur as a direct result of the coefficient of thermal expansion (CTE) mismatch between the repair patch and the underlying cracked metallic structure to which the patch is bonded. This research examines the response of a precracked, 24 inches x 6 inches x 0.125 inch, 7075-T6 aluminum panel repaired with a 15-ply graphite/epoxy patch. Two adhesives: EA 9696 and FM 73M were used with varying cure cycles. The hypothesis is that by reducing cure temperatures, the CTE mismatch will be less dramatic, thus yielding a more robust repair with a comparable fatigue crack growth rate. The research concluded that reducing the cure cycle temperature could decrease the thermal residual strains by as much as 26.5% between the graphite/epoxy composite patch and the aluminum structure when FM 73M adhesive is used to bond them together and 7.4% when EA 9696 is used. The research also concluded that a lower cure cycle temperature did not detrimentally affect the panels' fatigue crack growth rates.

15. SUBJECT TERMS
Composite Repair, Fatigue Cracking, Adhesive, Thermal Residual Strains, Graphite/Epoxy Patch, Bonded Repair

16. SECURITY CLASSIFICATION OF:			**17. LIMITATION OF ABSTRACT**	**18. NUMBER OF PAGES**	**19a. NAME OF RESPONSIBLE PERSON**
a. REPORT	**b. ABSTRACT**	**c. THIS PAGE**			Anthony N., Palazotto, AFIT/ENY
U	**U**	**U**	**UU**	138	**19b. TELEPHONE NUMBER** *(Include area code)* (937) 255-3636, ext 4599; e-mail: Anthony.Palazotto@afit.edu

Standard Form 298 (Rev. 8-98)
Prescribed by ANSI Std. Z39-18